A QUANTITATIVE ANALYSIS OF SHORELINE CHANGE, SARGENT, TEXAS

by

James E. Sealy,Jr. and Wayne M. Ahr

Department of Geology

August 1975

TAMU-SG-75-209

Partially supported through Institutional Grant 04-3-158-18
to Texas A&M University
by the National Oceanic and Atmospheric
Administration's Office of Sea Grants
Department of Commerce

$3.00

Order From

Department of Marine Resources Information
Center for Marine Resources
Texas A&M University
College Station, TX 77843

ABSTRACT

The constantly increasing urban and industrial demands on Texas shorelines have placed great stress on a delicately balanced environment. There are tremendous political and economic incentives for the development of methods which will predict the reaction of the coastal system to planned man-made changes on or near the coastline.

This thesis examines a method for shoreline stability analysis which could be used in conjunction with conventional studies of beach erosion rates to provide a more thorough understanding of the interaction of waves, the longshore current, and the coastal sediments. A method for the prediction of erosion and deposition rates related to the interaction of longshore currents and the sediment discharged at the mouth of a river is developed, and this method is applied to the new Brazos River delta near Freeport, Texas.

The potential for sediment displacement by the longshore current is calculated using the assumption that all of the wave energy dissipated in bottom friction is transferred into potential energy by causing the shoreward movement of sediments. The result is later correlated with observed rates of erosion caused by the longshore current at the Brazos River delta to show that the actual amount of sediment movement caused by wave energy dissipation is dependent upon the water depth and the bottom slope.

The potential for deposition of river sediments is modeled by a combination of diffusion processes whereby the bedload is deposited near the river mouth and the suspended load is distributed over a much wider area. Observed rates of deposition at the Brazos River delta are used to correct the predicted values.

The method is successful for predicting the trends of deposition and erosion in the Brazos River delta area for one and two year periods. It is postulated from the results that in some instances, the construction of dams on a river may seriously affect the balance between erosion and deposition on the coastline near the river mouth. In particular, it appears that a 50% drop in the calculated bedload of the Brazos River resulting

from dam construction since 1929 is partially responsible for accelerated erosion rates of the beach near Sargent, Texas, since 1930.

TABLE OF CONTENTS

LIST OF FIGURES

LIST OF TABLES

INTRODUCTION

Introductory Note

The Texas coastline is a 400-mile long arc with barrier islands separating the Gulf of Mexico from large bays and lagoons along 320 miles of this length (Fig. 1). This coastline is not static; rather, recent studies have determined that most of the Texas coast is presently retreating, and has been doing so for at least the past century (Seelig and Sorensen, 1973). Figure 2 shows the rates of change that have been estimated for various parts of the Texas Coast. The highest rate of shoreline advance is immediately southwest of Freeport, Texas, and reflects the development of the Brazos River delta since the diversion of that river in 1929. Southwest of the new delta, near Sargent, Texas, there is an extensive area which has a high rate of shoreline retreat--13 feet per year according to Figure 2. Most of this retreat has occurred since 1930, while the recession rate shown in the figure is the average rate for the years 1853 to 1946. The rate of shoreline retreat at Sargent is shown in more detail in Figure 3. Public and private land

---

The citations on these pages follow the style of The American Association of Petroleum Geologists Bulletin.

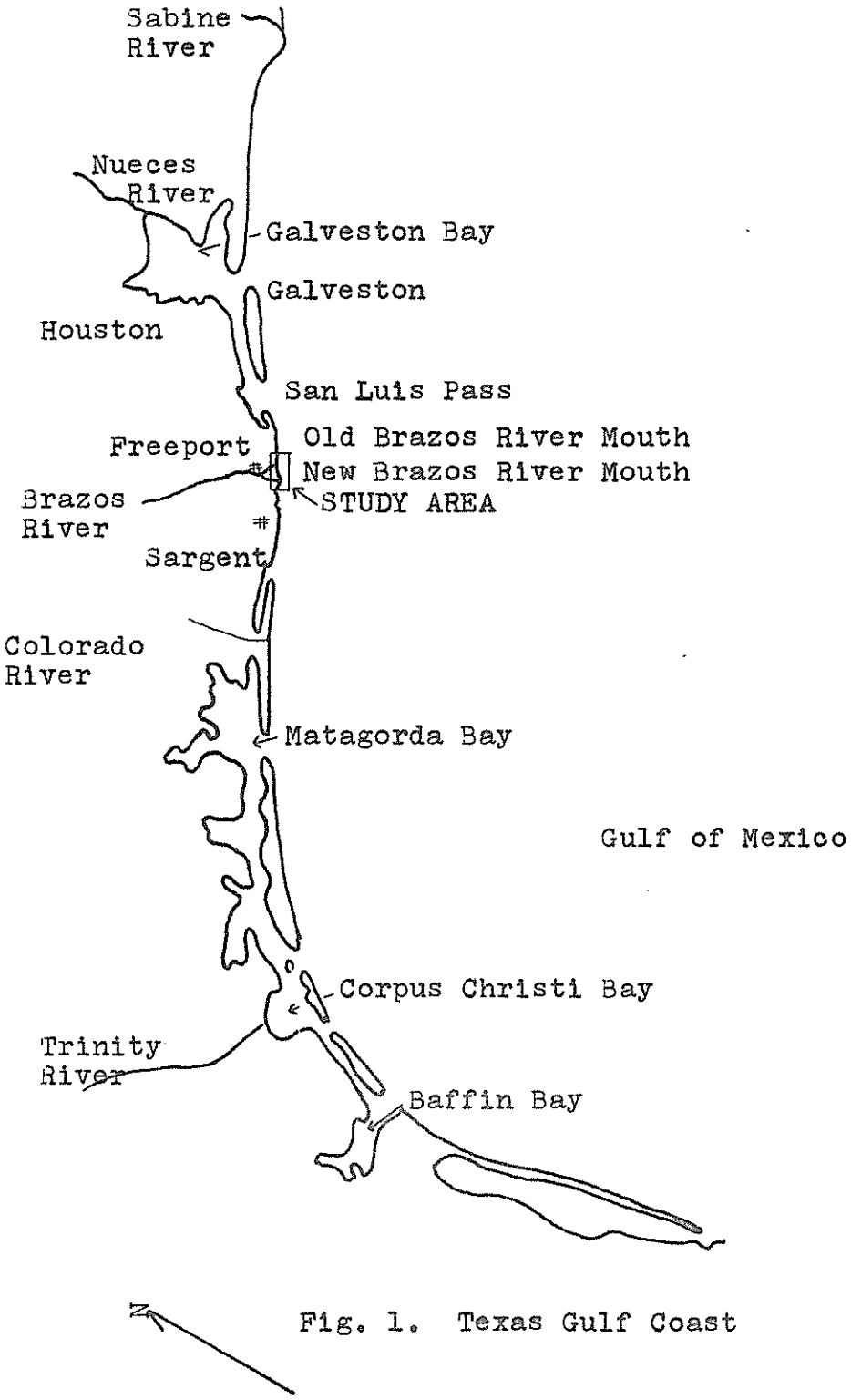

Fig. 1. Texas Gulf Coast

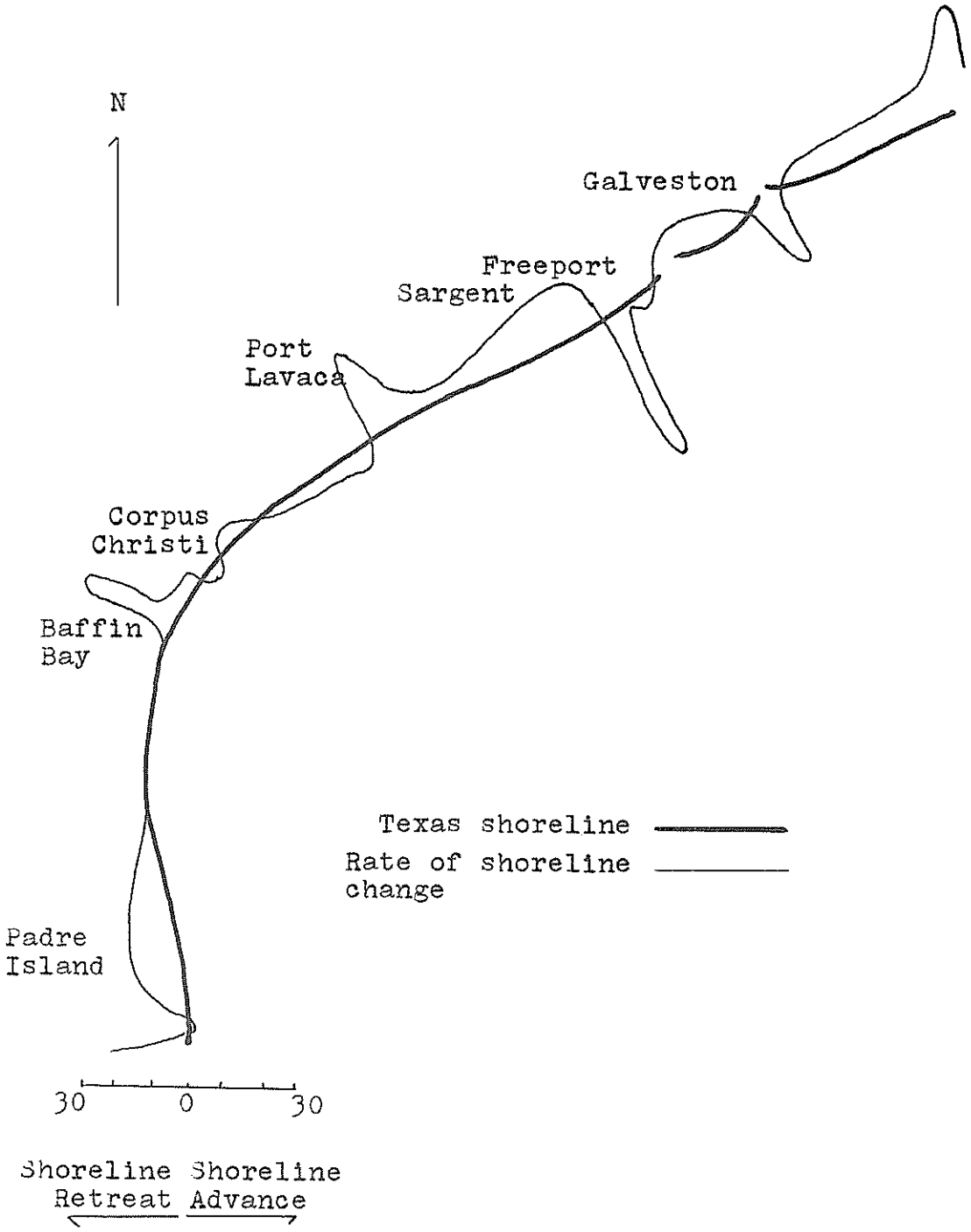

Fig. 2. Historic rate of change of Texas shoreline position. (from Seelig and Sorensen, 1973, figure 1).

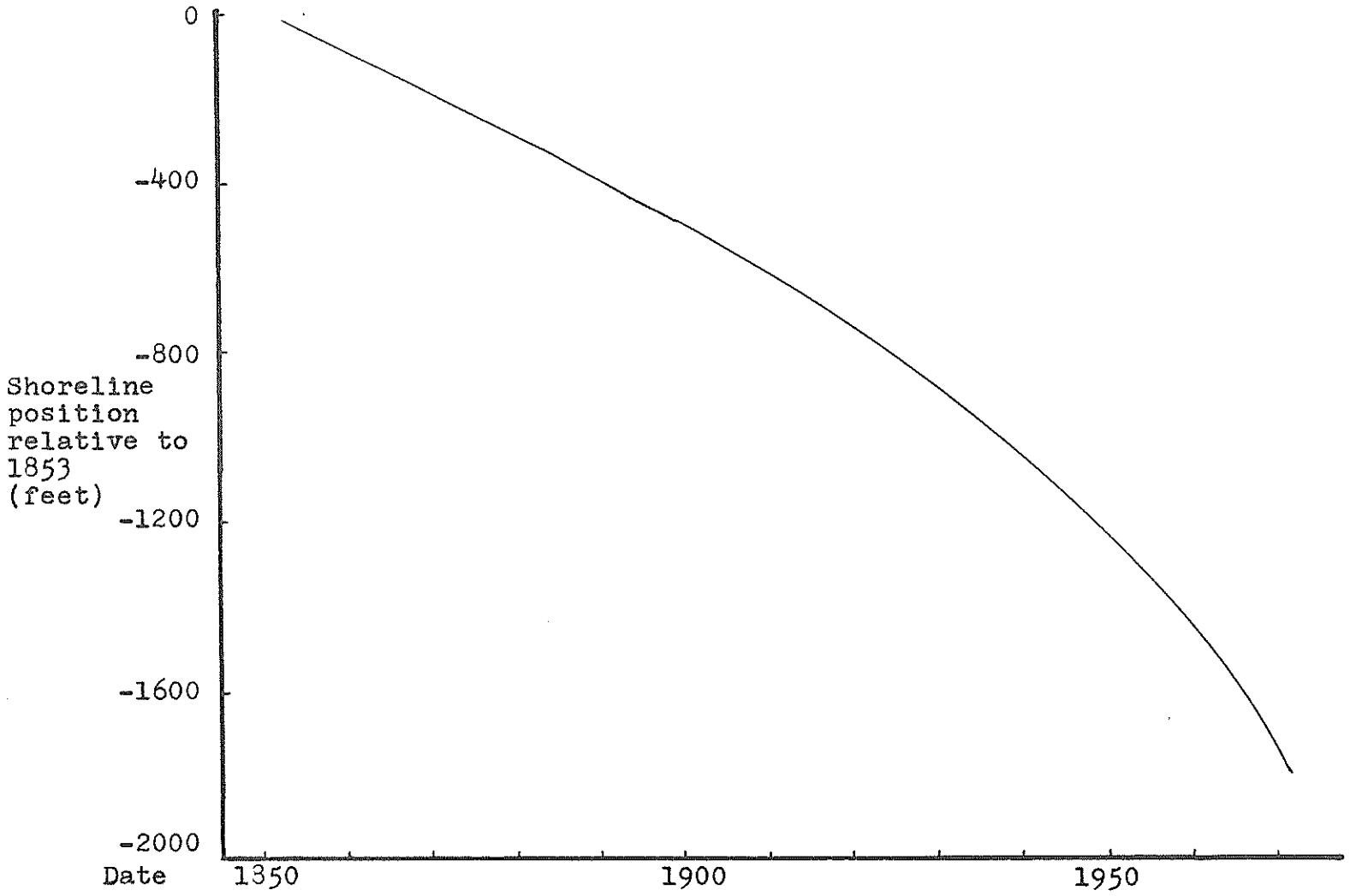

Fig. 3. Historical shoreline position for Sargent, Texas. (from Seelig, 1973, figure 13).

losses of this kind have become increasingly important during the last decade because of the continually greater demands placed on coastal areas by urbanization, industrialization, and tourism. Accordingly, the erosion of coastlines has come under intense study by engineers and geoscientists in the last few years, with the major emphasis falling on the causes and rates of erosion of sand beaches. In the particular case of coastline retreat at Sargent, Texas, it has been suggested (Sorensen, personal communication) that the delta development at the new mouth of the Brazos River, following the diversion of that river in 1929, might have altered the nearshore circulation pattern in the Sargent-Freeport area so as to cause the accelerated erosion rates depicted on Figure 3. The beach erosion at Sargent is therefore thought to be a small part of an overall change in the sedimentation pattern of the area. A study of the supposed cause of this change--the shift of the Brazos River mouth and delta--was proposed to reveal the extent to which the delta development and beach erosion might be related.

Statement of the Problem and Objectives

The Brazos River was diverted 7.3 miles above the

mouth in 1929, so that the river now enters the Gulf of Mexico 5.5 miles southwest of its original mouth. When the diversion was completed, a delta began to develop at the new river mouth, and the delta at the original mouth began to erode immediately. It was nearly completely eroded by 1952, and has not undergone any major changes since that time.

This thesis presents a simplified mathematical analysis of delta formation in which river deposition takes place in a tideless basin with wave induced longshore currents. The actual conditions of river sediment load, wave action, and bottom configuration at the site of the new Brazos River delta are then applied in the model, and the change in the nearshore circulation pattern in response to the growth of the new delta is examined. The results of this study are only generally applicable to the erosion at Sargent, as the available hydrographic charts limited the study to the area immediately around the two deltas. It is hoped, however, that this work may be useful in leading to the later development of a model which could be applied more universally and successfully to the problem of gross changes of offshore sedimentation patterns.

Application

The major contribution of this study is its systematic analysis of the natural processes involved in delta formation; it emphasizes 1) the degree to which a natural phenomena of this type may be approximated by simplified models, 2) the precision of the data available in such a large-scale sedimentological problem, and 3) some of the simplifying assumptions which can render such a system amenable to analysis.

More specifically, however, this study also contributes data to the problem of coastal erosion at Sargent, Texas, and should also be useful in land-use planning in the study area, where the use of the delta as a park is being considered, and in the Texas Gulf Coast as a whole.

PREVIOUS WORK

The importance of waves in beach erosion and in the nearshore transportation of sediments was first described by G. K. Gilbert (1885) in one of the earliest modern studies of shorelines. Gilbert's work was followed by that of Douglas Johnson (1919) whose genetic classification of shorelines was commonly accepted until F. P. Shepard's (1948) redefinition and reclassification of shorelines and coastal processes. Shepard's book included a discussion of wave properties, but did not fully examine the physical relationships between waves and beach development. He did, however, summarize the existing knowledge concerning seasonal beach profile changes, size distribution of beach sediments, and the theories of formation of beaches.

Several semi-analytical treatments of coastline and beach development followed Shepard; especially noteworthy are those by C.A.M. King (1959) and V. P. Zenkovich (1967), which contain lengthy discussions of sediment-wave interaction on beaches.

The author found it more useful to go to hydrodynamics texts for full discussions of theories of fluid and wave motion pertinent to sediment transport, and for explanations of refraction, shoaling, and breaking of

waves. Especially useful were Ippen (1966), Lamb (1924), and Graf (1971).

Recently some work has been done toward the prediction of changes in shape of originally straight beaches with uniform depths offshore (Grijm, 1960; Grijm, 1964; Bakker and Edelman, 1964). This work has thus far been completely theoretical and has not yet enabled the prediction of shoreline shape changes in actual field tests.

A model predicting the growth of a river delta into a long narrow body of standing water is given by Fowler (1957); this model does not allow for the effects of wave-induced erosion.

HISTORICAL BACKGROUND

Development of the Texas Coast

A number of the larger Texas bays are actually estuaries formed when rising sea level drowned Pleistocene river valleys at the end of the last glacial stage. Corpus Christi and Galveston bays, estuaries of the Nueces and Trinity rivers (Fig. 1), are examples of this.

It is thought that the Colorado and Brazos Rivers discharged into similar large estuaries after the last sea level rise. At that time the Colorado flowed in a wide river valley northeast of its present course, and the Brazos and Colorado river valleys merged near the coast. The Brazos and Colorado Rivers both developed extensive deltas which filled their estuaries and then coalesced, building a composite deltaic plain. This composite deltaic plain continued to develop until the natural diversion of the Colorado River a few hundred years ago.

Diversion of the Brazos River

Now only the Brazos flows across the composite Brazos-Colorado deltaic plain, and until the Colorado River delta's recent aggradation, the Brazos was the

only river to discharge directly into the Gulf (Leblanc and Hodgson, 1959). For this reason, it was inevitable that attempts would be made to use the Brazos for transportation between the Gulf and the interior of the state and that the river mouth would come into use as a harbor. There were, however, many problems encountered in these attempts.

The 1858 Coast Chart number 106 (Fig. 4) shows a subaerial bar about three quarters of a mile long and 100 yards wide southwest of the mouth of the Brazos River. The submerged extension of this bar formed a semi-continuous shoal around the river mouth, especially following flooding of the Brazos when the river's high sediment discharge exceeded the capacity of the longshore current (Wisner, 1891). A pass sometimes extended through the bar, but its course and depth changed continually. The first harbor improvement work at the mouth of the Brazos was an attempt to stabilize the pass; two jetties were constructed from the shoreline through the bar. Work began in 1880, but was unsuccessful and was abandoned in 1887 (Fox, 1931).

The beginning of sulphur production from the Bryan and Hoskins mounds and the development of the town of Freeport (Fig. 5) led to increased use of the lower few

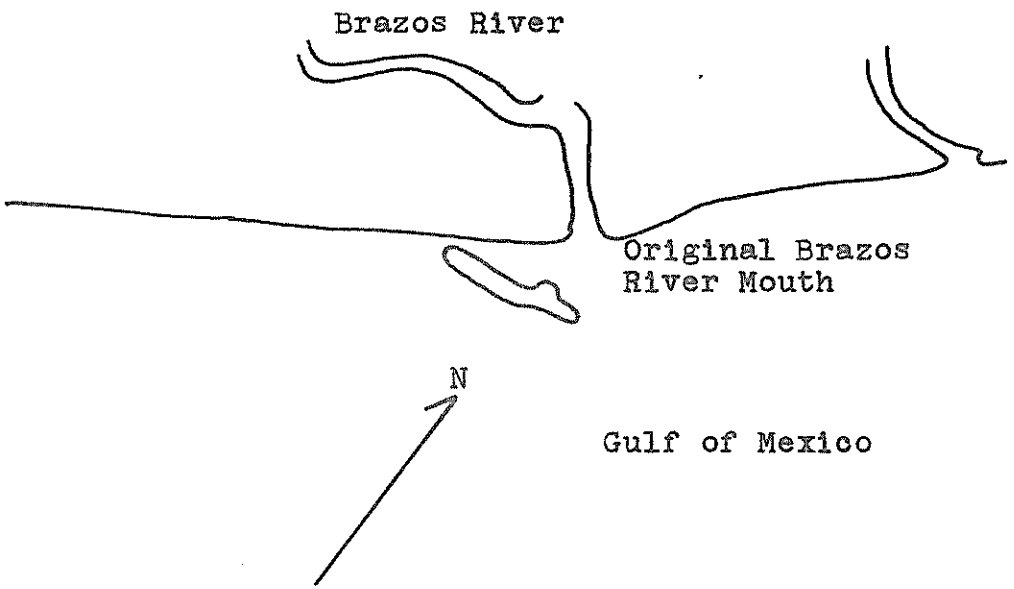

Fig. 4. Shoreline of the Texas coast at the mouth of the Brazos River, 1852. (from Coast Chart number 106, 1858).

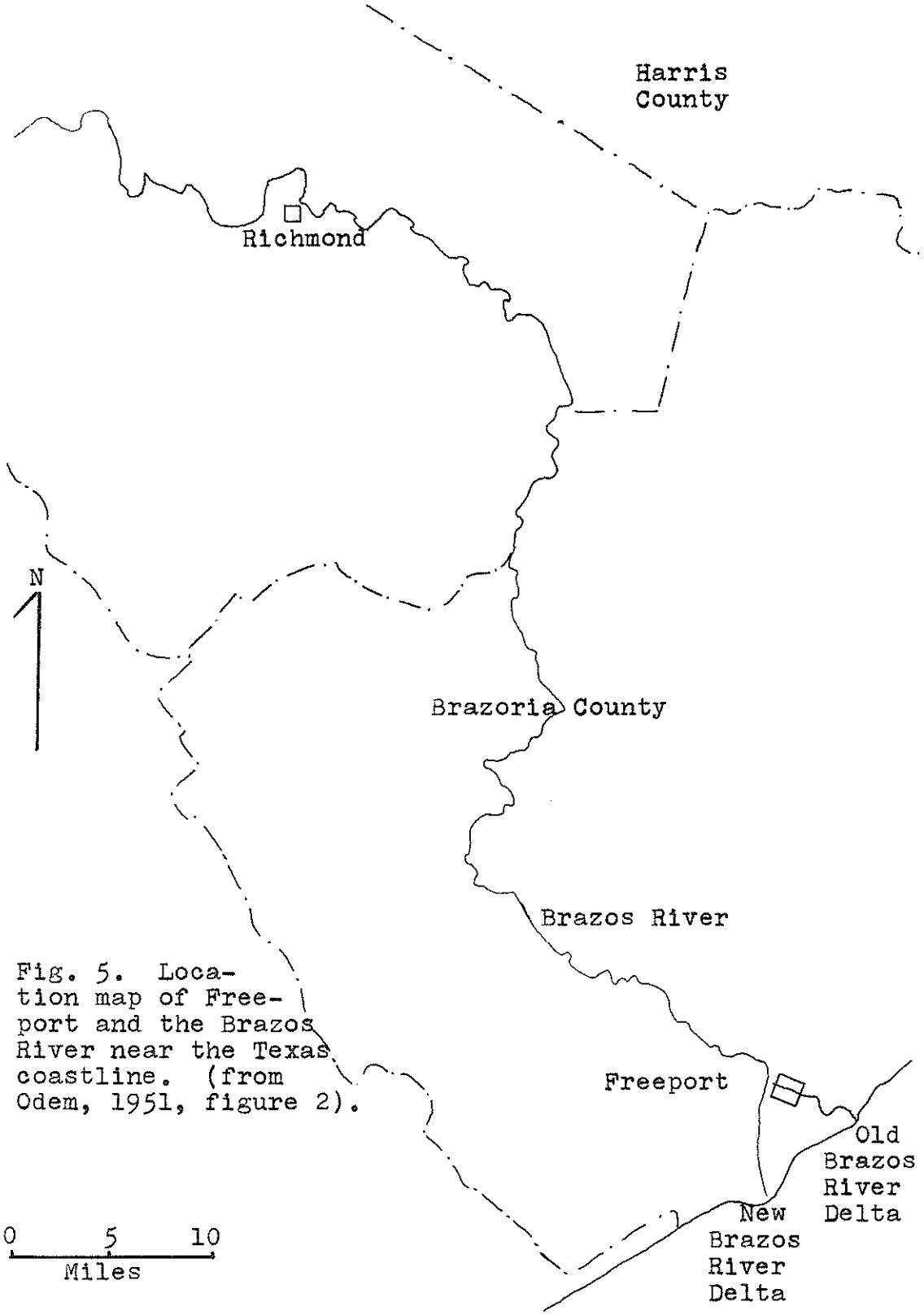

Fig. 5. Location map of Freeport and the Brazos River near the Texas coastline. (from Odem, 1951, figure 2).

miles of the Brazos as a harbor. It was then seen that flood stages caused silting up of the entire harbor, sometimes decreasing depth as much as twelve feet in a few hours (Odem, 1953). Dredging provided only temporary relief because flooding sometimes occurred immediately after the harbor was deepened or a channel through the bar was established. Jetties were constructed, but they were not completely successful in stabilizing the channel. The Corps of Engineers was called upon to solve this problem, and decided upon the diversion of the river, leaving the lower few miles at the original mouth as a tidal basin and harbor. This work began in August, 1928, and was completed in September of 1929 (Fox, 1931). The diversion site is 7.3 miles above the mouth of the old Brazos. The diversion channel is 29,000 feet long; the first 23,000 feet trended S 12°W, and the lower 6,000 feet trended S 6°E (Fig. 6). The channel originally crossed the Gulf Intracoastal Canal at an angle of 63°, but the portion of the canal southwest of the channel was later rerouted to a more landward position, and the canal was then positioned to cross the Brazos at right angles. The current velocity of the Brazos was too great for canal traffic to cross at this angle and new crossings had to be constructed (Fig. 6).

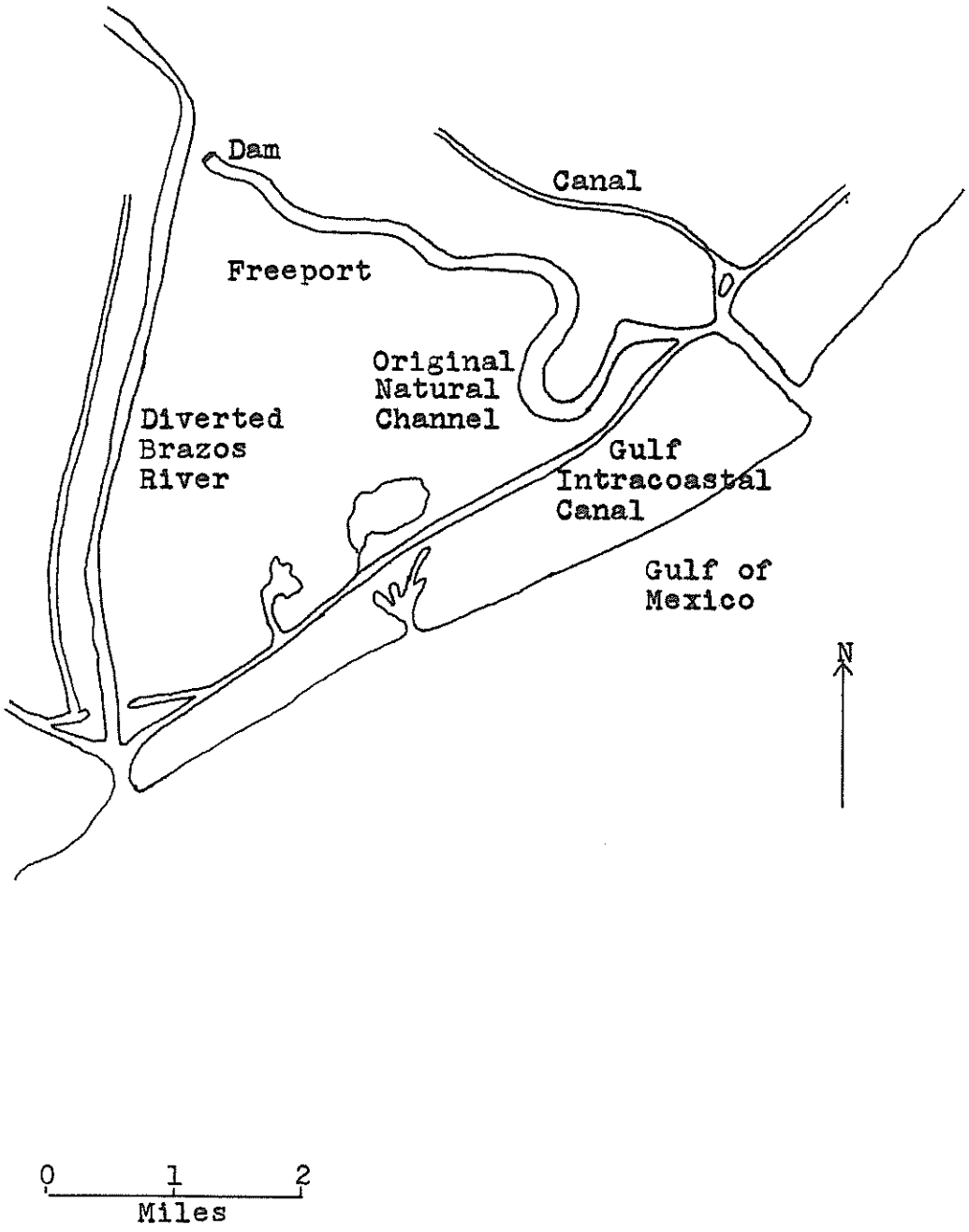

Fig. 6. The Brazos River channels (from Odem, 1951, figure 1).

The canal now intersects the Brazos at an angle of 60° from both sides and the new mouth of the Brazos is 5.5 miles southwest of the original mouth.

Construction and Destruction of the Brazos River Deltas

A brief chronological history of the area following the diversion of the Brazos River is now given; this is essentially as given by Seelig (1973).

1930. Aerial photographs of the study area (Tobin Surveys) show the old Brazos River delta extending one mile further into the Gulf than it appears on Coast Chart number 106. The shoreline at Sargent had undergone an average rate of erosion of 10 feet per year when compared with their 1856 position.

1933. Army Air Corps photos show a shoreline retreat of 100 feet at the old delta, from 1930, with continual construction at the new delta site.

1937. The first complete hydrographic survey in the study area showed the submerged portion of the delta.

1946. U.S. Department of Agriculture photographs show very little change in the subaerial aspects of the delta since 1937.

1948. U.S. Air Force photographs show that the

subaerial portion of the new Brazos River delta grew 8,000 feet into the Gulf from 1946-1948. The old delta continued to erode.

1952. The subaerial portion of the old Brazos delta was almost completely eroded, so that the shoreline was very nearly the same as in 1852.

1967. Surveys by the U.S. Army Corps of Engineers show an erosion rate of 70 feet per year at Sargent.

MODELING THE IDEAL DELTA

For the purposes of this study, it is assumed that the initial construction of the delta is entirely a function of river discharge and that the destruction of the delta is dependent on the erosive capability of the waves and the resulting longshore current. Once the delta has actually begun to form, this assumption will no longer be valid. Changes in shape of the depth contours will cause changes in the refraction of the waves and of the power of the wave propagation into shallow depths. Such changes cause the waves to have greater erosive capabilities in some areas than in others and the longshore currents will be, therefore, both destructional and constructional in nature for different areas of the delta.

The numbers calculated in the following discussion of erosion and accretion rates are obtained using the characteristics of the waves impinging on the Brazos River delta and the discharge rates of the Brazos River. It is not the intent of the author to imply here that the Brazos River delta can be modeled so simply, because the Brazos River delta is not ideal.

Longshore Sediment Transport

Surface waves produce oscillatory motions in water particles near the ocean bottom whenever water depth is less than one-half of the wave length. When the velocities of these motions exceed the critical erosion velocities of the bottom sediments, oscillatory motion will also be initiated in the sediments resulting in most cases in net sediment movement in the direction of wave propogation. If the direction of wave approach is not perpendicular to the depth contours, there will be a component of motion which is parallel to the contours (Fig. 7), which could be termed the longshore component of oscillatory sediment movement.

As waves propogate into shallower water and finally break, the undissipated energy of the wave causes a run-up of water on the beach. If the breaking waves and the run-up do not approach the beach from the perpendicular, a component of movement of water and sediment parallel to the beach results; this movement is commonly known as the longshore current. For the purpose of modeling the development of a delta, it will be assumed that the combination of longshore current and the longshore component of oscillatory sediment transport

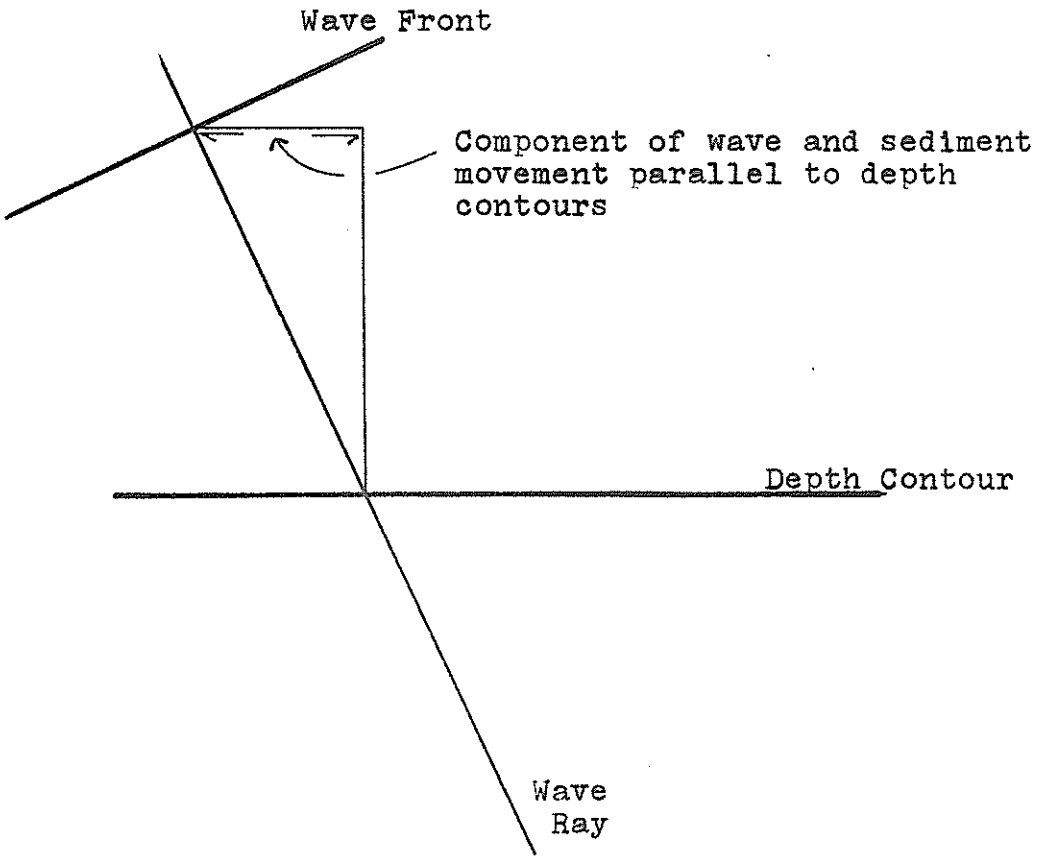

Fig. 7. Diagram showing wave not parallel to depth contour.

is responsible for all sediment erosion and transportation.

Longshore Transport Potential of Waves

The longshore transport potential is defined as the amount of sediment by weight that the waves entering the Brazos delta area are capable of transporting out of the area. The potential will be calculated in two parts: 1) for the area of offshore of the breaker zone, and 2) for the area between the beach and the breaker zone.

The breaker zone. When the oscillatory, wave-induced velocity of the water particles at the crest of a wave approaches the velocity of wave propagation, the crest tends to become steepened. If this trend continues, the wave oversteepens and "breaks". This has been found to occur when

$$u = 0.73C$$

where u = water particle velocity on the crest

C = wave propagation velocity.

A solitary wave (a standing wave) is the wave type for which there is the best agreement between predicted behavior, and the behavior of a breaking wave. The equation for the maximum orbital velocity in a solitary wave is:

$$u = \frac{H}{h} C$$

where H = wave height

and h = water depth.

Thus the depth at which a wave breaks is given by $h = H/0.78$. Six feet is considered to be the breaking depth for all of the waves here, because the resolution of most of the available charts is to the 6-foot depth contour.

Offshore of the breaker zone. The motion of individual water particles affected by a wave in intermediate depth or shallow water can best be examined using the velocity potential for a small amplitude wave:

Eq. 1 $$\Phi = \frac{ag}{\sigma} \frac{\cosh K(h+z)}{\cosh kh} \cos (kx - \sigma t)$$

where Φ = velocity potential of Airy (small amplitude) wave moving in the x direction

k = wave number = $\frac{2\pi}{L}$

a = wave amplitude, $\frac{1}{2}$ of the wave height

σ = wave angular frequency = $\frac{2\pi}{T}$

h = water depth

T = wave period

L = wave length

g = acceleration due to gravity

x = horizontal direction, direction of wave

propogation

t = time

z = vertical distance, with origin at surface

The velocity with which each water particle moves in the horizontal plane is given by the first partial derivative of this velocity potential with respect to the x axis:

Eq. 2a $$u = \frac{\partial \Phi}{\partial x} = \left(\frac{agk}{\sigma}\right) \frac{\cosh k(h+z)}{\cosh kh} \sin(kx - \sigma t)$$

2b $$u = \frac{agT}{L} \frac{\cosh \frac{2\pi}{L}(h+z)}{\cosh \frac{2\pi}{L} h} \sin 2\pi (x/L - t/T)$$

where u = velocity in the x direction.

This velocity is higher at the water surface than at the bottom, as is seen by substituting in z = 0 for the velocity at the surface:

Eq. 3a $$u = \frac{agT}{L} \frac{\cosh \frac{2\pi}{L} h}{\cosh \frac{2\pi}{L} h} \sin 2\pi (x/L - t/T)$$

3b $$u = \frac{agT}{L} \sin 2\pi (x/L - t/T).$$

Substitute z = -h in Equation 2b to obtain the velocity at the bottom:

Eq. 4a $$u = \frac{agT}{L} \frac{\cosh 0}{\cosh \frac{2\pi}{L} h} \sin 2\pi (x/L - t/T)$$

4b $$u = \frac{agT}{L} \frac{1}{\cosh \frac{2\pi}{L} h} \sin 2\pi (x/L - t/T)$$

Since cosh is always larger than one, the velocity given by Equation 4b must be smaller than that given by Equation 3b.

Theoretically, the decrease in the horizontal component

of orbital velocity is exponential, with the largest part of the decrease occurring in the first few feet of depth; however, the sediment-water interface is not frictionless, so there is a drastic decrease in orbital velocities from the non-moving bottom to the freely oscillating water particles. This velocity gradient and the resulting oscillating pressure gradient initiate movement in the bottom sediments.

The most straight-forward means of estimating the size of sedimentary particles which can be eroded by these local water particle movements is a comparison of orbital velocities with critical erosion velocities. The horizontal component of orbital velocity given by Equation 2 is the velocity most likely to effect erosion. The form of this equation most often used is given by:

Eq. 5 $$u = \frac{\pi H}{T} \frac{\cosh \frac{2\pi}{L}(h+z)}{\sinh \frac{2\pi}{L} h} \cos 2\pi(x/L - t/T)$$

where H = wave height.

This is obtained from Equation 2 by integrating with respect to t, using the identity $\sigma^2 = gk \tanh kh$, and differentiating the result with respect to t. Equation 5 gives the instantaneous horizontal component of velocity of the water particles. The maximum value of horizontal velocity is given when:

$\cos 2\pi(x/L - t/T) = 1$ so that

Eq. 6 $$U_{max} = \frac{\pi H}{T} \frac{\cosh \frac{2\pi}{L}(h+z)}{\sinh \frac{2\pi}{L} h}$$

It is well known that velocities necessary to entrain sedimentary particles are much higher than those necessary to transport them. It is assumed here that the maximum velocity will limit the size of the materials which can be eroded, while the average velocity, given by:

Eq. 8 $$U_{ave} = \frac{2H}{T} \frac{\cosh 2\pi\frac{(h+z)}{L}}{\sin h \frac{2\pi h}{L}}$$

will limit the particle sizes which can be transported. The sediment sizes which can be eroded or transported by given velocities can be estimated using Hjulstrom's curve (Fig. 8).

Erosive capability of waves offshore from the breaker zone. The wave energy per unit length of wave crest is given by:

Eq. 7 $$E = \frac{\gamma H^2}{8}$$

where E = wave energy per unit crest length

γ = specific weight of water

It is usually assumed that diffraction (lateral dispersion of wave energy) is negligible as a wave moves across parallel or near parallel contours. Thus the total amount of wave energy along a wave crest between two

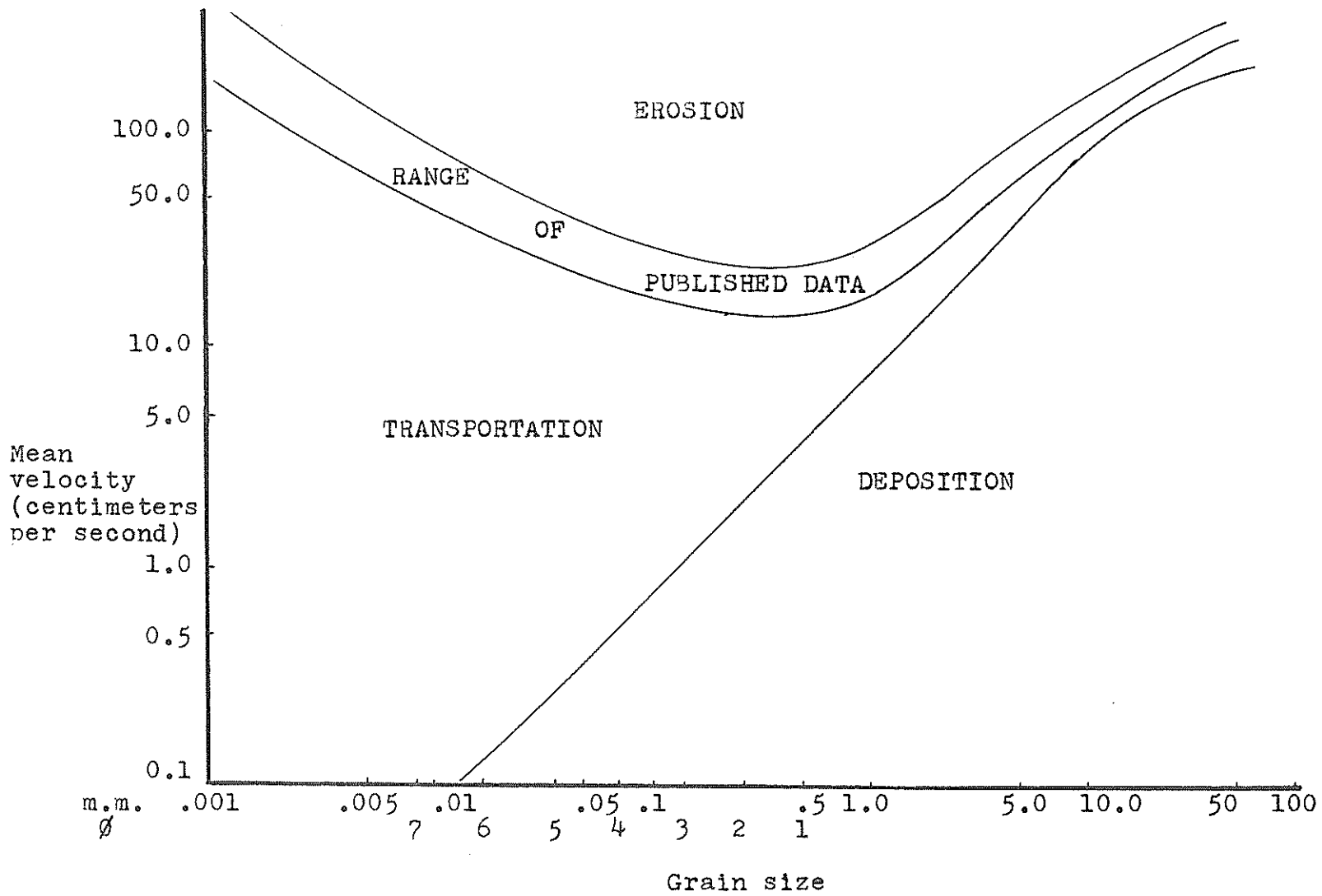

Fig. 8. Hjulstrom's curve showing critical velocities for erosion and deposition.

orthogonals to the wave front remains constant, if there are no energy losses due to friction or reflection. In Figure 9, wave refraction over a submarine low is shown; the wave energy originally concentrated along a wave crest of length b_o^* (total energy = $b_o E_o$, since E_o is given in energy per unit length of wave crest) is now diffused along a crest of length b_1 (total energy = $b_1 E_1$). From this, $b_o E_o = b_1 E_1$, thus $E_o > E_1$, in units of energy per unit crest length. Wave power, P_o, is given by $E\,C_G$ where C_G is the celerity of the wave group. Thus,

Eq. 8 $\quad P_o b_o = E_o b_o C_{Go} = P_1 b_1 = E_1 b_1 C_G$

again neglecting reflection and friction losses. As a wave propagates from deep water into shallow water, group velocity changes according to

Eq. 9 $\quad C_G = nC$

where $n = \frac{1}{2}\left(1 + \frac{2\,\frac{2\pi}{L}\,H}{\sinh 2\,\frac{2\pi}{L}\,h}\right)$

thus $P_o = E_o b_o C_o n_o$, and $P_1 = E_1 b_1 C_1 n_1$. Taking the ratios of these equations,

Eq. 10 $$\frac{E_1}{E_o} = \frac{b_o}{b_1}\,\frac{n_o C_o}{n_1 C_1}\,\frac{P_1 b_1}{P_o b_o}$$

Thus the energy E_1 at any given depth can be obtained in terms of the energy at deepwater conditions, E_o, if

---

*Note: The subscript o usually indicates deepwater wave conditions.

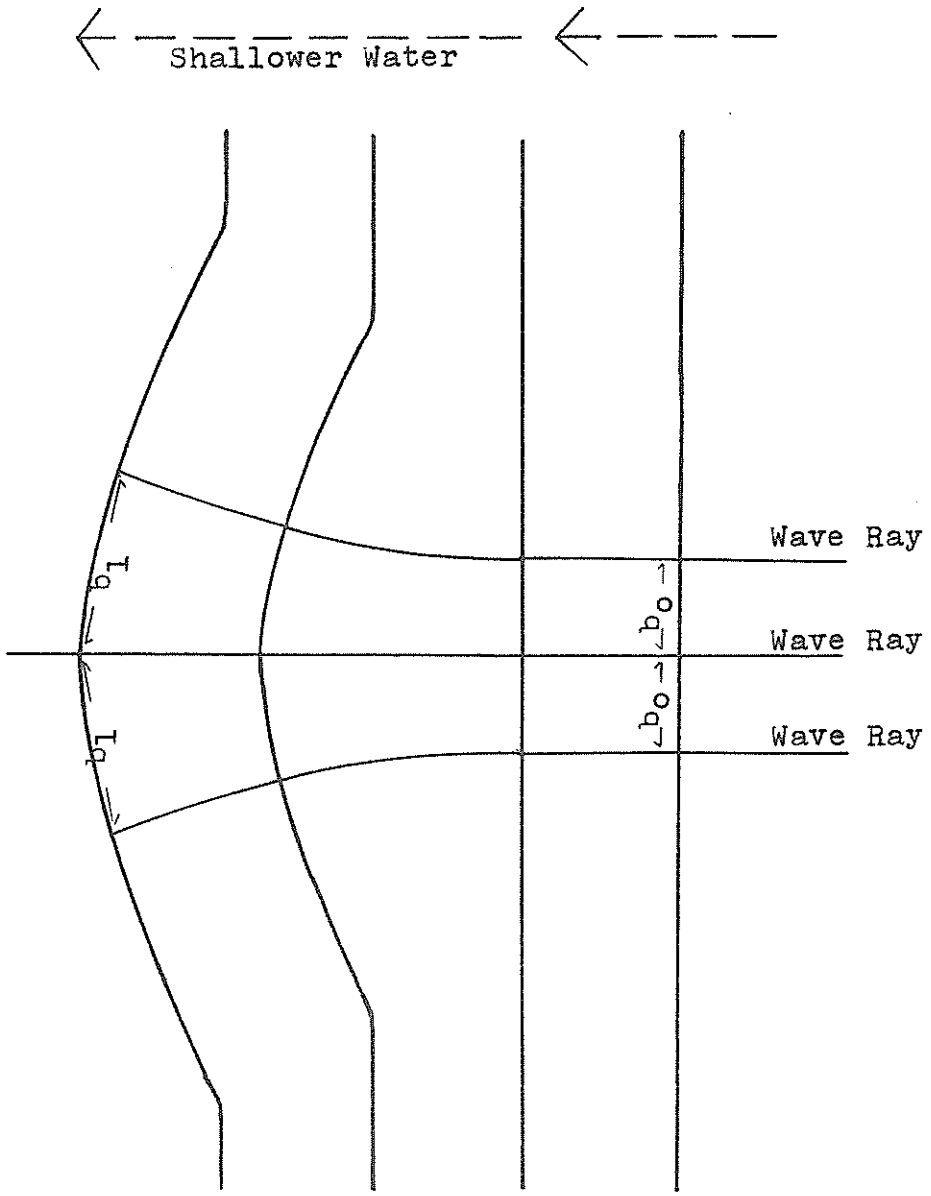

Fig. 9. Wave refraction over a submarine low.

b_o/b, n_oC_o/nC, and Pb/P_ob_o can be found.

The first of these factors, known as the refraction coefficient, k_r, can be calculated easily after refraction diagrams for a given wave have been drawn. The second, known as the shoaling coefficient, k_s, can be computing using Equations 9 and 11.

Eq. 11 $$C = C_o \tanh \frac{2\pi}{L} h.$$

The last factor is the friction-percolation coefficient k_{fp}; this factor is often ignored, as the value of the coefficient is a function of several empirical factors. For this study, energy losses due to percolation will be ignored, while those losses due to bottom friction can be picked from the graph in Figure 10.

Assume that the frictional energy losses of a wave moving into shallow water from depth h_2 to depth h_1 ($h_1<h_2$) can be related to the erosion of bottom sediments.

Eq. 12 $$E_1 = E_2 \frac{b_2}{b_1} \frac{n_2C_2}{n_1C_1} \frac{P_1b_1}{P_2b_2}$$

gives the wave energy per unit crest length at the shallow depth; if the frictional losses were zero, then the shallow depth energy would be:

Eq. 13 $$E_1^1 = E_2 \frac{b_2}{b_1} \frac{n_2C_2}{n_1C_1}$$

thus, the total energy dissipated between depths h_1 and

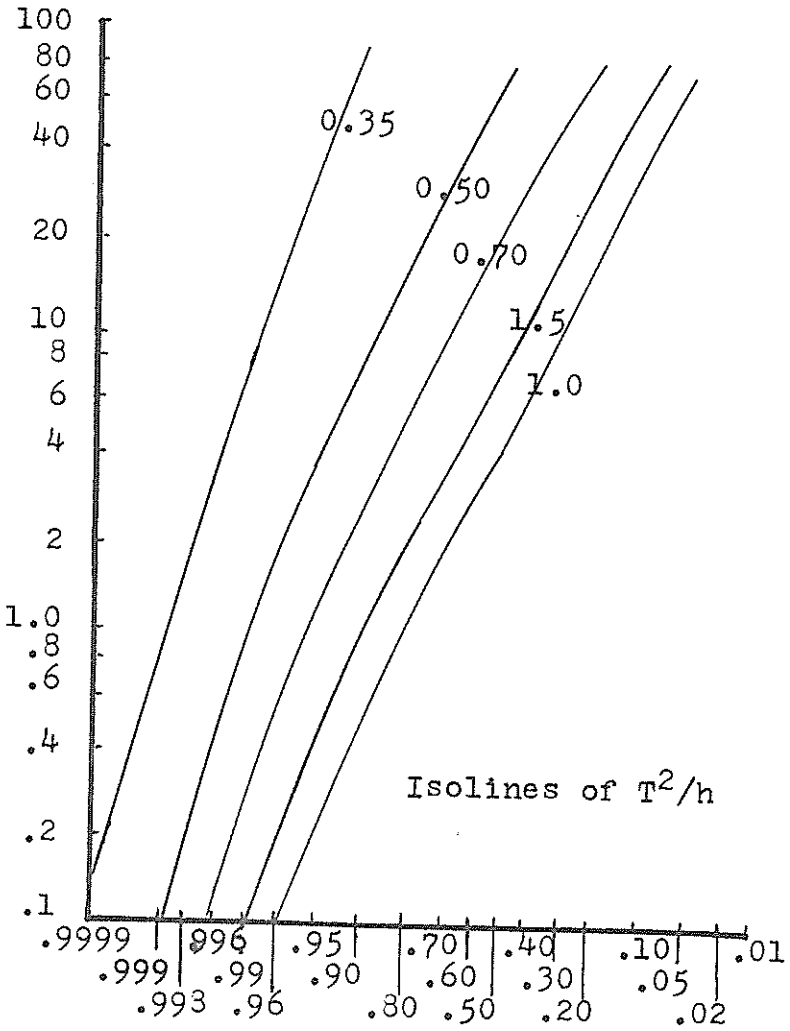

$\frac{fH_1\Delta x}{h^2}$

f = friction factor

Δ x = distance perpendicular to wave approach direction having a constant depth equal to h.

Fig. 10. Wave energy reduction factor k_f versus $\frac{fH_1\Delta x}{h^2}$. (from Ippen, 1966, page 169, figure 3.20).

h_1 is given by $\triangle E = E_1 - E_1^1$,

Eq. 14 $$E = E_2 \frac{b_2}{b_1} \frac{n_2 C_2}{n_1 C_1} - E_2 \frac{b_2}{b_1} \frac{n_2 C_2}{n_1 C_1} \frac{P_1 b_1}{P_2 b_2}$$

It is assumed here that $\triangle E$ is the energy available for sediment erosion and transportation.

Method for the calculation of possible sediment transport. Figure 11 shows the orthogonals of a wave propagating shoreward from deep water. Assume that the direction given by length S is the direction of wave movement and thus is the direction of net water and sediment particle transport by the waves. Length A then indicates the net longshore movement of the sediments; length B the net onshore movement. Let length B equal one-half the distance between the depth contours h_2 and h_3, or $(L_3-L_2)/2$. As some unit volume of sediment is moved a net distance S by waves, it moves a distance B onshore, and, since the bottom is not of constant depth ($h_3 > h_2 > h_1$) the sediment moves upward relative to sea level. For the average sedimentary particle found between the depth contours h_3 and h_2, the gain in elevation caused by a net movement equal to S is $h_2-h_3/2$.

If this unit volume of sediment weighs, for instance, one pound, then the net movement of S will result in a gain of potential energy by the sediment equal to

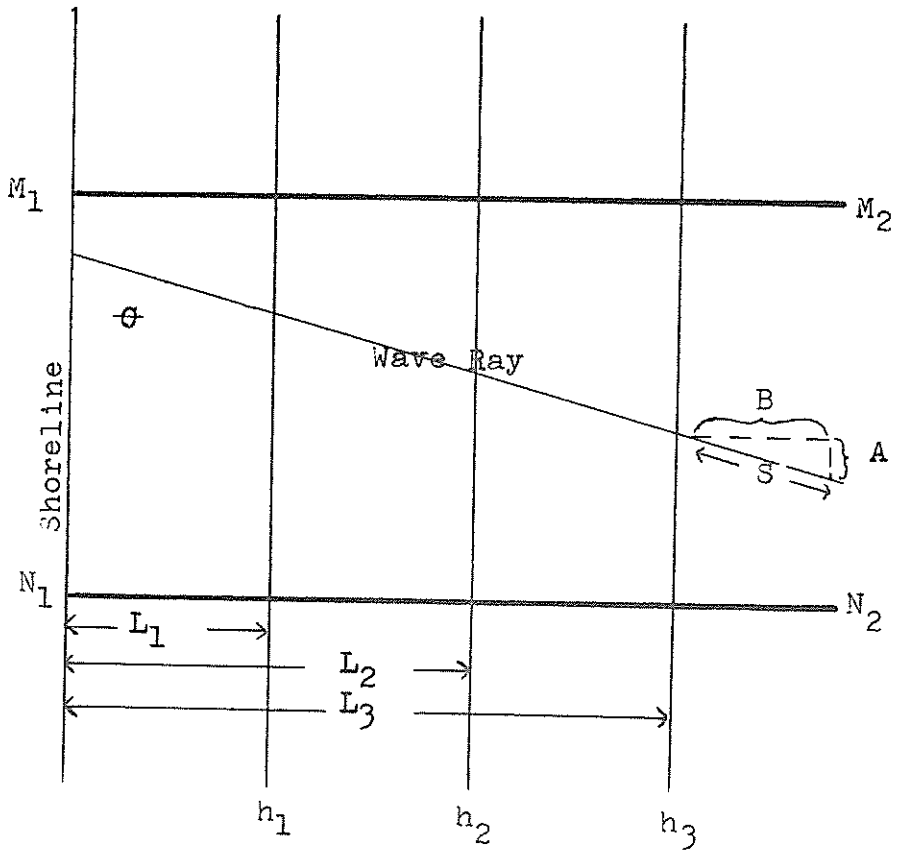

Fig. 11. Diagram showing a wave approaching shore.

$(h_2-h_3)/2$ ft.-lbs.* Let the lines N_1-N_2 and M_1-M_2, the shoreline and line N_2-M_2 define the region of interest in a particular problem. To find the amount of sediment which can be eroded from this area by wave action, look first at the sediment found between the h_1 depth contour and the shoreline. The average unit weight of sediment in that area gains $h_1/2$ ft.-lbs. of energy for every length C that the sediment moves in the direction of wave propagation. This net movement also results in a longshore movement equal to that given by length A. When the sediment has moved from the depth h_1 to the shoreline, it can no longer move in the onshore direction; it can, however, move in the longshore direction. For every $h_1/2$ ft.-lbs. of wave energy dissipated in frictional contact with the bottom, it might be said that one unit weight of sediment moves a distance A in the longshore direction. The average distance the sediment must move in order to be transported out of the area of interest is $\frac{1}{2}$ the distance between the lines N_1-N_2 and M_1-M_2, thus the ratio:

---

*Note: Remembering, however, the buoyant affect of water, the unit weight (one pound) of sediment will actually be a mass of sediment so that $(\rho_s - \rho_w)\, g$ = one pound, where ρ_s = density of the sediment and ρ_w = density of sea water.

$$\text{Distance} \quad \frac{A}{\frac{(N_1-N_2) - (M_1-M_2)}{2}}$$

enables one to calculate the total energy necessary to move the unit weight of sediment out of the area of interest.

The relationship between the amount of wave energy dissipated in frictional contact with the bottom and the amount of sediment which can be eroded and transported by the waves is unknown. It will be assumed here that the relationship is linear; that is, that one hundred percent of this dissipated wave energy is spent in sediment erosion. This is, of course, not true; energy is lost as heat due to internal turbulence, wind friction at the free water surface, and so on. However, the erosion predicted by a direct comparison of the energy dissipated in friction (ΔE) with that energy necessary for sediment erosion can be compared with measured erosion rates for the Brazos River delta in an attempt to calibrate the relationship. This calibration provides an idea of the actual percentage of dissipated wave energy which tends to cause sediment erosion and dissipation.

To find the amount of sediment which can be transported from the area and between the depths h_1 and h_2 or

h_2 and h_3, assume that the shallower depth contour is a barrier, shoreward of which the sediment cannot move, much as if it were a shoreline; thus the analysis is the same as that just discussed.

Velocity of the longshore current. In this portion of the nearshore circulation system it is also necessary to determine the sediment sizes which can be eroded. Even though there are waves inside the initial breaker zone, the oscillatory action of the waves on the bottom is not the agent responsible for particle erosion and transport. Rather, there is usually a type of flow which approximates a unidirectional steady current. Comparison of the mean velocity of this current with the critical erosion velocity (Fig. 8) will give the grain sizes which the current is capable of eroding and transporting.

There are several methods of computing the velocity of the longshore current which are discussed in Ippen (1966), Shepard (1963), King (1959) and Zenkovich (1967). Galvin (1967) presents an analysis of these methods and the data upon which they are based, and concludes that the best approximation of longshore current velocity is given by:

Eq. 14 $$V = \left[\frac{1}{(433.2\ (\text{bottom slope})\ (H_b)\ (\cos \theta_b)}\right]^2 + \left[\frac{1}{2.28g\ H_b \sin \theta_b}\right]^{\frac{1}{2}} - \frac{1}{(216.6)\ (\text{bottom slope})\ (H_b)\ (\cos \theta_b)}$$

where H_b = the height of the wave at breaking

θ_b = the angle that the breaking wave makes with the shoreline

g = the gravitational constant.

This equation relies on empirical correlation for the vague factors such as "amount of energy dissipated in breaking", and so on, which are usually found in theoretical equations but which cannot be measured precisely.

The velocity of the longshore current in the study area was calculated for several widely divergent values of slope, H_b and θ_b, and varied only between 114 and 128 centimeters per second. Comparison of this velocity to Figure 8 shows that nearly all sediment sizes can be eroded and transported by these velocities.

Erosion of sediments inside the breaker zone. Sediment erosion and transportation onshore of the wave breaking zone might also be estimated by a comparison of available energy with that necessary for sediment movement. In this zone, however, there is an added complication of energy dissipation by wave breaking.

Figure 12 shows that the energy of a wave immediately prior to breaking can be calculated in terms of the deep water wave energy and the shoaling, refraction, and friction-percolation coefficients. Not all of this energy, however, is propagated toward shore. As the wave breaks some of the potential energy of the wave is converted into kinetic energy, and some is lost as heat. The manner in which the wave breaks (plunging, surging or spilling) influences the amount of energy which is dissipated in breaking, but no quantitative relationships have yet been established. Unfortunately, there is no known certain way to calculate the amount of remnant energy which moves onshore.

If some arbitrary portion of the energy of the wave at breaking is assumed to be dissipated in the breaking process, then the remnant energy (that which propagates shoreward from the breaking zone) can be calculated, as can the amount of sediment which can be eroded by the friction dissipating process between the breaking zone and the shoreline. The correlation factor found for the energy dissipation-sediment erosion relationship in the offshore zone can then be applied in this near-shore zone. Then, the erosion rates measured in the Brazos River delta area can be compared to the predicted erosion

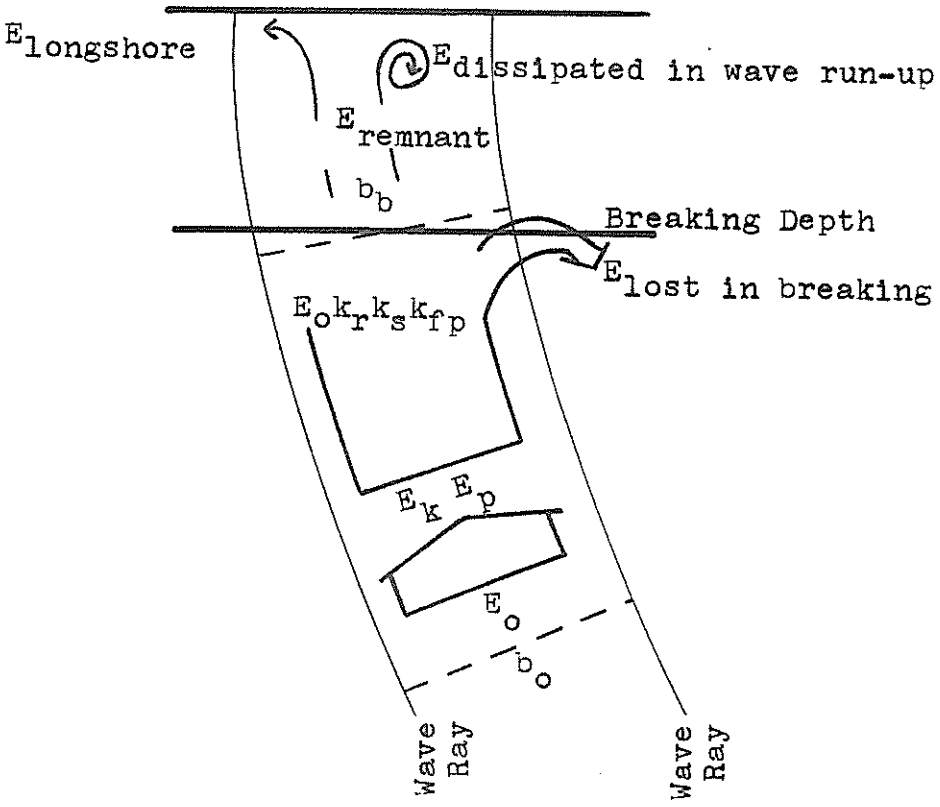

Fig. 12. Diagram showing wave energy at various depths.

rates in an attempt to correlate the assumed energy loss in breaking with the actual energy losses. Obviously, the precision of this correlation depends on that of the former correlation factor.

Sediment Load of the Delta Building River

River-transported sediments may move either in the suspended load or the bedload. If suspended, the weight of the particle is counterbalanced by turbulent velocity gradients and the attendant pressure gradients. In the bedload, the sediments roll and saltate along the channel bed, and the bed supports the particle weight.

The United States Geological Survey maintains gauging stations on major streams which make measurements for the purpose of calculating the stream discharge and suspended sediment load. The stations rarely measure bedload transport rate, because no reliable measurement techniques are yet known. In Texas, stream gauging stations are operated by the Texas Water Development Board. This agency has compiled monthly discharge and suspended load data for every Texas River. The length of these records varies from station to station.

Measurements of Stream Discharge

Non-soluble and non-colloidal sedimentary materials

in natural streams and rivers begin to move whenever a certain critical flow velocity or shear stress is exceeded. Once motion is initiated, these materials are subject to two main modes of transport. The sediments are called suspended load sediments if, during their motion, they are completely surrounded by fluid at all times, or bedload sediments, if they roll, slide or saltate over the bottom. There is no universal dividing line in size between sediments which will be transported in the bedload and those transported in the suspended load, as slight variations in the hydraulic conditions of a stream may cause the suspension of certain bedload sizes, or the precipitation of certain suspended load sizes. The equations that predict the downstream movement, the dispersion, and thus the discharge of the two load types have completely different physical bases, and will be discussed later.

When it becomes necessary to compute the sediment discharge, the empirical and theoretical mathematical formulas are useless without knowing the size ranges present in the sediment, the relative percentages of the load carried as bedload, or suspended load, etc. Direct measurements of the total discharge can only rarely be made. In order to get an accurate measure of stream dis-

charge, it is necessary to take bedload and suspended load discharge samples, and using the predicted sediment concentration distributions, calculate the sediment discharge over the entire cross sectional area of the stream.

Suspended Load Discharge

Factors affecting suspended load concentration. The effect of turbulence on a sedimentary particle is analogous to the effects of diffusion processes on a molecule. In a fluid which moves particles at a velocity v, the concentration of a particular molecule or of a sediment size is given by:

Eq. 15 $$\frac{\partial C_r}{\partial t} = -v \nabla C_r + \epsilon_t \nabla^2 C_r$$

where ϵ_t = the coefficient of turbulent diffusion

C_r = concentration

t = time

v = flow velocity.

That is to say, the change of the concentration C_r of sediment at a given point in a 3 dimensional reference system with respect to time, is equal to the sum of the changes caused by the convective motion, $v \nabla C_r$ and the change due to turbulent diffusion. For a turbulent flow

field, v will have different values in different directions, as will t. Experiments have shown that the equation 15 will give valid predictions of $\frac{\partial C_r}{\partial t}$ for sedimentary particles. Combining this equation with the logarithmic velocity profile expected in open channel flow, the concentration at any distance; from the bottom in a channel of total depth D can be found by:

Eq. 16 $$\frac{C_r}{C_{ra}} = \left(\frac{D-j}{j}\,\frac{a}{D-a}\right)^{Z_k}$$

where C_{ra} = the concentration at a standard depth a from the bottom

$Z_k = \frac{\text{settling velocity}}{.4\ U_*}$, a constant for a particular situation.

The concentration as a function of depth and Z_k according to equation 16 is given in Figure 13 as a graph of j-a/D-a versus C_r/C_{ra} (Vanoni, 1946). The coarser the sediment fraction under consideration, the greater the variation in concentration with depth; that is, with high Z_k, the concentration is much greater close to the bed (low values of j) than near the free surface (high values of j). As the magnitude of Z_k decreases, C_r becomes closer in value to C_{ra} throughout the stream depth, so that very small particles have a nearly constant concentration distribution (Task Commit-

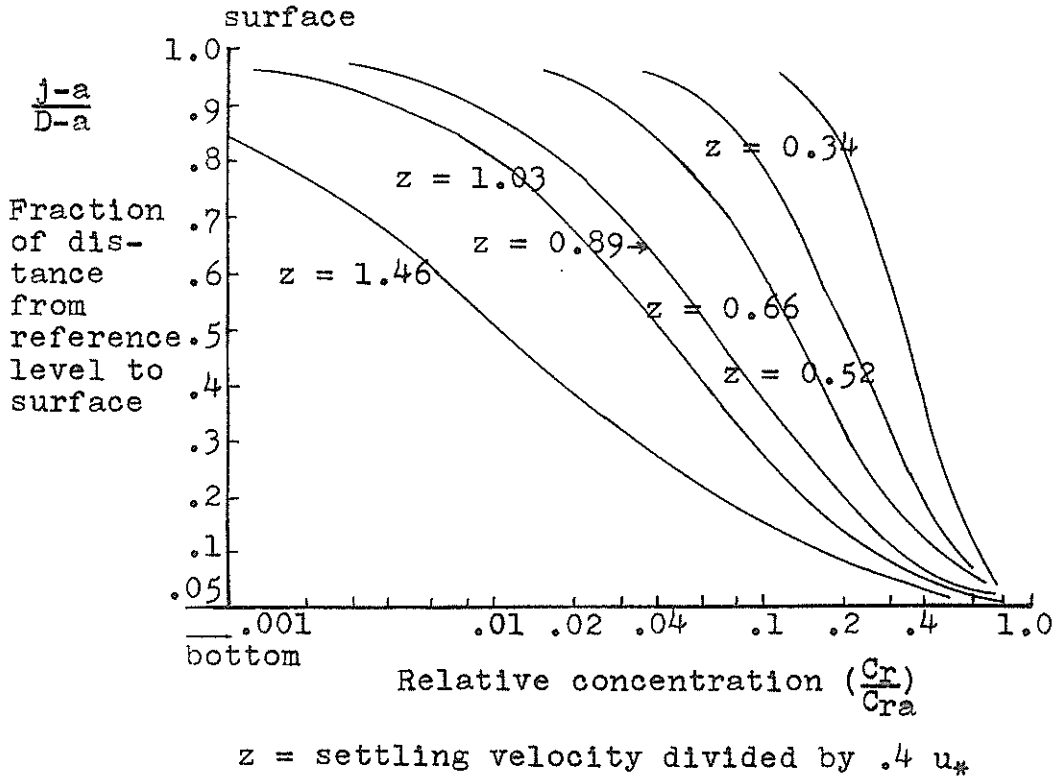

Fig. 13. Vertical distribution of suspended sediment in a river. (after Vanoni, 1946).

tee, 1969, p. 1478).

The variation in C_r with U_* makes the choice of the position (both in the cross section and long section of the stream) of the point of measurement of C_{ra} very important (Task Committee, 1969, p. 1430).

The concentration at $j = 0$ should be infinite, according to equation 16, but this equation is based on the particle being completely surrounded by the fluid, and thus does not apply at $j = 0$.

The total suspended load discharge, g_{ss}, should be equal to:

$$\int_{j=0}^{j=z} C_r u \, dj$$

for a vertical section. Einstein has shown that by combining the equation for C_r/C_{ra} with that for g_{ss}, an equation is derived which gives the suspended load rate per unit time and width of vertical channel section for a given size fraction (Graf, p. 191).

Eq. 17 $$g_{ss} = \int_{j=0}^{j=D} f\left(C_{ra}, \left[\frac{D-j}{j}\ \frac{a}{D-a}\right]^{Z_k}\right)$$

Suspended load measuring devices. There are essentially three types of sampling mechanisms which can be used to sample suspended load: 1) the instantaneous sampler, 2) the integrating sampler, and 3) the continuously recording sampler (Graf, 1971).

The instantaneous sampler is an open container which can be lowered and oriented with the flow direction so that water flows through the sampler. A messenger causes both ends to close, capturing only the water and sediment flowing at a known depth and a particular instant in time.

The integrating samplers are of two types. The point integrating sampler is in essence a bottle which is lowered into position and opened; it fills slowly and thus will contain the water sediment mixture which flowed past the sampling point for an extended time period giving a sediment concentration averaged over that time period. The depth integrating sampler is an open bottle which is lowered into the flow and withdrawn, resulting in a concentration averaged over a given depth range. Both the instantaneous and integrating type samplers give sample which must be taken to a laboratory for additional processing to determine the sediment concentration.

Continuously recording samplers work by measuring the difference in the properties of clear water and those of water containing suspended sediment, in which the attenuation of light, sound, and x-rays are measured. An illuminator or transducer is used in conjunction with

a pumping apparatus which draws off a continuous sample. These samplers give a direct measurement of sediment concentration in parts per million, or like units, without further lab work (Graf, 1971).

Once the samples are taken, they must be correlated to give a concentration distribution for the entire stream cross section. If single samples are taken in a vertical section, these sample concentrations are then taken as C_{ra}, and the C_r throughout the rest of the vertical section height, from j near zero to j = D, is calculated for every size range present, because each size range will have a different exponent Z_k. Variations in average velocity and in turbulence across the width of a stream require measurement of several vertical sections at one position in the stream; this can be done by lowering instantaneous or time integrated samplers. Then the total suspended load discharge is:

Eq. 13 $$G_{ss} = \sum_{\text{width}} g_{ss}$$

for every size range present.

Bedload Discharge

Factors affecting bedload discharge. The bedload sediments are all materials which move in more or less constant contact with each other and with the bed. Since

the velocity at the bed is essentially zero and increases rapidly upward to the water-bedload "interface", the bedload sediments may experience large velocity and pressure heads gradients. These gradients would act to lessen the magnitude of $\tau_{o\ crit}$ (critical bed shear) necessary for movement initiation. Assuming that the bedload discharge rate is related to τ_o, and approximating this relationship by a power function so that:

Eq. 19 $$q_s = K_1 + K_2 \tau_o + K_3 \tau_o^2 + \ldots$$

where τ_o = shear stress at bed

q_s = sediment discharge

then if $\tau_o = 0$ at some layer within the bedload, q_s must also equal zero, and so must K_1. If $\tau_o = \tau_{o\ crit}$, q_s is still zero, for τ_o must be greater than $\tau_{o\ crit}$ for motion. Thus,

$$K_2 \tau_{o\ crit} = K_3 (\tau_{o\ crit})^2$$

$$K_2 = -K_3 \tau_{o\ crit}.$$

For sand-sized particles, τ_o is a low value, and the higher order terms of the series can be ignored. Thus,

Eq. 20 $$q_s = K_3 \tau_o (\tau_o - \tau_{o\ crit})$$

This is a duBoys equation for bedload movement using a critical shear stress criterion (Graf, 1971). The discharge of bed material depends on the differences between the tractive stress set up by the stream and the

tractive force necessary to initiate motion. The shear stress however, in an open channel, is rarely, if ever, uniformly distributed over the wetted perimeter, and distribution appears to be dependent upon the slope of the channel walls, the ratio of channel width and depth, and the overall shape of the channel.

Existing samplers and sampling schemes for the measurement of bedload discharge of a stream are innaccurate and difficult to use; as a result, knowledge of the bedload discharge of a stream is based on empirical estimates. There is doubt as to which empirical method is most reliable, even though some methods require much more precise data for their application, and thereby may be assumed to be more accurate. One of the simplest and most accurate methods is given by Colby (1957). Using data from selected natural streams and from flumes, he found the relationships between stream velocity and sediment load shown in Figures 14 and 15. These figures give the concentrations of suspended sediment and the bedload discharge expected for a given stream velocity. The geology of the stream valley determines to a certain extent the amount of sedimentary particles available for transport. Therefore, not all streams will have the values of sediment discharge given by Figures 14 and 15.

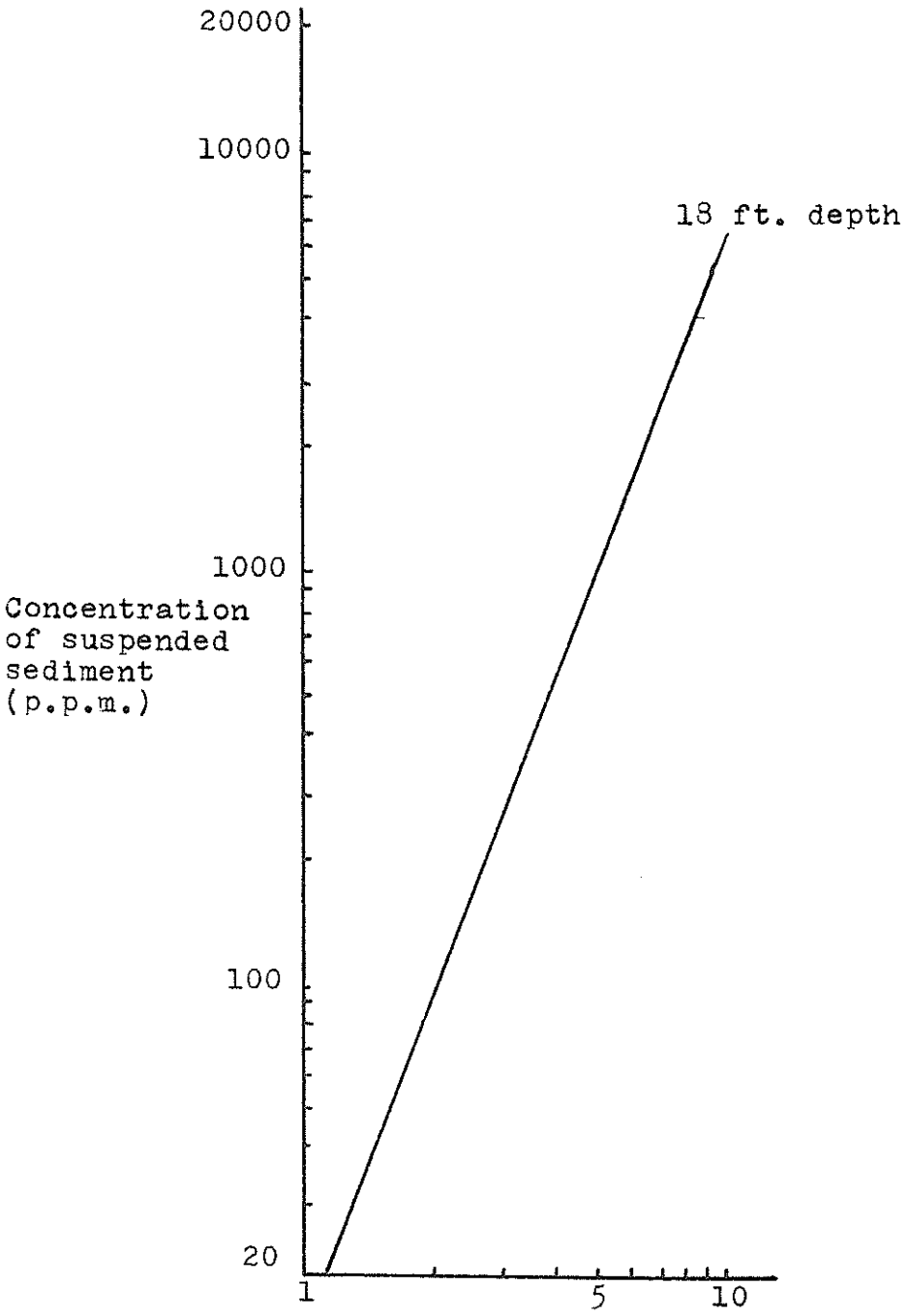

Fig. 14. Suspended sediment concentration vs. stream velocity for natural streams. (from Colby, 1957, figure 7).

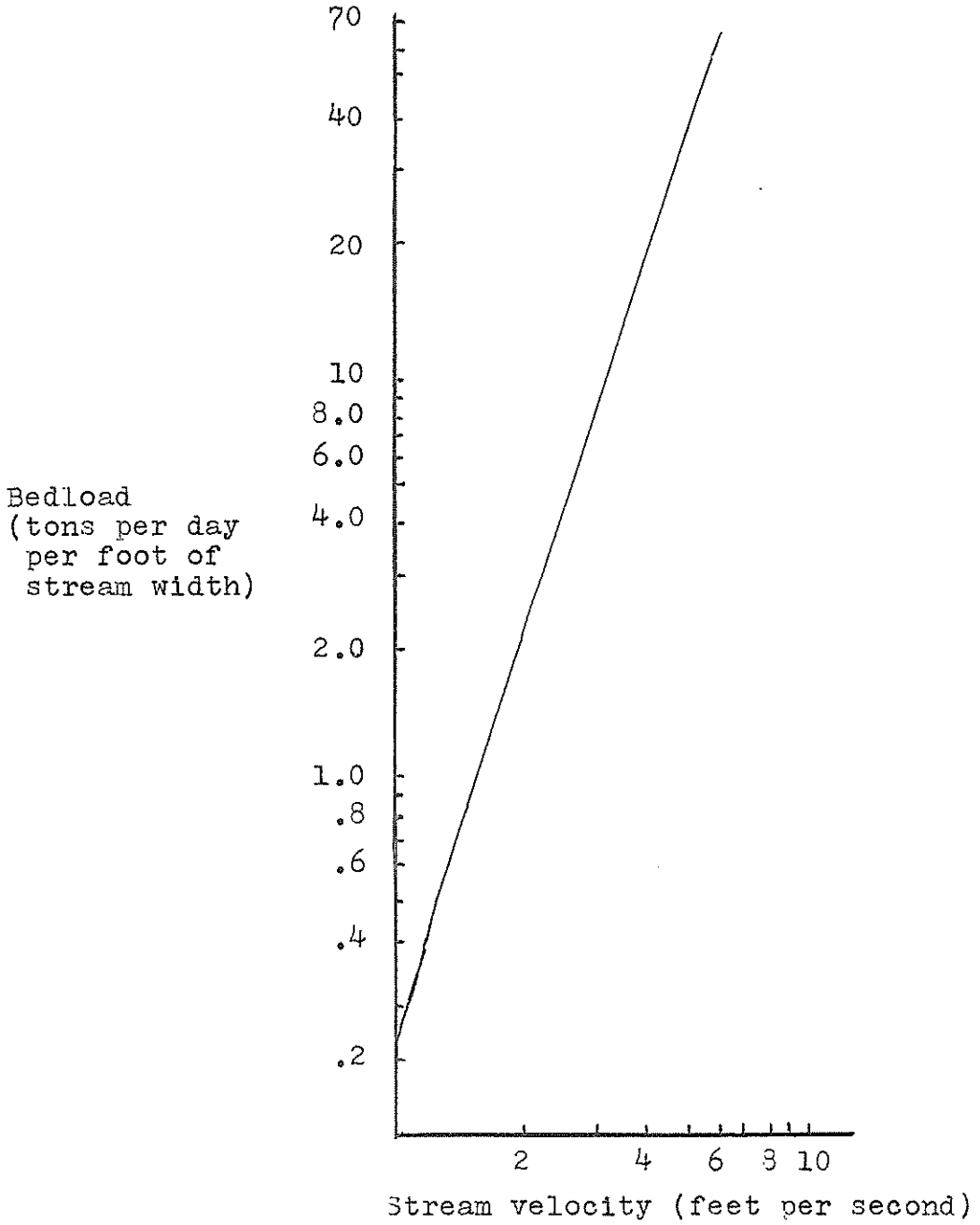

Fig. 15. Bedload vs. stream velocity for natural streams. (from Colby, 1957, figure 5).

Colby uses the ratio of the estimated suspend load concentration to the predicted suspended load concentration to arrive at a correction factor (Fig. 16). When this correction factor is applied to the predicted bedload, a corrected and supposedly more accurate value of bedload discharge is obtained.

A more convenient method for calculating bedload discharge in most cases involves a relationship between river discharge and bedload transport, because discharge is the most commonly measured river characteristic. A few such equations exist and have been applied to particular rivers (Graf, 1971), but the equations were developed using empirical data from tests involving primarily coarse (granules, etc.) bed materials, and should not be applied indiscriminately to sand bed rivers.

Regardless of the method used to calculate stream bedload, the results are usually subject to dispute. Several of the empirical correlations of stream flow characteristics with bedload discharge discussed by the Task Committee (1971) were evaluated by the author in collaboration with W. N. Seelig of Texas A&M University, and the results were found to vary by amounts ranging from 100% to 1000%. Most discouraging was the fact that in every correlation tested, the increase of bedload

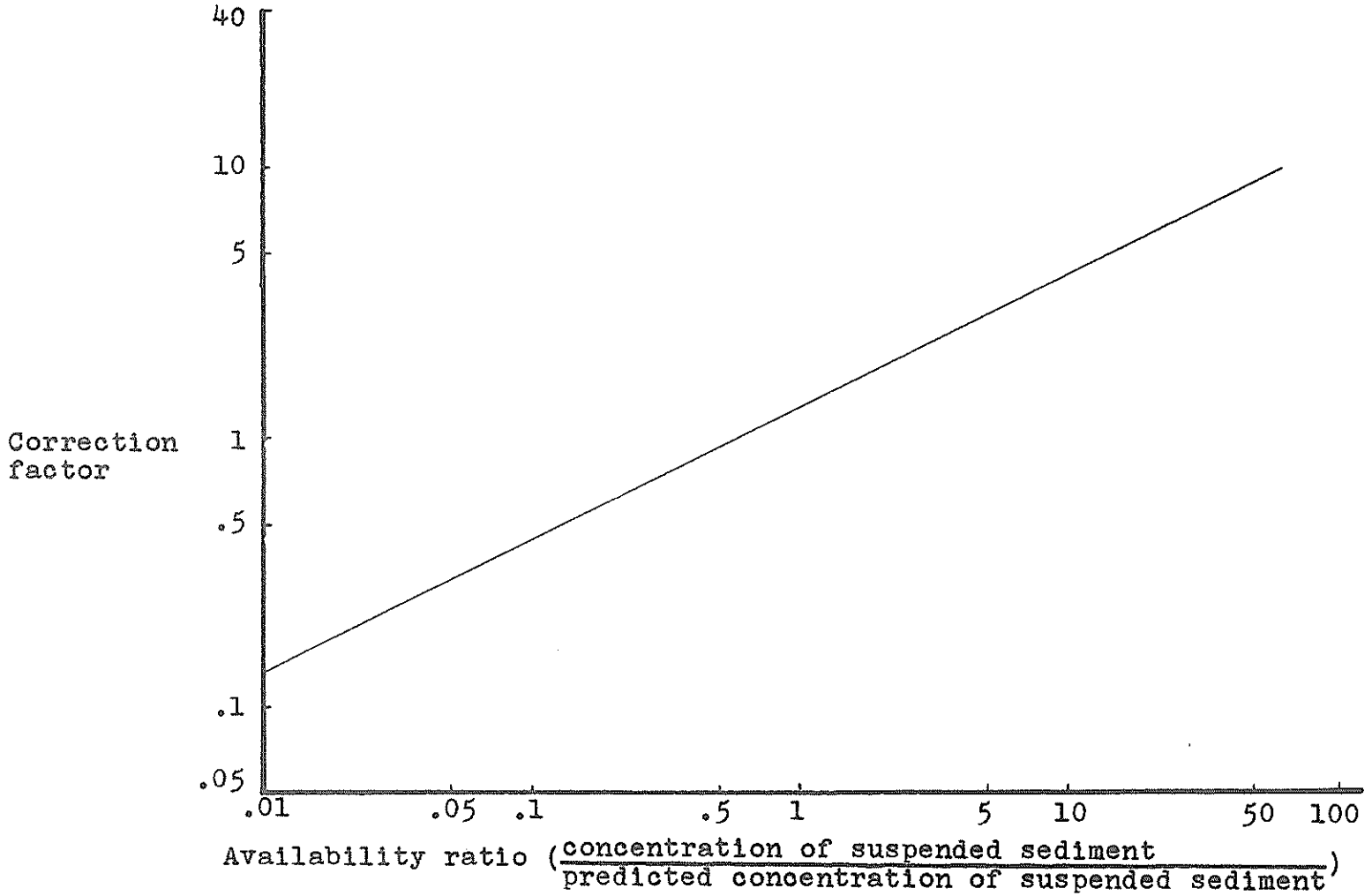

Fig. 16. Correction factor for calculating bedload vs. availability ratio for natural streams. (from Colby, 1957, figure 8).

transport with increasing flow velocity or increasing discharge was exponential rather than linear. Measurements recorded at most gaging stations give, at best, a daily average of stream flow; there is no way of estimating the frequency or periodicity of intervals of high velocity or discharge, or the bedload discharge during those periods. It seems that until some reliable measurement techniques have been developed, the best estimates of bedload discharge that can be obtained are minimum values based on daily, weekly, or monthly stream flow averages. Seelig (1973) has found for example, that in at least one case when instantaneous measurements of stream velocity taken daily for a month are used to compute the bedload discharge for that month, the resulting discharge values agree to within five percent with those obtained by using the monthly velocity average.

Distribution of Sediment Load at the Mouth of the River

When the total sediment load of a river is known, the pattern and rate of deposition of this load at the river mouth must be determined in order to compare the deposition of river sediments to the wave-induced sediment erosion.

Bates (1953) has shown that for a river flowing into

more dense basin waters, the stream does not immediately lose its integrity, rather, it propagates outward with the width at any given distance from shore approximately equal to 3 X until the current is dissipated at:

Eq. 21 $X_m = 2000\ (W)$

where X_m = distance from shore

W = channel width at mouth.

The velocity of the stream flow is given by Figure 17.

Bates states that in most cases the bedload sediments begin to be deposited at a distance from the mouth equal to approximately 4 times the channel width at the mouth. He shows that for most rivers flowing into saline basins the vertical mixing of fresh and salt waters is minimal, with the stream flowing out over the top of the basin waters. If this is generally valid, then it may be assumed that the deposition of suspended sediment is proportional in some way to the decrease in stream turbulence.

As sediment escapes the influence of the river it is not immediately deposited; rather, it probably tends to diffuse away from the mouth as a function of wave-generated turbulence. With these factors in mind, the deposition of the suspended load of a river is approximated in this thesis using steady state diffusion patterns

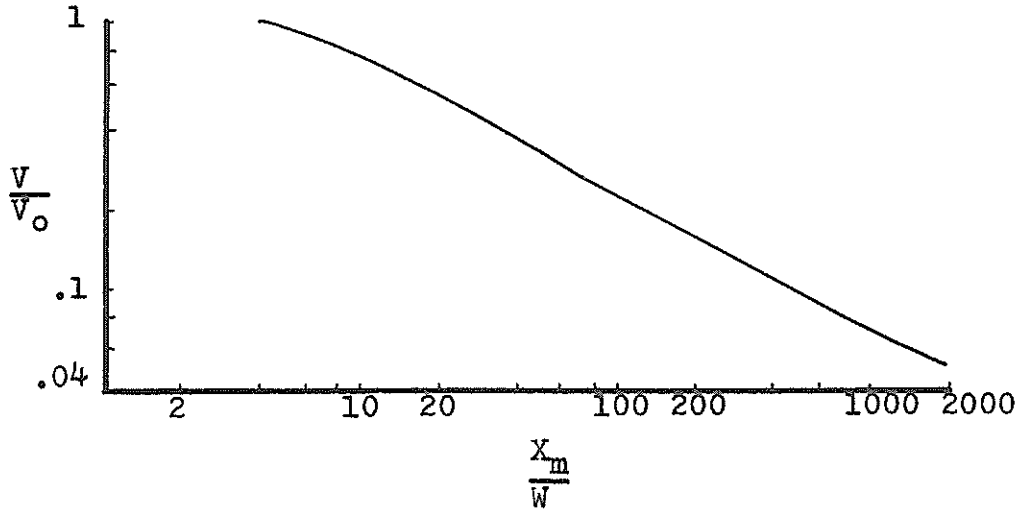

V = stream velocity at any distance from the mouth

V_o = stream velocity at the mouth

X_m = distance from shore

W = channel width at the mouth

Fig. 17. The decrease in stream velocity at increasing distances from the river mouth. (from Bates, 1953, Figure 1).

of sediments diffusing from a succession of point sources having source strengths inversely proportional to their distance from the river mouth. This principle is applied to the Brazos River in a later section.

The diffusion of sediment away from the mouth is given by:

Eq. 22 $$\frac{\partial C_s}{\partial t} = \epsilon_m \nabla^2 C_s$$

where C_s = concentration of suspended sediment

t = time

ϵ_m = diffusion coefficient

and $$\nabla^2 = \frac{\partial^2}{\partial x^2} + \frac{\partial^2}{\partial y^2} + \frac{\partial^2}{\partial z^2}$$

After a certain length of time the diffusion process must approach equilibrium, so that for any given element of volume of basin waters offshore from the river, the concentration must change very little with advancing time. Therefore,

$$\frac{\partial C_s}{\partial t} = 0 \quad \text{and}$$

Eq. 23 $$\nabla^2 C_s = 0$$

To simplify this equation further, assume that the diffusion is essentially <u>two-dimensional</u> as shown in Figure 18. When the river discharges into the basin, the lower specific gravity fresh water will float on the basin water, and the density contrast between the waters will

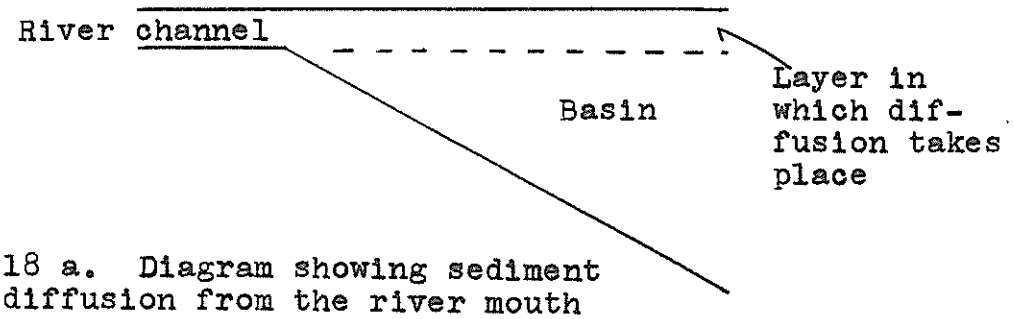

Fig. 18 a. Diagram showing sediment diffusion from the river mouth into the basin in the plane of the water surface and the mixing zone.

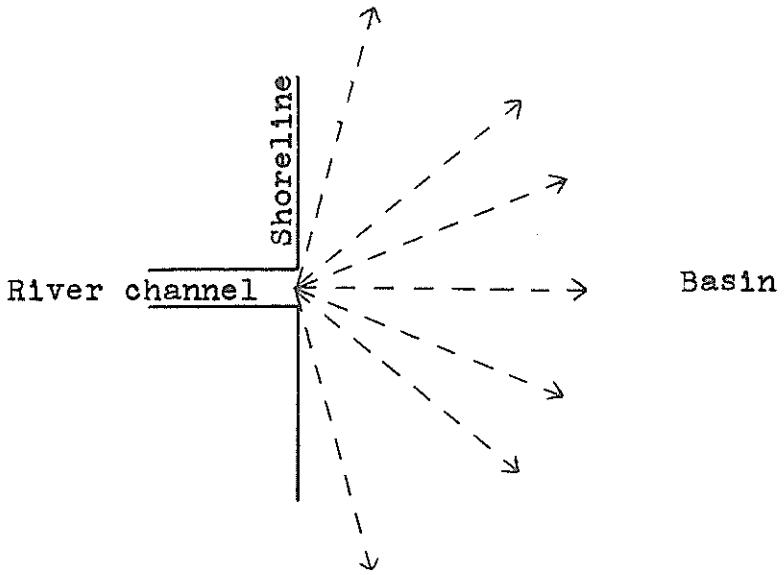

Fig. 18 b. Diagram showing sediment diffusion from the river mouth into the basin in all directions, in the plane of the water surface and mixing zone.

dampen vertical mixing (Bates, 1953). The Laplacian in equation 23 then reduces to:

$$\frac{\partial^2 C_s}{\partial x^2} + \frac{\partial^2 C_s}{\partial y^2}$$

where the x-y plane is the plane of the surface of the basin.

The diffusion pattern resulting from this type of model is shown by Figure 19. The concentration at a particular point in the basin will depend on the distance of that point from the river mouth, and not on the direction of the point from the mouth, assuming no coastal currents. With this in mind, equation 23 reduces to:

Eq. 24 $$\frac{\partial^2 C_s}{\partial R^2} + \frac{1}{R}\frac{\partial C_s}{\partial R} = 0$$

where $R = \sqrt{x^2 + y^2}$, the distance of the point from the origin, (river mouth). Integrating equation 24 twice yields:

Eq. 25 $$C_s = a \ln_R + b$$

where a and b are constants of integration. To solve these constants, the concentration, C_s, must be known at two points. The first point at which the concentration is known is where R is very near zero; here, the concentration will be given by the measurements of the river sediment concentration. There is no other point at which the concentration is known, but obviously the use

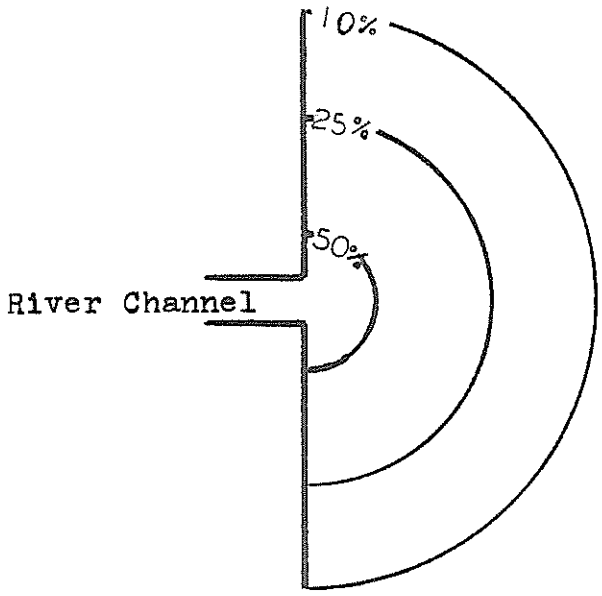

Fig. 19. Diagram showing sediment concentration in basin waters decreasing as a function of distance from the river mouth.

of the model can proceed no further without at least an estimate of concentration at some point. This estimate, however, must be tempered by the knowledge of the relationship of the concentration at some point to the deposition rate at that point. Figure 20 illustrates an example of the steady state concentrations in a basin resulting from diffusion away from a river mouth. The contour lines connect points at which the estimated concentration is 50%, 25%, and 10% of the concentration at the river mouth. If the concentration in the river were such that 100 tons of suspension were discharged from the river in a year, the steady state diffusion pattern shown in Figure 20 might be interpreted as showing that of this 100 tons, 50 tons are deposited yearly within the area defined by the shoreline and the 50% contour line, and that 75 tons are deposited within the area defined by the shoreline and the 25% contour, and so on. If this model is to be applied to an already existing delta for purposes of growth rate prediction, the sedimentation rates at the periphery of the delta should be examined through the use of isopach maps showing delta thickness, so that a concentration at delta periphery can be estimated. That is, if a delta is nearly symmetrical and the influence of the delta extends

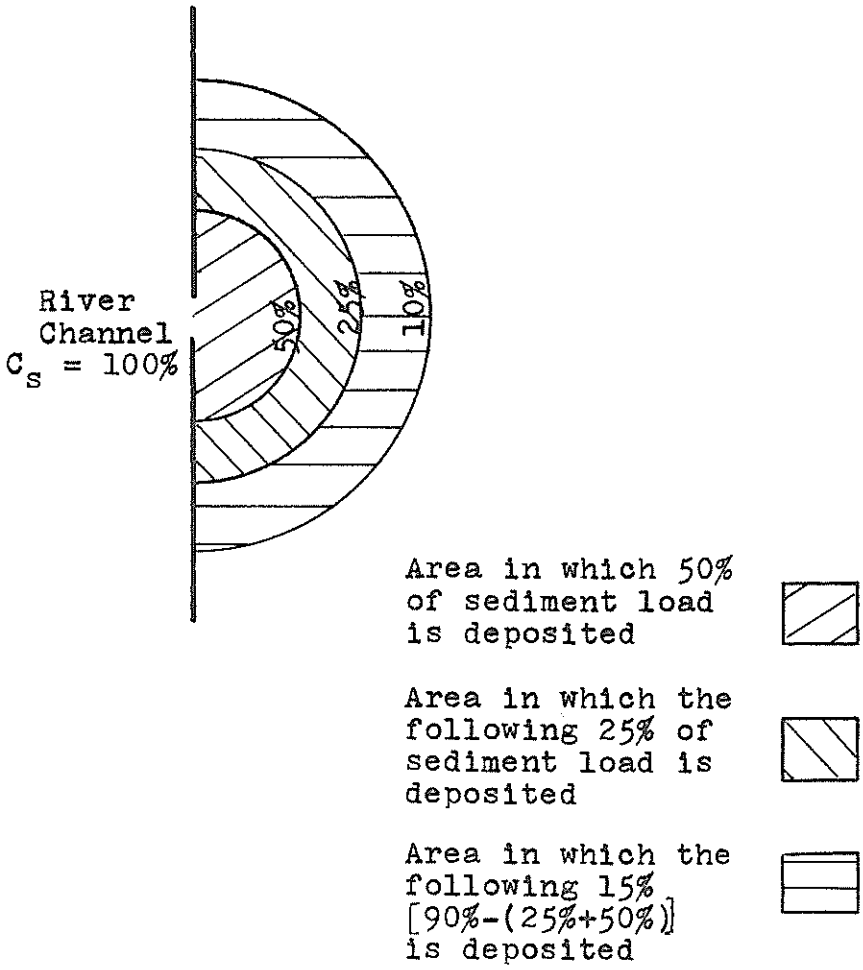

Fig. 20. Diagram showing the relationship between isoconcentration contours and deposition rates.

seaward to a point 5 miles from the river mouth (R = 5), and the deposition rate at that point is some number of pounds of sediment per year, then the approximate concentration at that distance can be determined if the concentration of suspended sediment at the river mouth is known.

If a diffusion model having point sources of decreasing strength with increasing distance from the mouth were desired, equation 25 must be solved for several values of C_s where R is very near zero. The simplest example of the procedure is to model the diffusion from two points. On Figure 17, at a point a distance from the mouth given by $\frac{X_m}{W} = 25$, the velocity of the river is approximately $\frac{1}{2}$ the velocity at the mouth. Assume that a distance from the mouth of $\frac{X_m}{W} = 1000$ is basinward of the delta periphery. It might be assumed that at $\frac{X_m}{W} = 25$, the concentration of the stream is $\frac{1}{2}$ the original value and that it is 1/10 the original value at $\frac{X_m}{W} = 1000$. At least 1/10 of the suspended sediment load is lost to the delta. If the diffusion of $\frac{1}{2}$ the suspended sediment load from the mouth is modeled (solve Equation 24 using $C_s = \frac{1}{2} C_{so}$ for a value of R very near zero), and the diffusion of 4/10 of the suspended load from a point $\frac{X_m}{W} = 25$ from the mouth is modeled, a

pattern similar to that given in Figure 21 results.

Figure 21a shows the diffusion away from the mouth of $\frac{1}{2}$ of the sediment load; the percentages represented by the contour lines are percentages of the <u>total</u> sediment load, not of $\frac{1}{2}$ the load. Figure 21b shows the diffusion of .4 of the sediment load away from the second point, which is a distance $\frac{X_m}{W} = 25$ away from the mouth. Again, the percentages shown are of the total sediment load, rather than of .4 of the sediment load. When these two are plotted together, the distance $\frac{X_m}{W} = 25$ in 21b may be larger than R in Figure 21a, and thus Figure 21c results. When this occurred in modeling the Brazos River delta, the author drew an ellipse with a semi-minor axis given by R and a semi-major axis given by $\frac{X_m}{W} = 25+R_2$ with an averaged interior concentration; this was found to be the simplest and most direct way to average the concentrations between the two source points. The result is shown in Figure 21d.

The stream loses contact with the bed when the stream waters begin to float on the denser basin waters. As a result the bedload would not tend to undergo diffusion away from the mouth as is shown by Figure 21d. The constant wave and longshore current action at the river mouth would tend to make the bedload move away from the

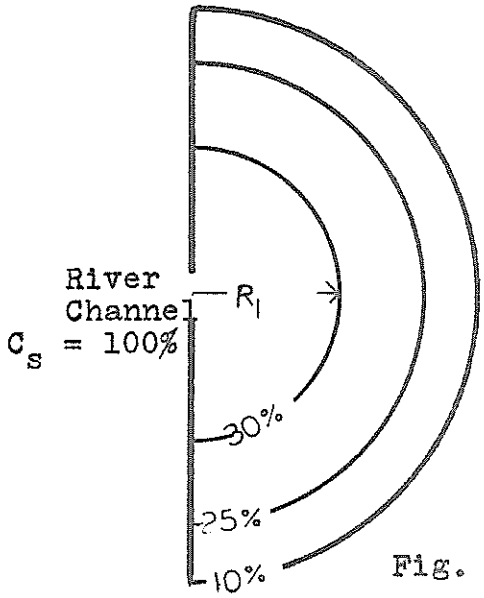

Fig. 21 a. Diagram showing diffusion of 50% of the sediment into the basin from the river mouth.

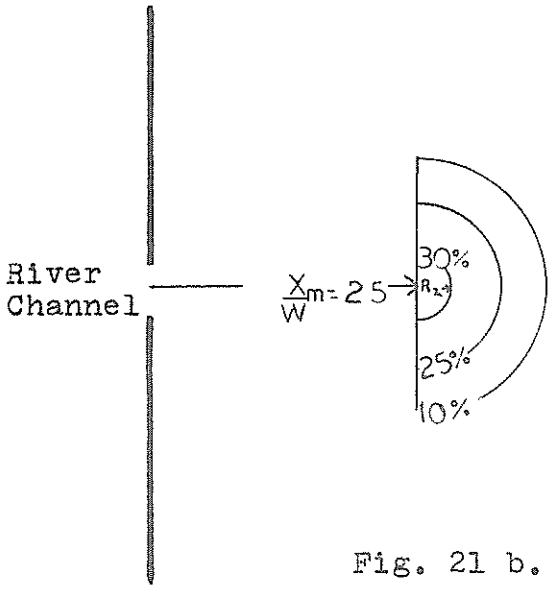

Fig. 21 b. Diagram showing diffusion of 40% of the total sediment from a point $\frac{X_m}{W} = 25$ distant from the mouth.

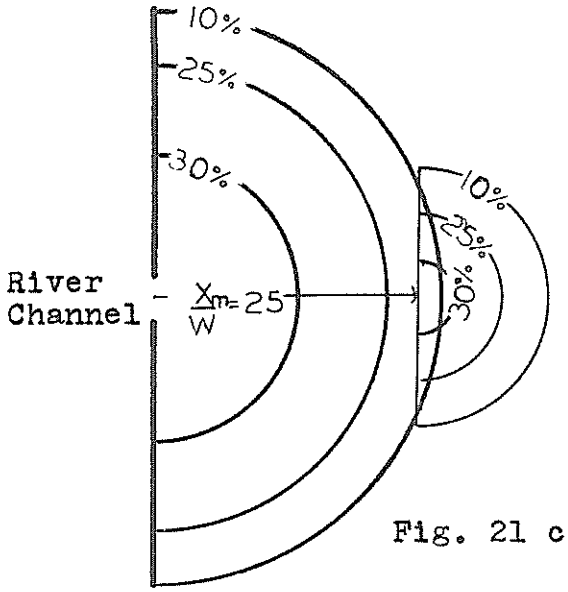

Fig. 21 c. Diagram showing the two prior diffusion patterns superimposed, with 10% of the total sediment escaping.

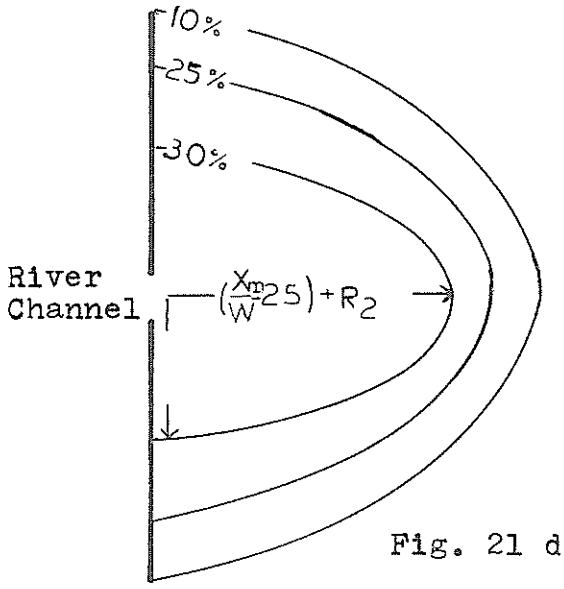

Fig. 21 d. Diagram showing the averaged diffusion pattern obtained from averaging the two patterns shown above.

mouth in a manner similar to diffusing. However, it is assumed that the dispersion of the bedload would be in a spherical pattern, as is shown in Figure 21a.

APPLICATION OF THE DELTA MODEL TO THE NEW BRAZOS RIVER DELTA AREA

The theory and assumptions on which a simplified model of delta development is based have been enumerated to this point. Now this model will be applied to the development of the Brazos River delta. This is done for two reasons: 1) to provide an example of the method of application of the model, and 2) to examine, within the framework of the idealized model, the relationships of delta growth at Freeport with erosion at Sargent Beach.

The available data concerning the wave climate at Freeport and the sediment load of the Brazos River are first presented and discussed, and then the calculations of erosion and deposition are given.

As a basis for comparison with predicted erosion-deposition rates, isopach maps were constructed for the intervals July, 1930 to July, 1931; July, 1931 to June, 1932; June, 1932 to October, 1934; October, 1934 to August, 1937; and August, 1937 to May of 1973. There are no reliable maps of the area for the years immediately preceding the diversion of the river, so that it was impossible to draw an isopach for the first year of delta development.

The 1973 chart was constructed on the basis of field

work by the author and W. N. Seelig of Texas A&M University during April and May of 1973. This work was done with the assistance of the Oceanography and Civil Engineering Departments of Texas A&M University, both of which provided a ship with continuous depth recorders for various phases of the work.

All other figures are based on work done by the United States Coast and Geodetic Survey as reported in USCGS Chart No. 1283 (January, 1931, December, 1931, March, 1933, October, 1934, May, 1940) and in Nienaber (1963). Editions of USCGS Chart No. 1283 are available for dates after May, 1940, but the data on these maps for the area near the new Brazos River delta were measured in 1937.

Sediments of the New Brazos River Delta

Offshore Sediments

The sediments offshore from a 25 mile-wide-strip of shoreline around the old and new Brazos River Deltas were studied by Nienaber (1963). His is the only major sedimentological work in the area. Nienaber's study included grain size, heavy mineral and clay mineral analyses for samples on 5 traverses which extended from the surf zone to the 100 foot isobath. Sediments at depths

greater than 60 feet reflect the presence of a topographic high--a relict feature of unknown origin--rather than the influence of the Brazos, and will not be discussed.

The sediments from the shoreline to the 60-foot isobath show a decrease in mean grain size with increasing distance from shore. The mean grain size ranges from 4 to 10 ϕ, where ϕ is an expression of grain size equal to the negative logarithm, to the base two, of the grain size in millimeters ($\phi = -\log_2 d_{mm}$). The mean grain size trend is shown in Figure 22. Figure 23 shows the standard deviation of the diameters of these sediments. The most noticeable characteristic of the two maps is the similarity of trends; the coarser sediments are the better sorted, while the finer ones are poorly sorted. The nearshore sands are unimodal, generally leptokurtic. Further offshore, the sediments quickly become bimodal, with one mode in the 3ϕ size range and one in the 10-14ϕ range. The clay mode, which is first seen at water depths of about 20 feet, becomes increasingly dominant offshore, but there are no pure clays being deposited in the study area.

Although the mean grain size map shows a predominance of silt sizes in the area, none of the individual samples

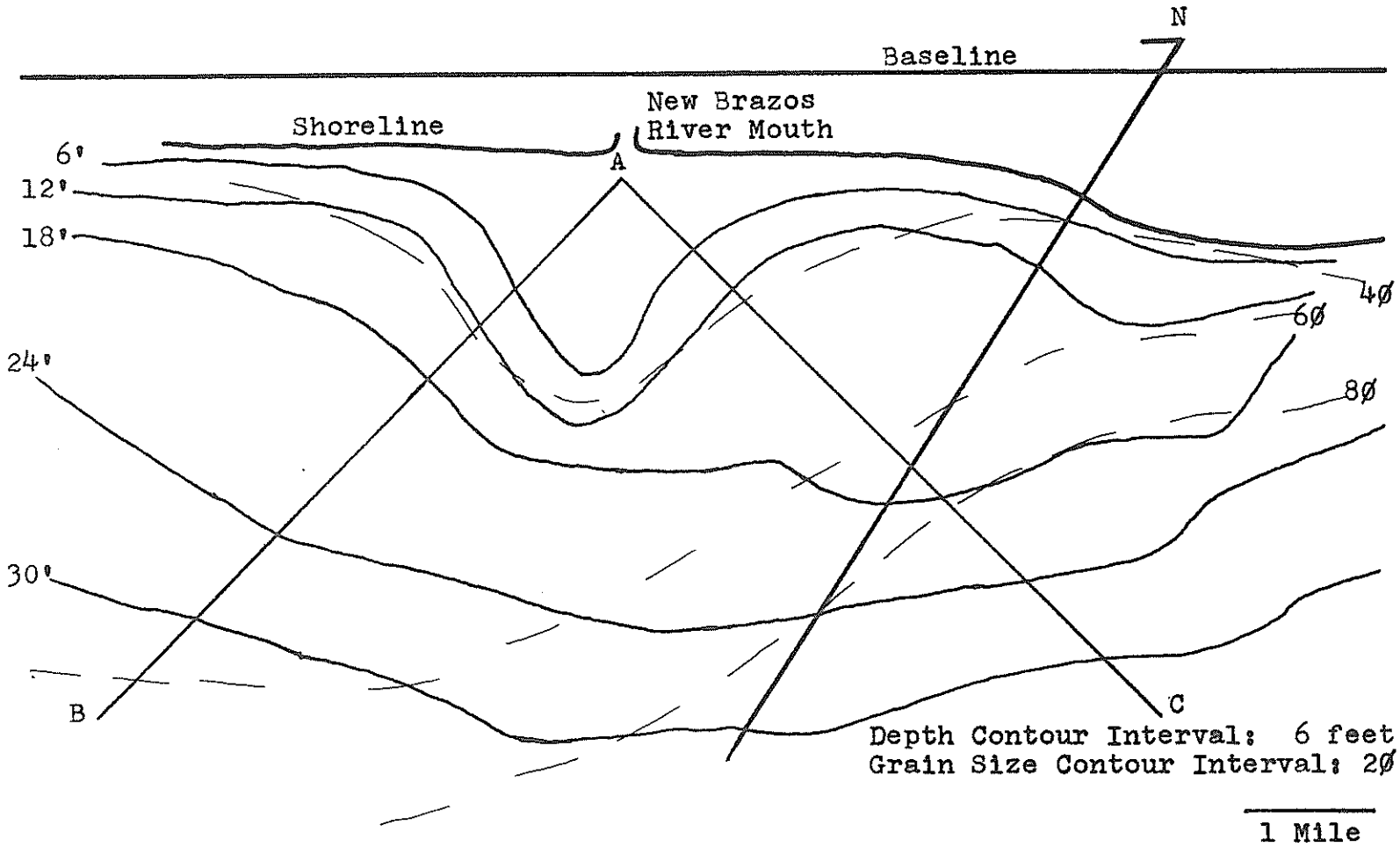

Fig. 22. Contour map of mean grain size in phi units plotted on the August, 1937 depth contours. (from Nienaber, 1963, figure 28).

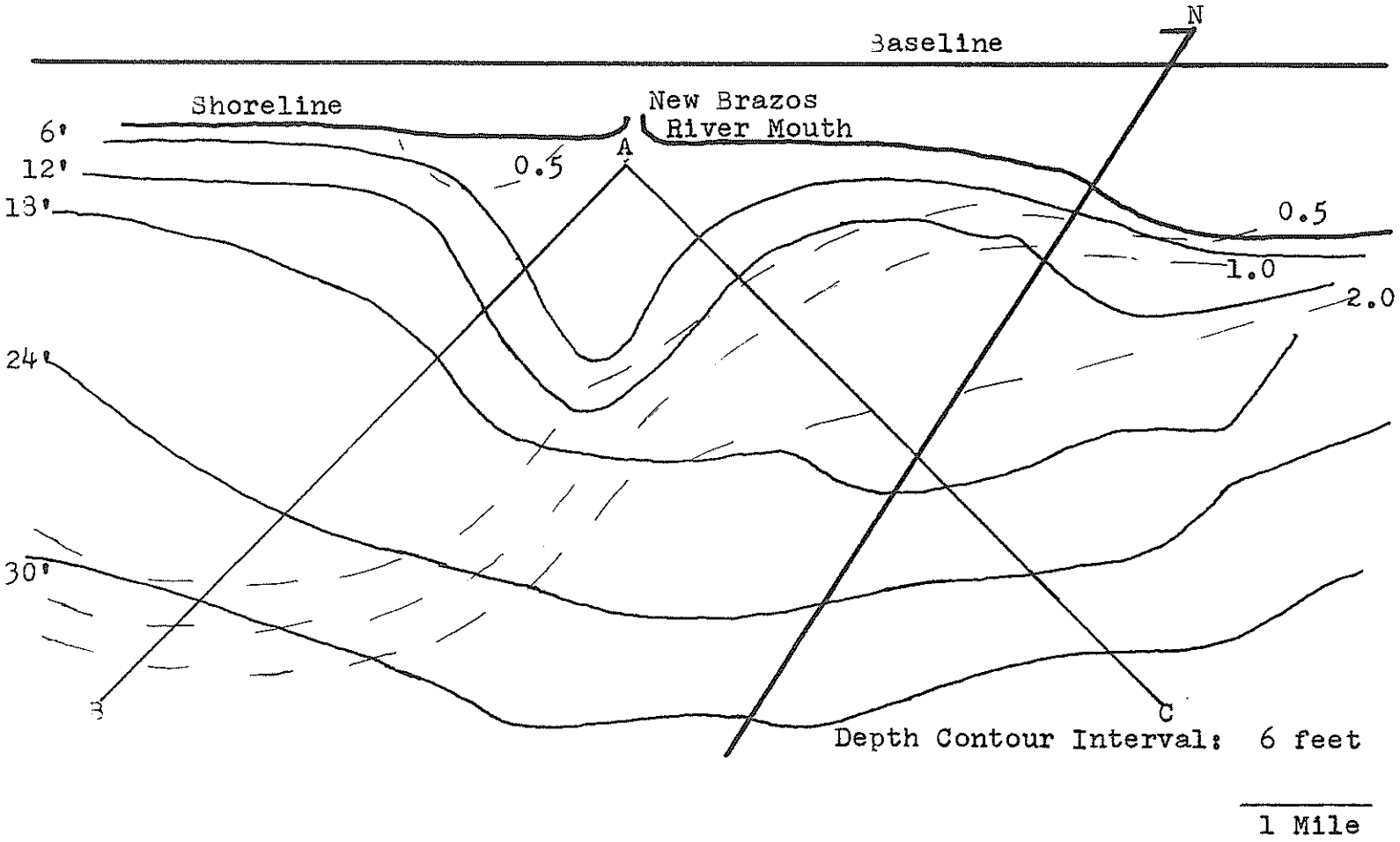

Fig. 23. Contour map of standard deviation plotted with the August, 1937 depth contours. (after Nienaber, 1963, figure 29).

actually had a mode in the silt size range. Data in Figure 24, a frequency distribution curve for all of samples taken by Nienaber, illustrate this point, but there is reason to question its validity insofar as the hydraulic characteristics of the sediments are concerned.

Matthews (1972) states that clay minerals (illite and chlorite) in a channel on the Yukon River are flocculated into particles of a much larger equivilent diameter as the river comes into contact with marine water along a salt wedge. This same effect has been noted in the Mississippi River (Ahr, personal communication). Studies currently underway at Texas A&M University (Mathewson, personal communication) show that in the Brazos River a majority of the clay particles in suspension have flocculated far upstream from the salt wedge. The mechanism of the flocculation is unknown, and is probably unlike that of the flocculation seen on the Yukon and the Mississippi. If further flocculation occurs at the salt wedge, almost all the clays should be aggregating into larger particles, but this has not yet been documented (Mathewson, personal communication). In his analysis, Nienaber wet sieved his samples and added a dispersant to the fine fraction, thus destroying all floccules. He did note, however, that illite and chlorite

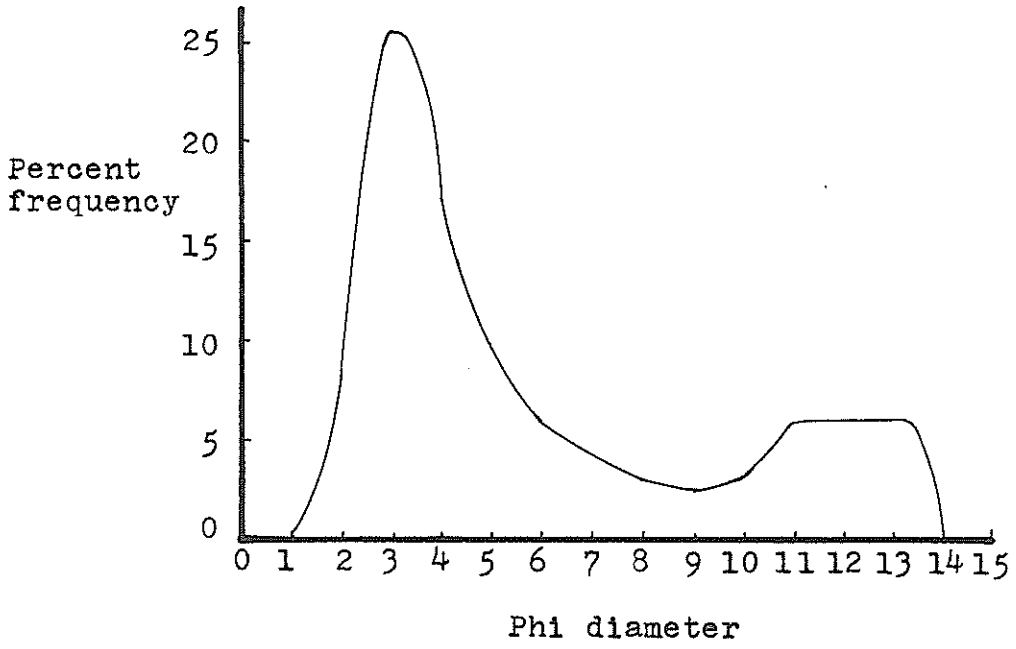

Fig. 24. Frequency distribution of size grades for all sediment samples taken by Nienaber. (from Nienaber, 1963, Figure 18).

were usually deposited closer to shore than other clays (especially montmorrillonite). These data compare favorably with those of Matthews (1972).

Using a scanning electron microscope Mathewson (personal communication) has seen that flocculated clays in the upper Brazos River form essentially two-dimensional sheets. The median diameter of these sheets reaches 5-6ø but low density clay aggregates have fall velocities more in the 7-8ø range. This range includes fine and very fine silt; thus it seems probable that these floccules may have acted as silts during transportation and deposition.

Nienaber (1963) noted a divergence between depth contours and the contours of mean grain size and standard deviation. The rate of change of grain size (or standard deviation) with depth along line A-B is much different than that along A-C (Fig. 22, 23). Seelig (1973) points out that the pattern of the grain size contours is that expected when the effect of longshore drift on river outflow is taken into account. However, this asymmetric pattern presumably would relate to standard deviation and to rates of deposition as well. For example, deposition could be expected to be faster downdrift than updrift from the river mouth, and the grain size (and standard

deviation) contours should roughly parallel the depth contours. It seems that this probably happens, with the deviations of the contour lines from the depth contours in Figures 22 and 23 resulting from the difference in the dates of Nienaber's work, which was done in 1958, and that of the hydrographic work, 1938. In 1938 the old Brazos River delta still exerted considerable control on the depth contour shapes, especially in the area northeast and east of the new river mouth.

Beach Sediments

Seelig (1973) collected beach sediment samples at ½ mile intervals from Brown Cedar Cut to San Luis Pass. The upper centimeter of sand in the zone of wave run-up was scraped into a jar for analysis in the visual accumulation tube, which measures the speed at which particles fall through a water column, thus their "fall-diameter". This analysis assumes sphericity, which is reasonable for beach sands, and also that the density of the particles is close to that of quartz. These beach sands are about 95% quartz (Nienaber, 1963) so both assumptions are reasonable.

Seelig's analyses show that the mean grain size of the beach sands from San Luis Pass to the mouth of the

San Bernard River is approximately .15 mm (2.75Ø), and increases to .3 mm (1.75Ø) at Sargent. These values are the same as those given by Odem who took four foot cores near the water line on the new and old deltas. Odem found that these cores were composed almost entirely of fine sand (78-94%), and very fine sand. None of Odem's samples contained sand larger than 2Ø in diameter. Seelig (1973) examined Odem's core logs, and has estimated that the delta is composed of a minimum of 90% of fine sand (2.5-3Ø diameter); beach sands north and south of the delta area average 3-3.5Ø in diameter (Odem, 1952).

Sediments Available for Erosion

Nienaber shows that there is not a continuous range of grain sizes available for erosion in the area. Figure 22 shows mean grain sizes ranging from less than 4Ø to 8Ø, but Figure 24 points out that these are mixtures of 3-4Ø and 9-13Ø modes. Using these two figures, the grain sizes available for erosion from depths of 6-12 feet, 12-18 feet, 18-24 feet and 24-30 feet, have been estimated, and the values are given in Table I. As an example of how these values were calculated assume that at depths greater than 48 feet, the average grain size is 9Ø. The sediment in this sample is probably a nearly

Table I

Sediment Sizes Available for Erosion for Various Depth Intervals Offshore from the Brazos River Delta

Depth Interval (feet)	Mean Grain Size Present (Ø)	Components (percent by weight)				
		2Ø	3Ø	4Ø	7Ø	11.5Ø
0-6	2.5	20	80	0	0	0
6-18	3	15	80	5	0	0
18-24	4	10	40	50	0	0
24-30	5	0	20	65	15	15

even mixture of 9 through 13Ø. Choosing 11.5Ø as an average size of the clay mode, the sample must be approximately 70% 11.5Ø in size and 30% 4Ø in size. The components by weight of the other samples are estimated on this same principle, assuming that the coarser sand, 2-3Ø in size, increases in abundance nearer the beach. The column in Table I labeled 7Ø shows that in the opinion of the author the 9-13Ø sediments are deposited as 7Ø-sized floccules, and therefore this is the size which must be eroded, rather than the 11.5Ø average of the clay mode.

Wave Data

Two sets of wave data are available for the study area: 1) hindcasts of deep water wave parameters for Caplen, Texas averaged for the years 1950-1952, and 1954 (Bretschneider, 1956), and 2) gauge measurements made at Galveston.

To compare the data from these two sources, Seelig (1973) has refracted the hindcast deep water waves into the gauge at Galveston. The total energy of the hindcast waves at the gauge was 25% higher than that measured by the gauge, but Seelig states that this difference could be caused by the use of different measurement techniques.

Because the data seem to agree, it is assumed that the wave climate at Freeport can be approximated through the use of the data from Caplen. Galveston is closer to Freeport than Caplen is but no wave direction is available for the gauge measured waves. A general direction of wave approach is given in the hindcast data, however. These data, given in Table II, show the average number of hours of occurrence per year of waves of a given period and mean height. The original data were tabulated for wave heights ranging from 1-2 feet to 12-13 feet and for periods of 3-4 seconds to 11-12 seconds. Weighted averages of the data are given here. All wave types in the original data which occur less than .1% of the time were ignored in the compilation of Table II. It is assumed that their contribution of energy to the coastline is negligible.

To simplify the modeling process, two typical waves are constructed from the waves listed on Table II, one causing longshore flow to the northeast, and one causing longshore flow to the southwest. To do this, the annual longshore component of energy of each wave type was calculated using the formula:

Eq. 26 $$E = \frac{\gamma}{8} H^2 (\sin \theta) \text{ (Total hours per year)}$$

where θ can be read from Figure 25.

Table II

Characteristics and Longshore Component of Wave Energy of the Average Waves in the Brazos River Delta Area

Direction of Wave Approach	Sine θ	H (feet)	Hours	Longshore Component of Energy (feet-pounds per foot of wavecrest)
E	.839	3.6	303	2.6347×10^4
E	.839	6.1	110	2.7462×10^4
E	.839	7.7	8	3.1824×10^3
	Sub Total		421	5.6991×10^4
SE	.208	3.2	1105	1.9056×10^4
SE	.208	4.7	587	2.1567×10^4
SE	.208	6.1	73	4.5180×10^3
	Sub Total		1765	4.5142×10^4
	TOTAL		2186	10.2133×10^4
S	.552	3.2	939	4.2457×10^4
S	.552	5.1	400	4.5391×10^4
S	.552	5.76	19	2.7834×10^3
	Sub Total		1358	9.1179×10^4
SW	.980	3.3	173	1.4769×10^4
SW	.980	6.4	52	1.6697×10^4
	Sub Total		225	3.1464×10^4
	TOTAL		1583	12.2643×10^4

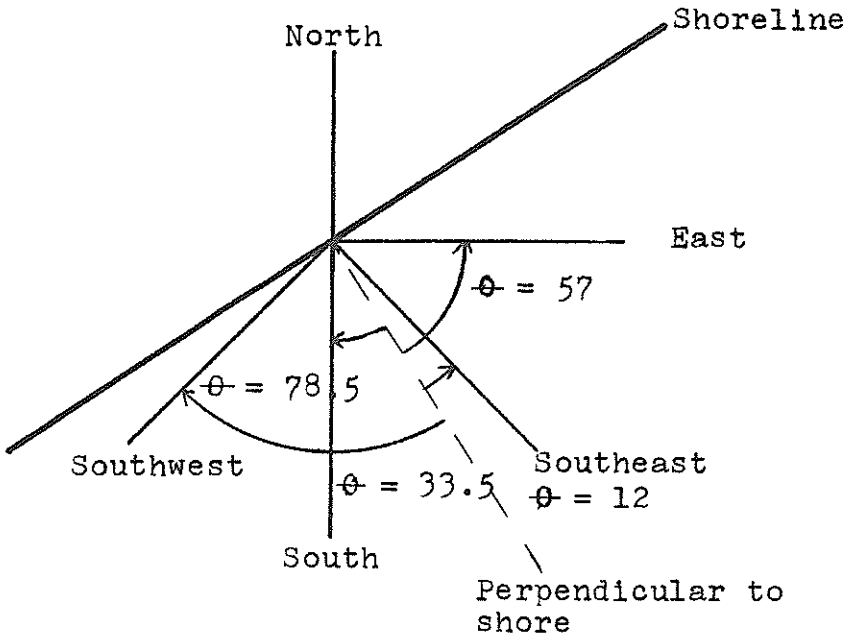

Fig. 25. The angle θ for the four major directions of wave approach.

Refraction was ignored, because it causes θ to change both in space and in time. The calculated values of E are given in the right hand column of Table II. Concentrating first on those waves causing longshore drift to the southwest, note that waves from the east contribute a total of 5.6991×10^4 ft.-lbs. per year to this simplified longshore system pictured here, with 421 hours of occurrence, while waves from the southeast contribute 4.5142×10^4 ft.-lbs. per year, occurring 1765 total hours. The combined total is 10.2133×10^4 ft.-lbs. annually, and 2.86 hours. Working equation 26 backwards,

$$H^2 = \frac{(10.2133 \times 10^4 \text{ ft.-lbs.})\ (8)}{\sin \theta}$$

We see that if θ is known, H can be calculated. The energy contributions from the two directions are nearly equal. Therefore, assume that the typical wave approaches shore from the east-southeasterly direction. Referring to Figure 25, $\sin \theta$ is seen to be .566, and H is then found to be 3.2 feet. The period is found to be 5.83 seconds by taking a weighted average of the periods of the waves from the east and southeast; then, since $L_o = 5.12T^2$, the wavelength is found to be 174 feet, and this wave type occurs 2186 hours annually. The "typical" wave causing longshore drift to the northeast was found in a similar way to have a height of 4.2 feet, a period

of 5.62 seconds, a wavelength of 161.7 feet, to occur 1583 hours annually, and to approach from the south.

Sediment Load of the Brazos River

The stream discharge and suspended load calculated from the measurements made at each gauging station on the Brazos River and its tributaries can be found in Cook (1967, 1970), Adey and Cook (1964), and Stout and others (1961).

The values calculated from measurements at the Rosenberg-Richmond gauging station, which is approximately 100 miles upriver from the mouth of the Brazos, are given in Appendix I. It is assumed here that the values of stream discharge and suspended load given in Appendix I reflect the stream discharge and suspended load of the Brazos at the river mouth. No other gauging station is useful in terms of estimating the sediment load discharged into the Gulf, as all the others are upstream from a dam or natural reservoir which would remove sediment load carried by the river to that location.

The quantity of suspended load of the Brazos River as reported by the Water Development Board is based on three measurements of concentration of suspended sediment, one each at points located 1/6, 1/2 and 5/6 of the width

of the streamflow. The average of the percentage by weight of suspended sediment of these three samples is then multiplied by 1.102 to obtain an average concentration of suspended sediment for the entire stream cross section. The grain sizes of the suspended sediment are not measured. This is a much shorter method for calculation of suspended load than that outlined earlier, and is based on correlations of these three measurements of concentration with the concentration as calculated using the method previously discussed.

The Water Development Board does not specify the method used for computation of stream discharge. It seems reasonable to assume, however, that the stream velocity is measured at a number of points, and the average then multiplied by some empirically derived constant similar to the 1.102 above to give an average velocity for the entire stream. This velocity is then multiplied by the cross sectional area of the stream flow to obtain the discharge.

Relationship of Stream Discharge to Suspended Load

It is generally assumed that the suspended load discharge is directly proportional to water discharge. To examine this assumption, look first at Figure 26, a plot

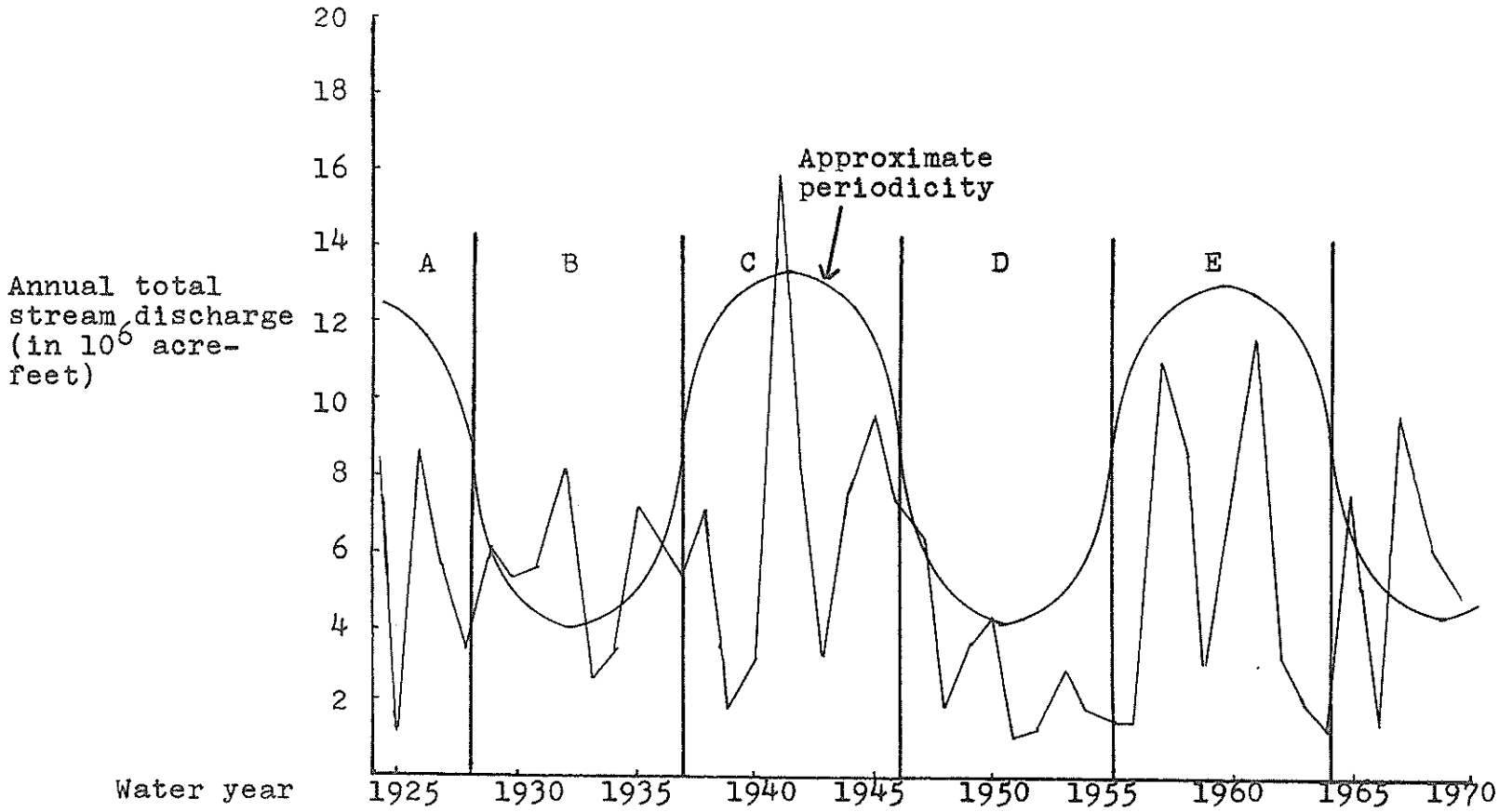

Fig. 26. Annual totals of stream discharge showing possible periodicity.

of the annual totals of water discharge. These totals seem to show a periodicity, the trend of which is outlined by the sinusoidal curve superimposed on the plot. The amplitude and nodal points of this sine curve can only be estimated because the record is not long enough for the characteristics of the period to be more clearly discerned.

For further discussion the discharge record will be divided into time periods A, B, C, D and E (see Figure 26) coinciding with the years 1924-28, 1928-37, 1937-46, 1946-55 and 1955-64, respectively, where periods B and D are low discharge portions of the period and A, C and E are high discharge portions. The averages of annual water discharge for these intervals are shown in Table III.

The annual totals of the suspended sediment discharge are plotted in Figure 27. This figure shows that the suspended load totals do not completely reflect the periodicity of the water discharge. On a year to year basis, high water discharge yields a high sediment discharge, but the amount of sediment discharged per unit of water discharge decreases from interval B to intervals C, D and E. This is shown in Table IV, where we see that the low discharge interval (interval B) has the highest ratio of suspended sediment discharged per unit of water

Table III

Average Stream Discharge of the Brazos River

Water Years	Interval	Average Stream Discharge (10^6 acre feet)
1924-28	A	5.978
1928-37	B	5.300
1937-46	C	7.229
1946-55	D	2.745
1955-64	E	6.278

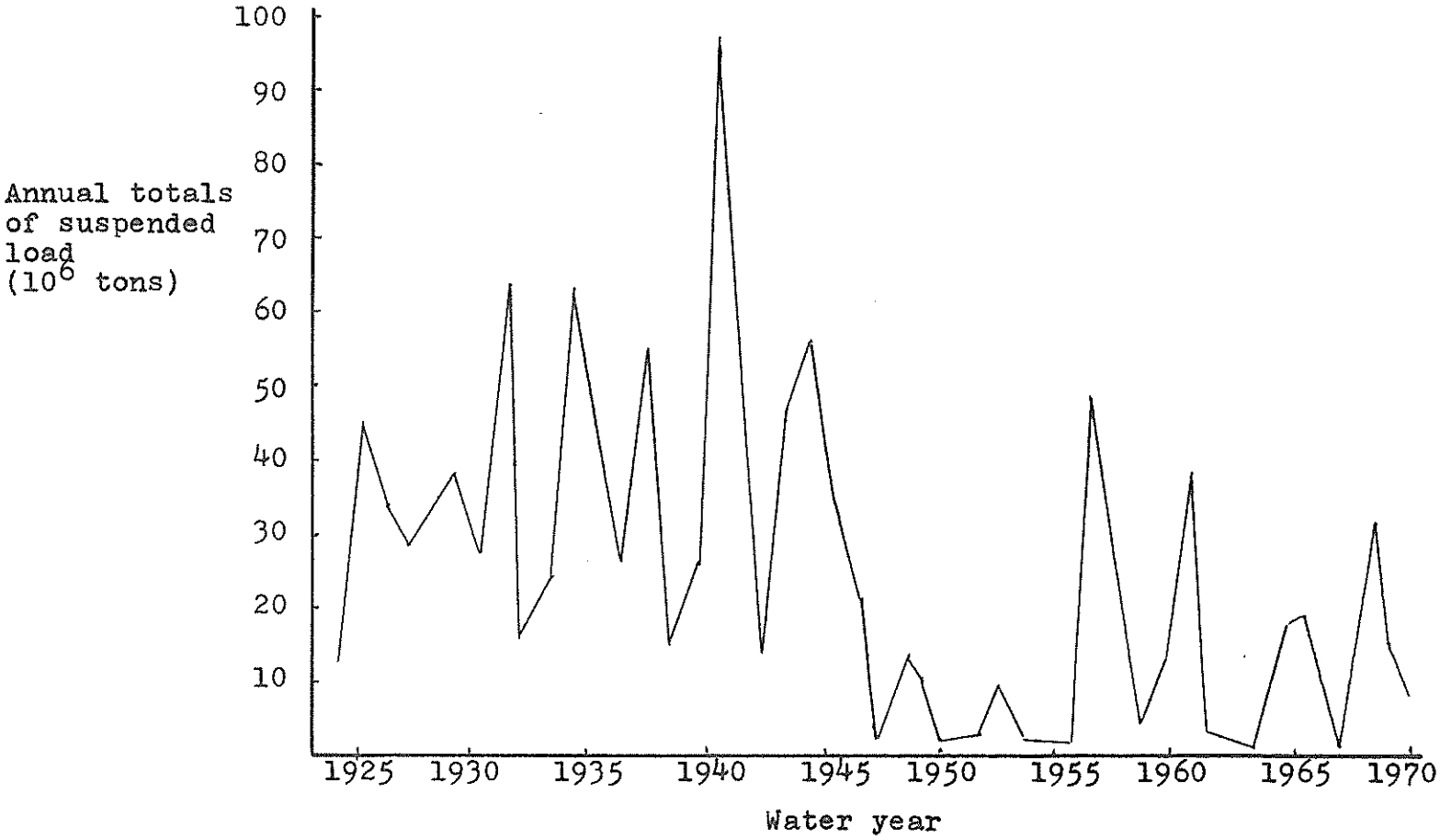

Fig. 27. Annual totals of suspended sediment discharge of the Brazos River.

Table IV

Average Suspended Sediment Load Discharge of the Brazos River

Water Years	Interval	Average Suspended Load Discharge (10^6 tons)	Average Suspended Load Discharge (10^6 tons) / Stream Discharge (10^6 acre feet)
1924-28	A	30.05	5.03
1928-37	B	36.7	6.92
1937-46	C	45.9	6.35
1946-55	D	7.8	2.88
1955-64	E	15.8	2.51

discharge, with this ratio decreasing steadily. For the cause of this trend, look at Figure 28, the plot of annual averages of suspended sediment concentrations. This figure and Table V show a nearly constant suspended sediment average for the years 1924-1943, after which the concentration drops to approximately 50% of its former value.

In the opinion of the author, this decrease was caused by the construction of dams on the Brazos River and its tributaries. These reservoirs would tend to trap all of the incoming sediment, reducing the suspended load concentration without affecting the discharge, because reservoir capacity is usually very small compared to the total stream discharge. The first large dam built directly on the Brazos was the Possum Kingdom Dam, which began to impound water in 1941. Figure 27 shows that by 1943 the suspended load concentration of the Brazos had been cut by approximately 50%. Earlier workers (Odem, 1953; Nienaber, 1963) stated that dam construction had no effect on the suspended load. These studies, however, were made during interval D, a low portion of the discharge cycle, and these workers might have assumed that this was the cause of the low suspended load concentrations.

Fig. 28. Annual averages of suspended sediment concentration of the Brazos River.

Table V

Average Suspended Sediment Concentration of the Brazos River

Water Years	Interval	Suspended Sediment Concentration (percent by weight)
1924-28	A	.552
1928-37	B	.478
1937-46	C	.469
1946-55	D	.185
1955-64	E	.164

By 1964, 24 dams had been constructed on the Brazos. Not all of these dams affect the sediment load because some have been built upstream from an existing dam. Eight major dams which could affect the sediment load were built after the Possum Kingdom Dam. The capacity of these dams and the date on which they began to impound water, are given in Appendix II.

Dams would reduce the total suspended load in two ways: 1) by providing a reservoir in which the sedimentary particles can settle out, and 2) damping the peak streamflow by storing water during high rainfall cycles. Figure 14 shows the effect of the damping by showing that small increases in stream velocity give an order of magnitude change in sediment concentration.

Dams thereby reduce the total suspended load by reducing the concentration of sediments in suspension. The total suspended load discharge in some unit time, however, is still proportional to the total stream discharge in that unit time. Assuming that the proportionality of sediment discharge to water discharge of interval A is unaffected, the reduction in load caused by the upstream dams is summarized in Table VI.

Suspended Sediment Size

The sizes of the sediments carried in suspension by

Table VI

Progressive Decrease of Suspended Sediment Discharge per Unit Stream Discharge for the Brazos River

Water Year	Interval	Percent Decrease
1924-28	A	---
1928-37	B	0
1937-46	C	8.3%
1946-55	D	58.3%
1955-64	E	63.8%

the Brazos River vary with the discharge, with the geology of the channel, and so on. There are no records of sediment size comparable to the continuous records of sediment load or discharge; the few measurements available are summarized in Table VII.

For the grain sizes finer than .008 mm, the range of reported percentages were extremely wide, and were not averaged, for, as stated previously, it is the opinion of the author that a majority of the particles in the fine silt and clay sized ranges are actually carried as floccules of 5-6Ø size. Assuming that most material finer than 7Ø is carried as 7Ø floccules, the percentages of each size are given by Table VIII.

Bedload Discharge of the Brazos River

There are no published measurements of the bedload discharge of the Brazos River; to estimate the amount of material carried by the Brazos as bedload, Colby's (1957) method was used. C. T. Welborn of the U.S. Geological Survey, in Austin, Texas (personal communication) has used Colby's method to construct Figure 29, which gives the bedload discharge in tons per day as a function of mean daily velocity. This work is based on suspended load and stream flow measurements taken recently, however,

Table VII

Grain Sizes of Sediment Carried in Suspension by the Brazos River at Richmond, Texas

Grain Sizes (Ø)	Average Percent by Weight Coarser than
3	2.0%
4	10.7%
5	21.9%
6	31.97%
7	40.3%

Table VIII

Apparent Grain Sizes of Sediments Carried in Suspension by the Brazos River at Richmond, Texas

Grain Diameter (Ø)	Percent by Weight
3	2.6%
4	8.1%
5	11.2%
6	10.07%
7	68.03%

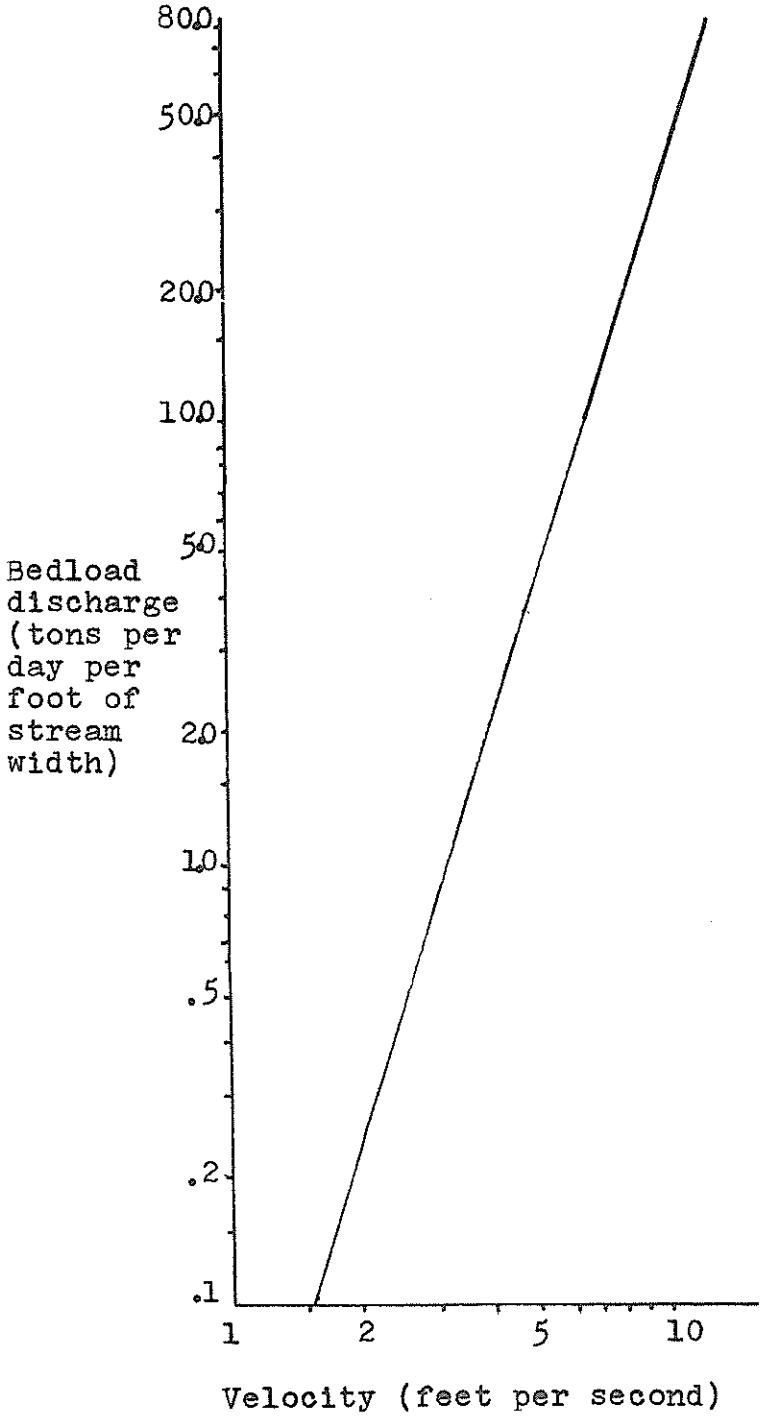

Fig. 29. Bedload discharge vs. mean daily velocity for the Brazos River at Richmond, Texas. (from Welborn, unpublished figure).

so that the availability ratio factor (Fig. 16) which he used to predict the bedload shown in Figure 29 probably is correct only for the years after the dams began to decrease the amount of sediments in suspension.

Welborn constructed a chart, (Fig. 30) for the conversion of the published values of stream discharge at the Rosenberg-Richmond gauging station to mean daily velocity at that station. Knowing the mean daily velocity, one may obtain the bedload discharge in tons per day per foot of width from Figure 29. Figure 31, also from Welborn, shows the correlation between stream discharge at the Richmond-Rosenberg gaging station and stream width at that station. Using these three figures one may obtain the bedload discharge of the Brazos for the years 1923 through 1972. Seelig (personal communication) has calculated the daily bedload discharge of the Brazos for several one month periods. He found that the predicted discharge was unaffected regardless of whether daily or monthly mean discharge values were used in the calculations. The calculated values of bedload discharge are given in Table IX. The predicted discharge values for the years prior to 1943 are probably lower than the actual value because, as was mentioned above, Welborn's figures are based on data taken recently and

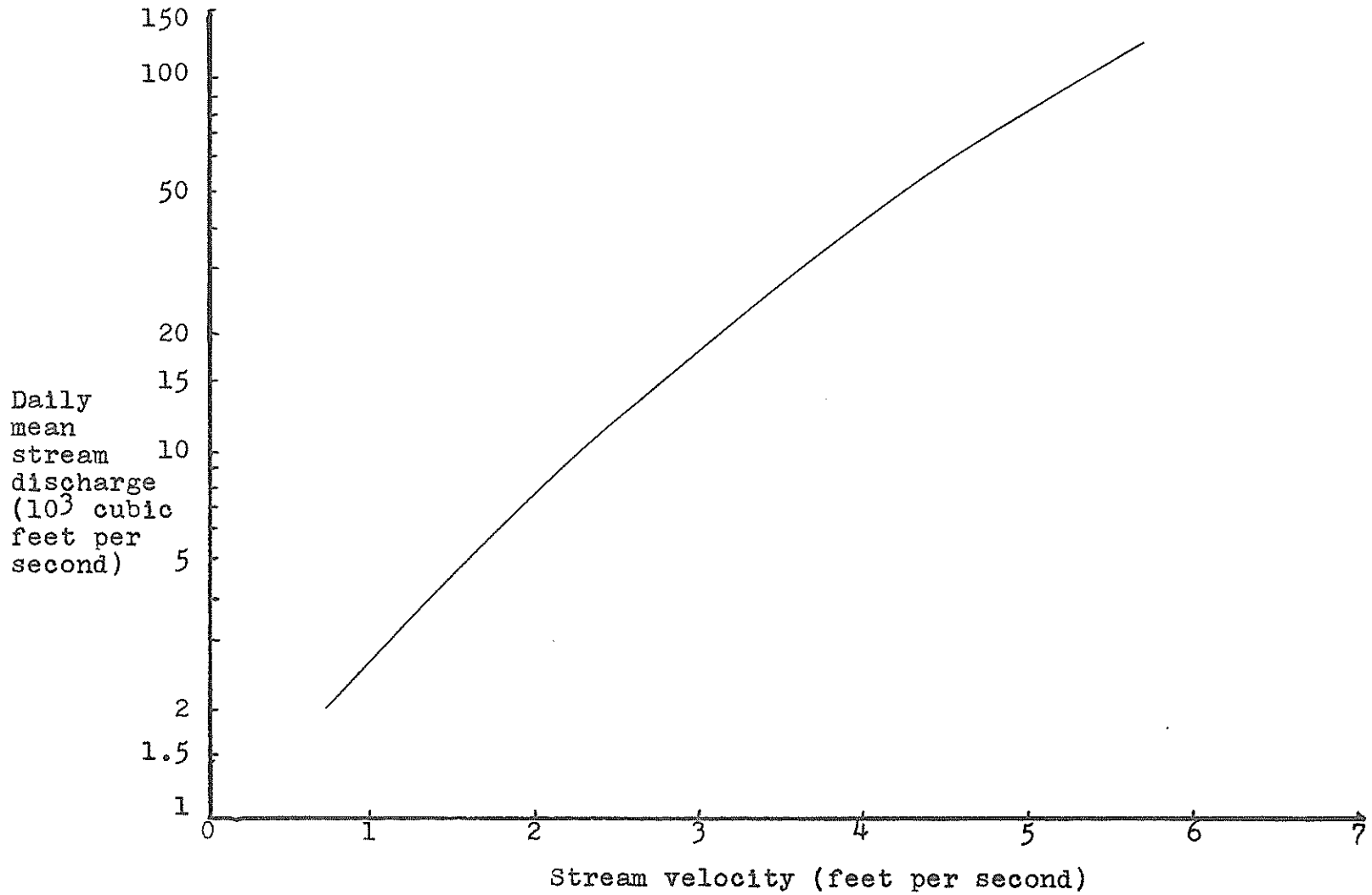

Fig. 30. Daily mean stream discharge vs. stream velocity for the Brazos River at Richmond, Texas. (from Welborn, unpublished figure).

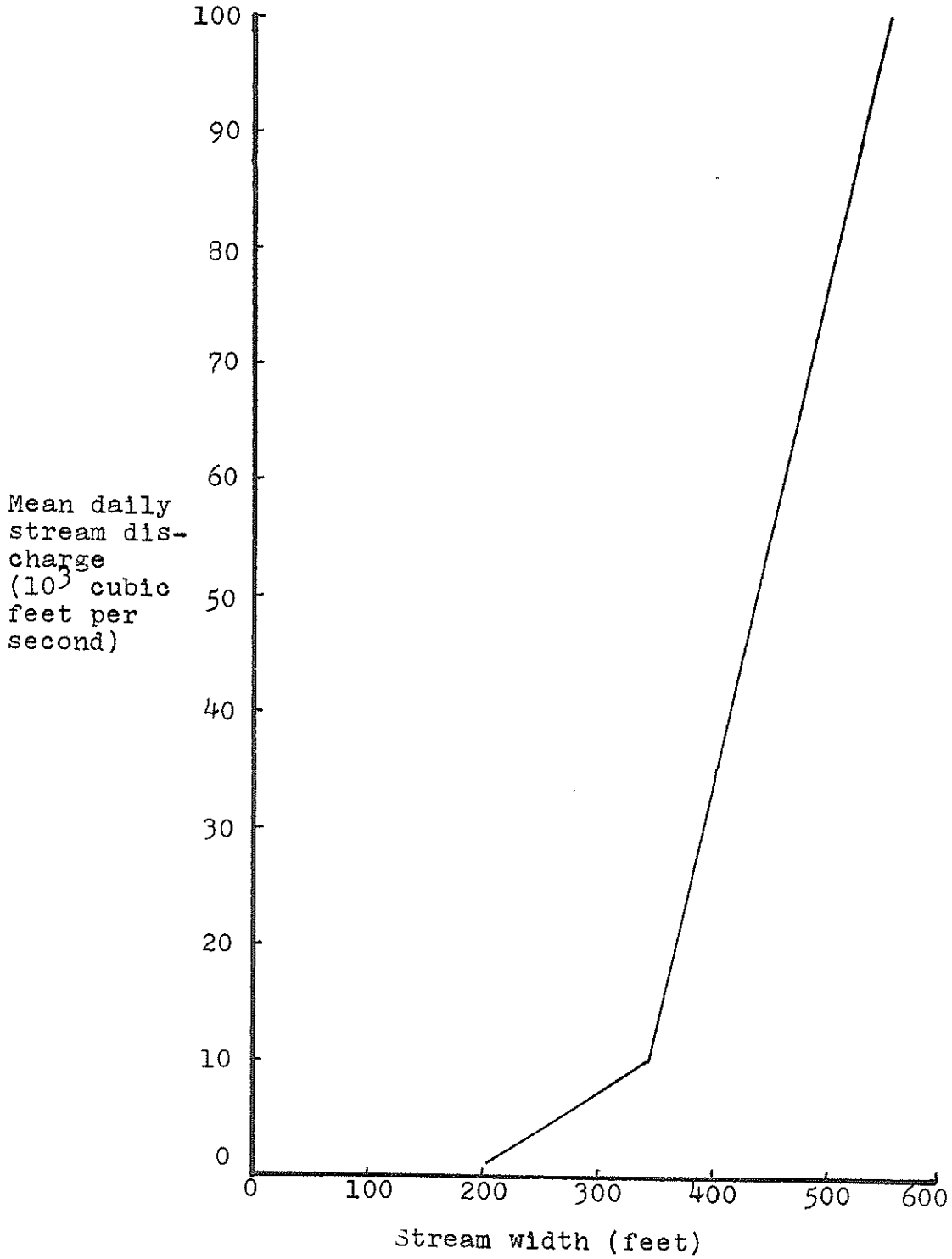

Fig. 31. Mean daily stream discharge vs. stream width for the Brazos River at Richmond, Texas. (from Welborn, unpublished data).

Table IX

Uncorrected Annual Bedload Discharge of the Brazos River

Year	Bedload (cubic feet per year)	Year	Bedload (cubic feet per year)
1923	$.42633 \times 10^7$	1948	$.22747 \times 10^7$
1924	$.95543 \times 10^7$	1949	$.34905 \times 10^7$
1925	$.14030 \times 10^7$	1950	$.47392 \times 10^7$
1926	$.11665 \times 10^8$	1951	$.11725 \times 10^7$
1927	$.57989 \times 10^7$	1952	$.15858 \times 10^7$
1928	$.36831 \times 10^7$	1953	$.38165 \times 10^7$
1929	$.99495 \times 10^7$	1954	$.17045 \times 10^7$
1930	$.98157 \times 10^7$	1955	$.20025 \times 10^7$
1931	$.54427 \times 10^7$	1956	$.17060 \times 10^7$
1932	$.93234 \times 10^7$	1957	$.30102 \times 10^8$
1933	$.31074 \times 10^7$	1958	$.10221 \times 10^8$
1934	$.36264 \times 10^7$	1959	$.36402 \times 10^7$
1935	$.15362 \times 10^8$	1960	$.70126 \times 10^7$
1936	$.59827 \times 10^7$	1961	$.17143 \times 10^8$
1937	$.57194 \times 10^7$	1962	$.40158 \times 10^7$
1938	$.73704 \times 10^7$	1963	$.23239 \times 10^7$
1939	$.21576 \times 10^7$	1964	$.13333 \times 10^7$
1940	$.33183 \times 10^7$	1965	$.12547 \times 10^8$
1941	$.30613 \times 10^8$	1966	$.96680 \times 10^7$
1942	$.12453 \times 10^8$	1967	$.15280 \times 10^7$
1943	$.37472 \times 10^7$	1968	$.12731 \times 10^8$
1944	$.12802 \times 10^8$	1969	$.64653 \times 10^7$
1945	$.14371 \times 10^8$	1970	$.51908 \times 10^7$
1946	$.80046 \times 10^7$	1971	$.13666 \times 10^7$
1947	$.65102 \times 10^7$	1972	$.35303 \times 10^7$

thus his correction factors would not be applicable to flows before dam construction. To correct these values, go to Figure 16 which shows the correction factor as a function of the availability ratio. Using this correction factor, the values prior to 1950 were recalculated. W. N. Seelig and this writer found that the following equations gave the best fit of the curves relating Brazos bedload sediment discharge with streamflow:

Eq. 27 $Q_{us} = -.4775 \times 10^{3} + .3519\ Q - .3334 \times 10^{-4}\ Q^{2} + .1459 \times 10^{-8}\ Q^{3} - .2148 \times 10^{13}\ Q^{4} + .1048 \times 10^{-18}\ Q^{5}$

Eq. 28 $Q_{us} = .1\ Q$

Eq. 29 $Q^{A}_{us} = 1.5\ Q_{us}$

Eq. 30 $Q^{B}_{us} = 1.2\ Q_{us}$.

In these equations,

Q_{us} = bedload sediment discharge in tons per day for water years 1950 to present.

Q = streamflow discharge

Q^{A}_{us} = bedload sediment discharge water years 1923-1940 in tons per day

Q^{B}_{us} = bedload sediment discharge for water years 1940-1950 in tons per day.

Equation 27 applies only for $3000 < Q < 77,500$ cubic feet per second, while equation 28 applies for lower flows.

Corrected values of bedload discharge are given in Appendix I.

Use of the Modeling Procedure at the Brazos River Delta Area

If the data on sediment size, wave climate, and sediment input in the area of the mouth of the Brazos River are known, there remains only the task of incorporating these conditions into a workable model.

Sediment Erosion

Before modeling the sediment movement caused by wave erosion, it is first necessary to insure that the orbital velocities and longshore velocities caused by the waves are sufficient to erode the sediment sizes present. Table X shows the average and maximum velocities caused by the two characteristic waves at the 6, 12, 18, 24, and 30 foot depths, and the grain sizes which can be eroded and transported by these velocities. These sizes were found by a comparison of the velocities with Hjulstrom's curve (Fig. 8). A comparison of these sediment sizes with those in Table II shows that in every case the wave induced velocities are capable of eroding and transporting the available sediments.

Table X

Comparison of U_{max} and U_{ave} with Grain Size

Depth (feet)	U_{max} (cm/sec)	Erodable Grain Size	U_{ave} (cm/sec)	Transportable Grain Size
Wave direction: South				
6	304	7Ø to -6Ø	194	7Ø to -4Ø
12	148.5	7Ø to -4Ø	94.6	7Ø to -4Ø
18	94.6	7Ø to -3Ø	60.1	7Ø to -3Ø
24	66.8	7Ø to -2Ø	42.5	6Ø to -1Ø
30	49.4	7Ø to -1Ø	31.5	6Ø to 0Ø
Wave direction: East-Southeast				
6	241.6	7Ø to -4Ø	153.6	7Ø to -4Ø
12	118.3	7Ø to -3Ø	75.4	7Ø to -4Ø
18	75.3	7Ø to -3Ø	48.1	7Ø to -3Ø
24	53.7	7Ø to -2Ø	34.2	6Ø to -1Ø
30	40.3	7Ø to -1Ø	25.6	6Ø to 0Ø

Calculation of the Sediment Displacement Potential

The calculated sediment displacement potential is defined as the number of feet of sediment which the model predicts will be moved to or from a given area in a given unit of time.

The first step in this calculation is the construction of wave orthogonals for the years of interest; this was done for the charts dated June, 1930, June, 1931, July, 1932, October, 1934, August, 1938, and May, 1973. The orthogonals arrays were constructed for both characteristic waves using the wave-front method described in Ippen (1966), in which the advance of the wave front during one wave period is a function of water depth. These wave orthogonals are shown in Figures 32 through 43. In the construction of these figures, wave refraction seaward of the 30 foot contour was ignored for two reasons: 1) the new data on most of the charts was landward of this depth, and 2) the wave directions given by the wave hindcasting method and those calculated for the characteristic waves of the area are very generalized, and are not well enough known to make use of refraction data outside the 30 foot contour.

Each map has a baseline and a north arrow for easy comparison with other charts; the variability of the

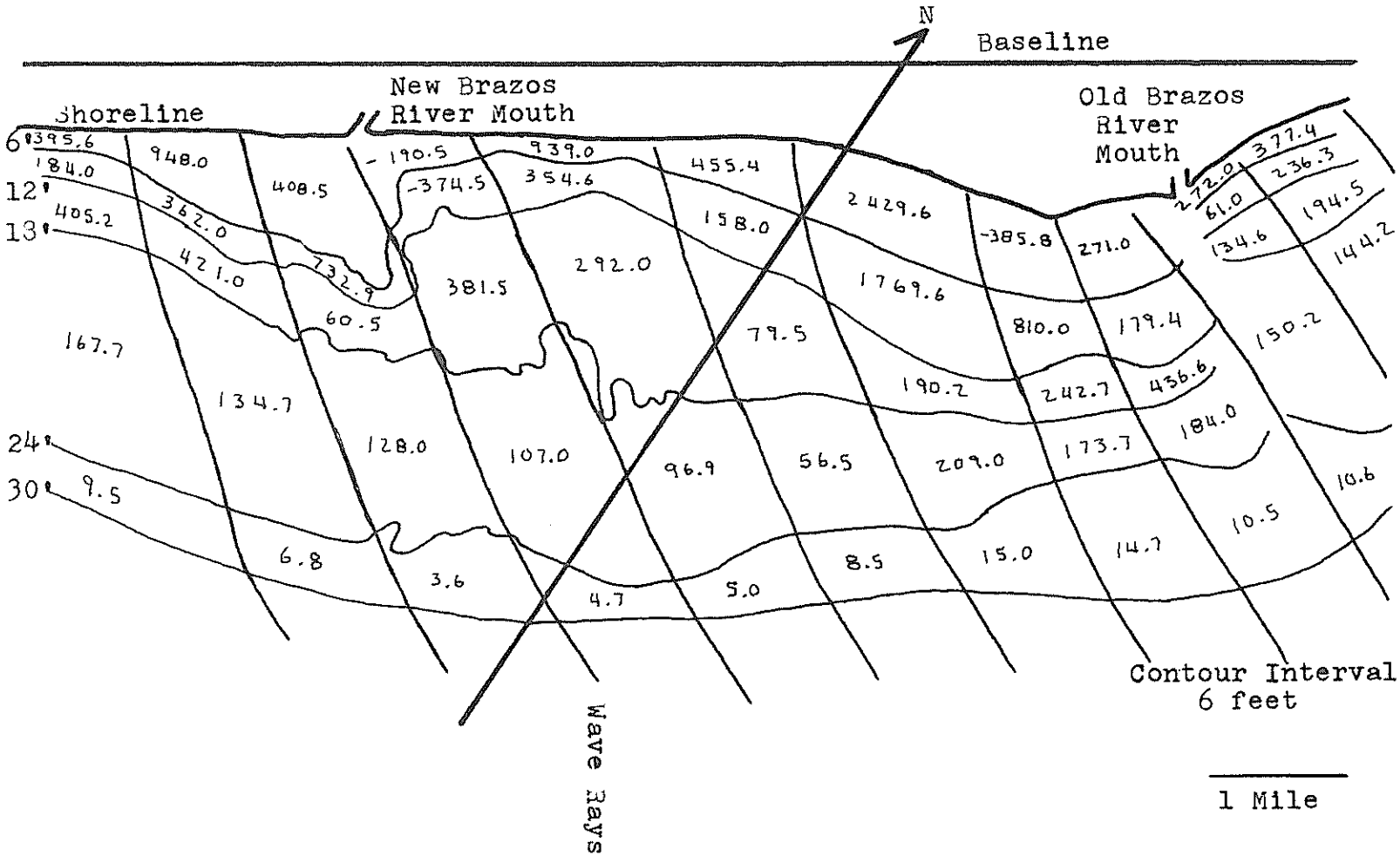

Fig. 32. Wave ray diagram for July, 1930, for waves approaching from the East-Southeast. Values given are 10^6 pounds.

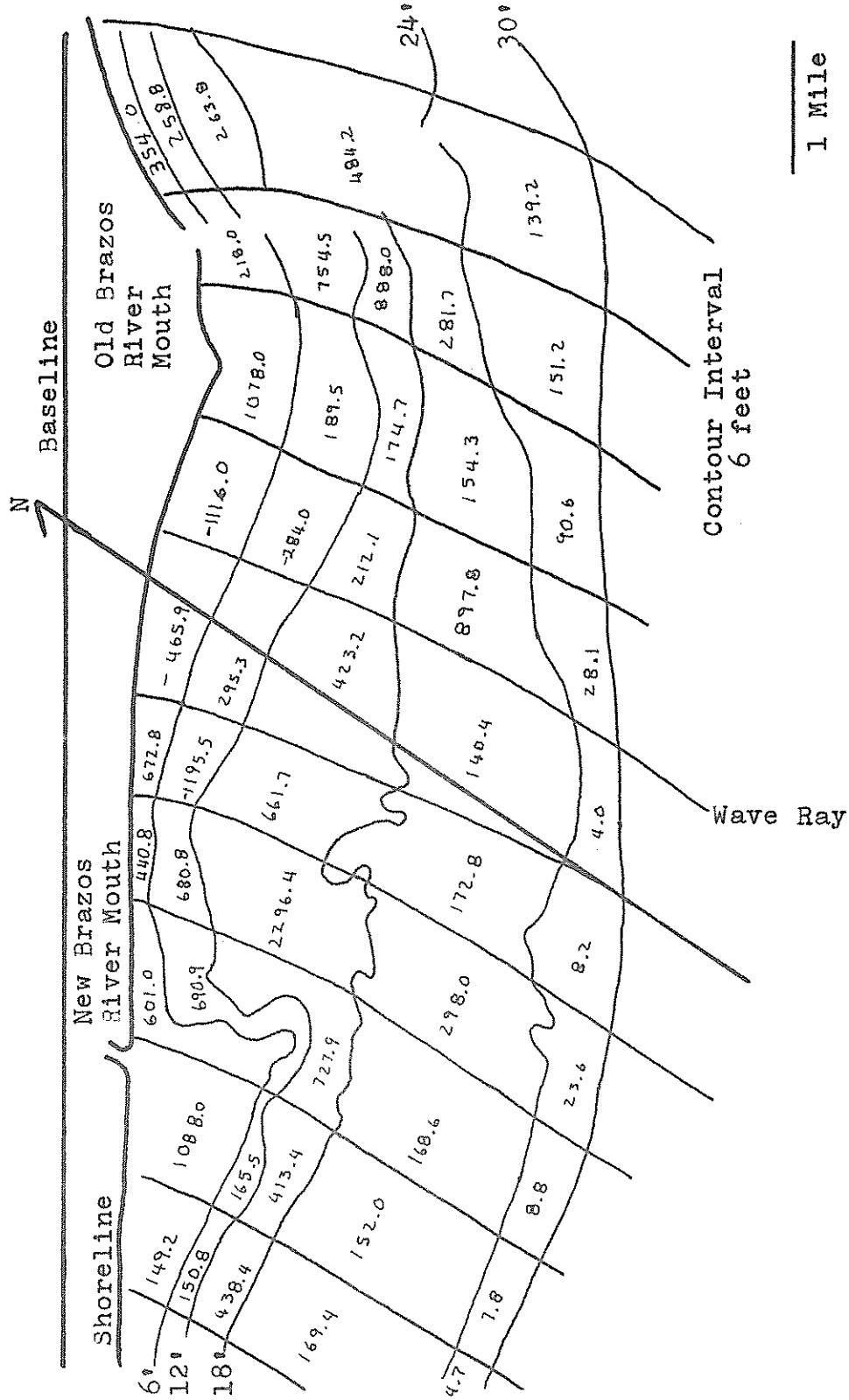

Fig. 33. Wave ray diagram for July, 1930, for waves approaching from the South. Values given are 10^6 pounds.

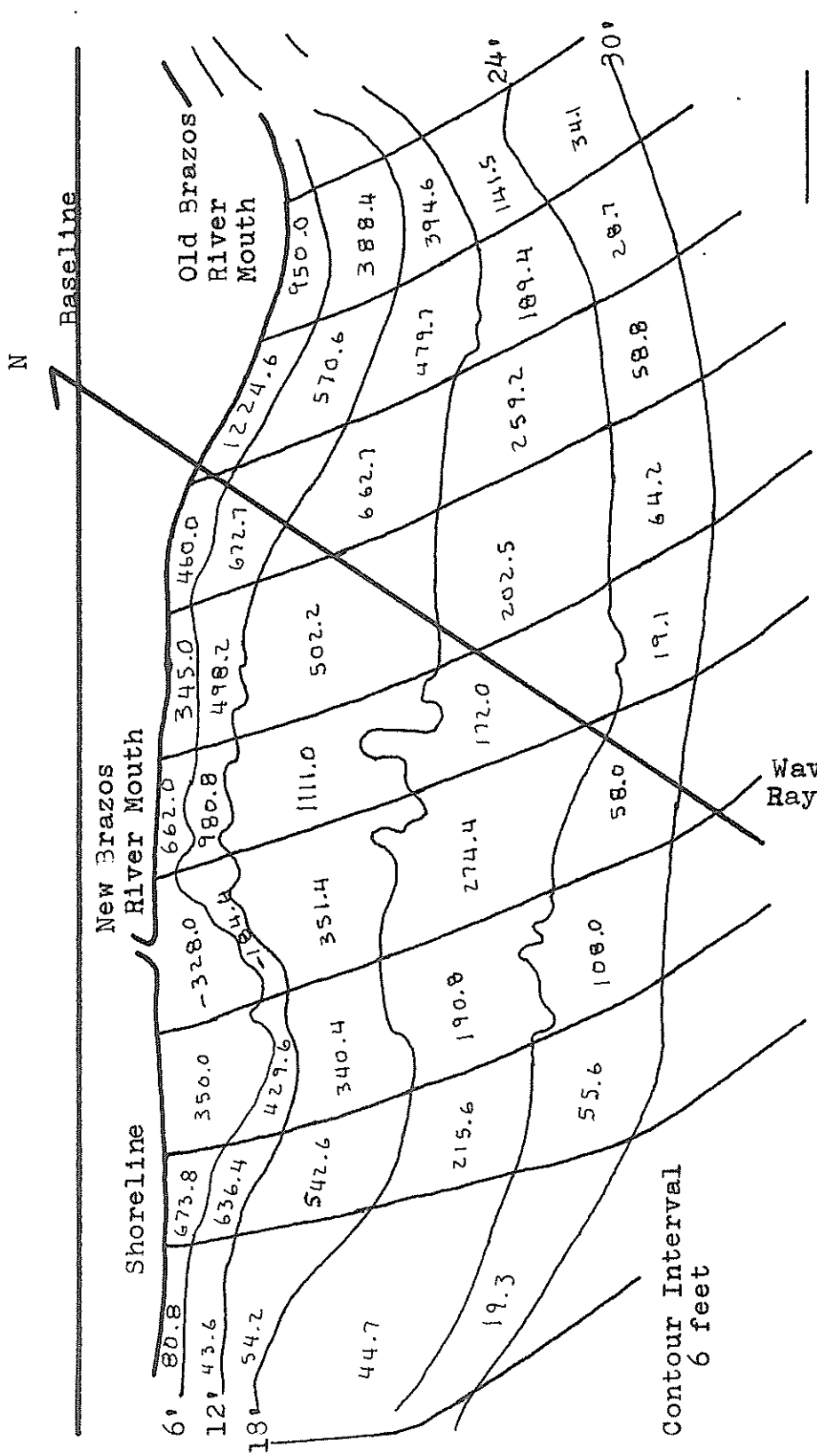

Fig. 34. Wave ray diagram for July, 1931, for 6 wave approaching from the East-Southeast. Values given are 10^6 pounds.

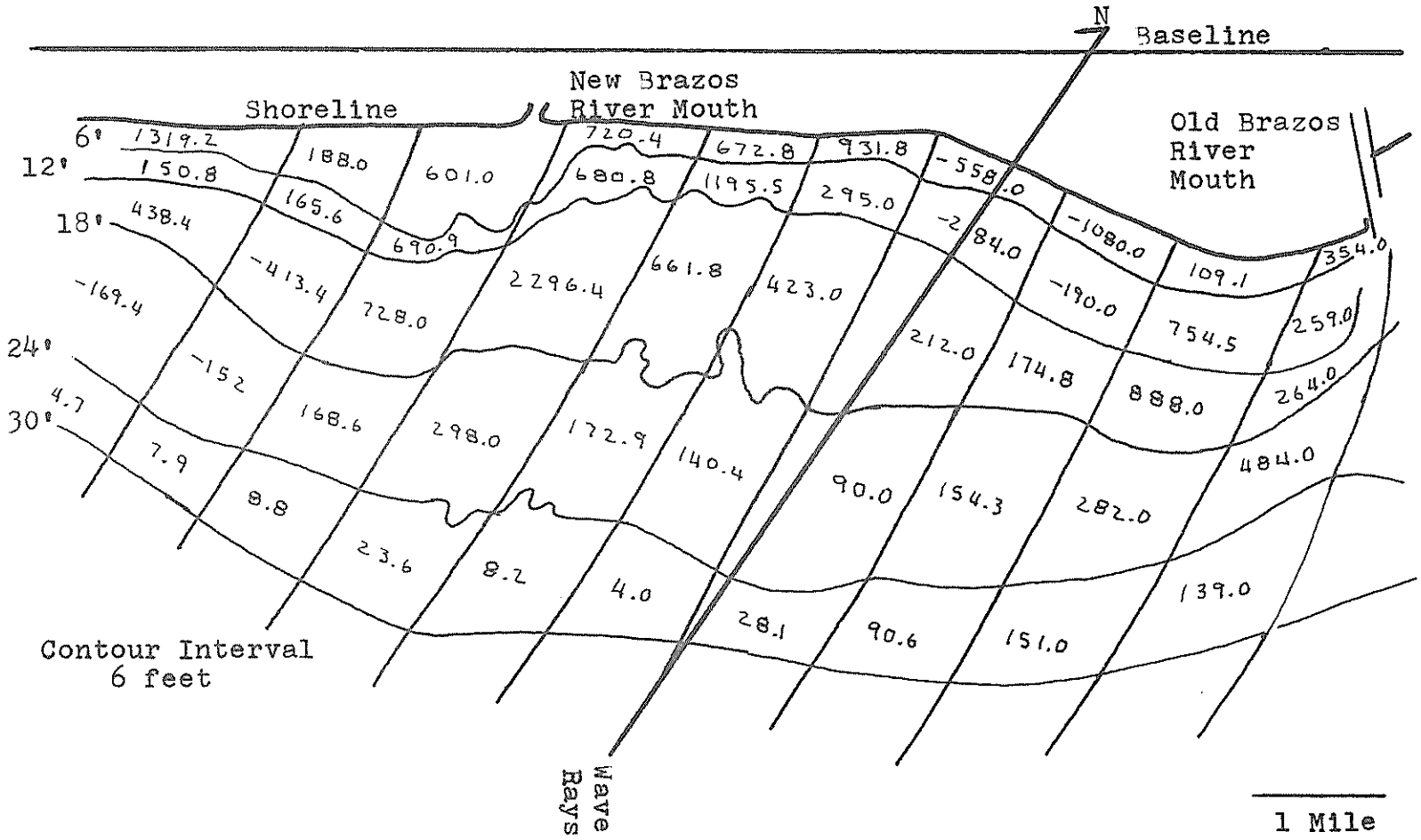

Fig. 35. Wave ray diagram for July, 1931, for waves approaching from the South. Values given are 10^6 pounds.

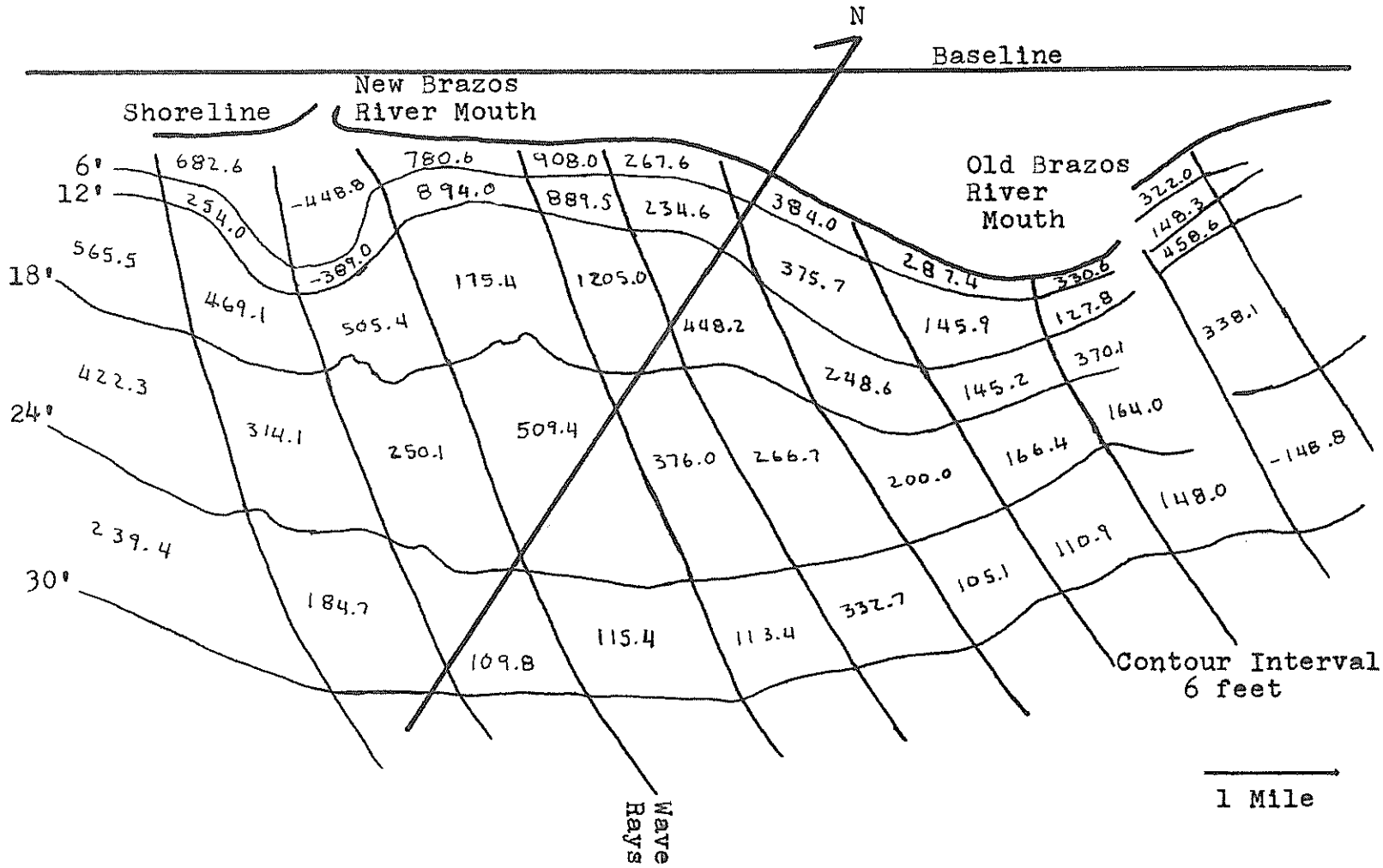

Fig. 36. Wave ray diagram for June, 1932, for wave approaching from the East-Southeast. Values given are 10^6 pounds.

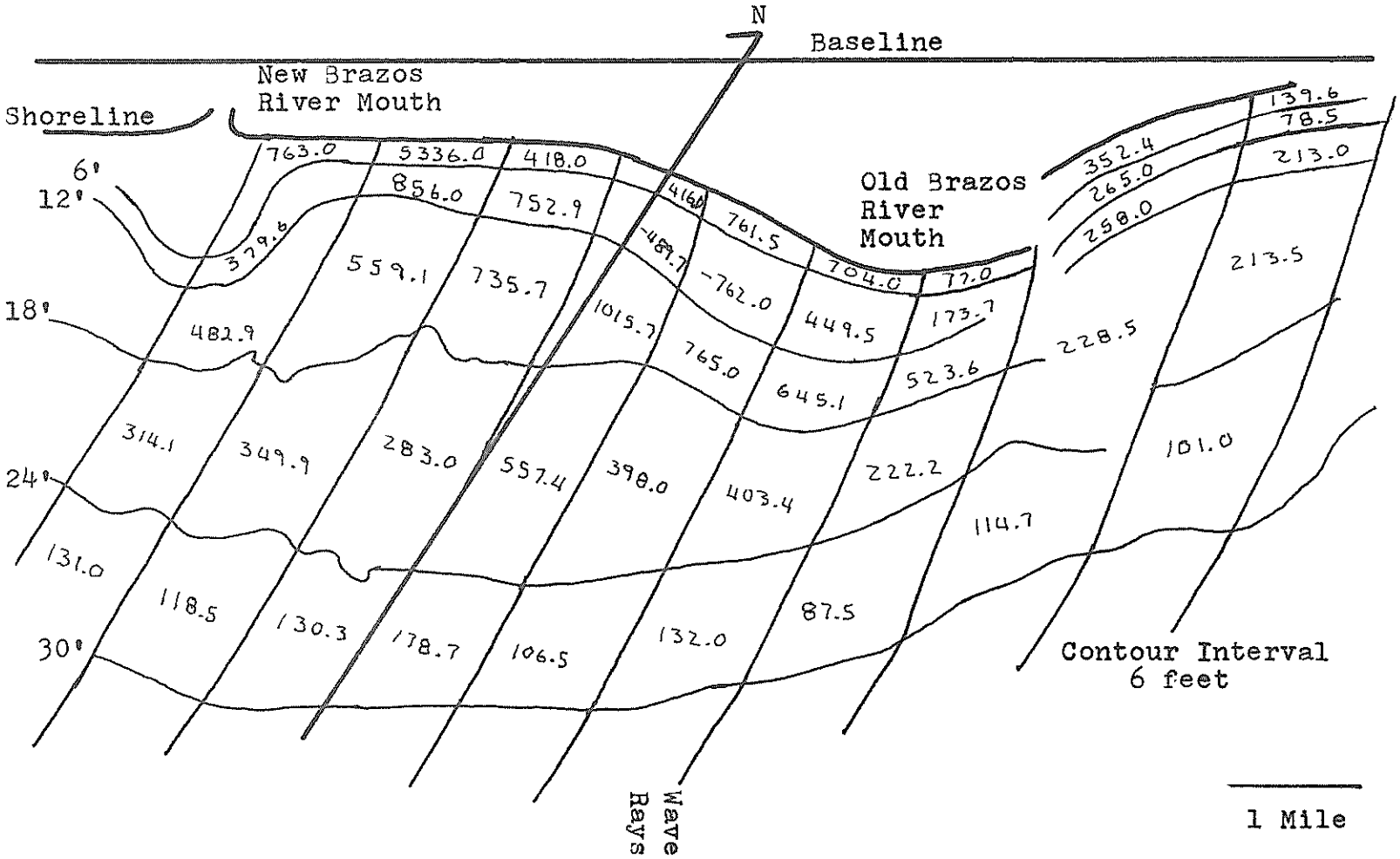

Fig. 37. Wave ray diagram for June, 1932, for waves approaching from the South. Values given are 10^6 pounds.

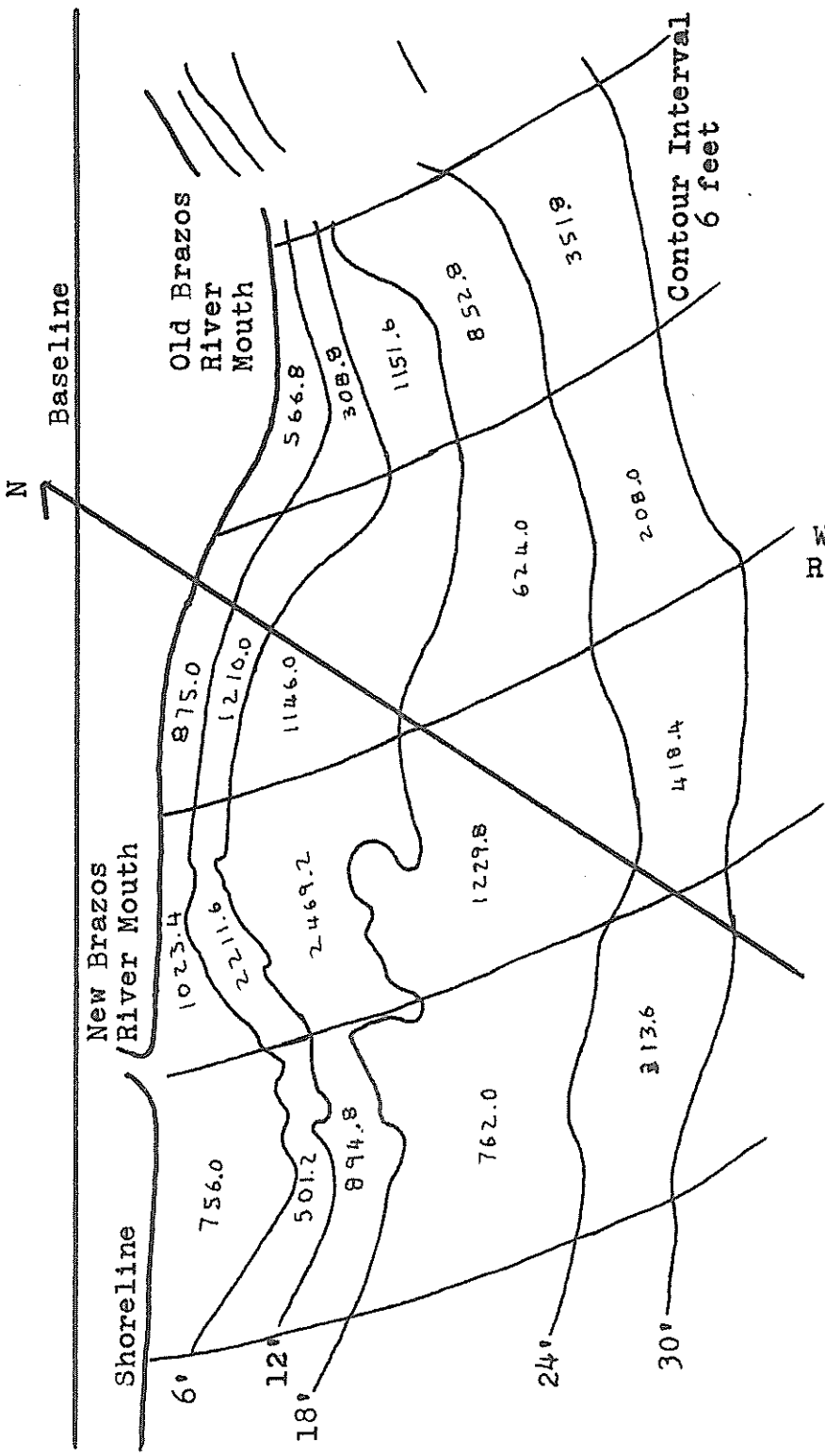

Fig. 38. Wave ray diagram for October, 1934, for waves approaching from the East-Southeast. Values given are 10^6 pounds.

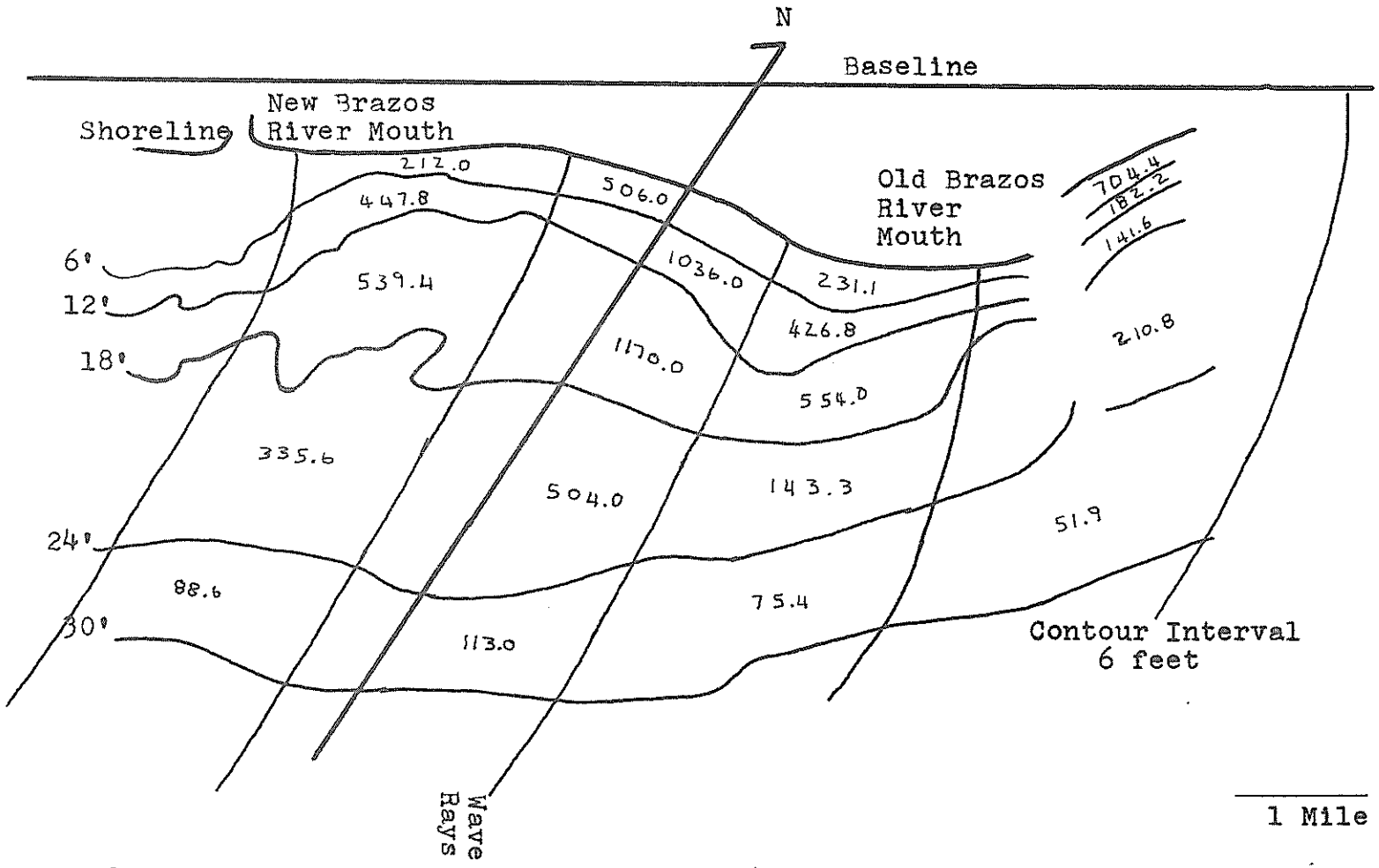

Fig. 39. Wave ray diagram for October, 1934, for wave approaching from the South. Values given are 10^6 pounds.

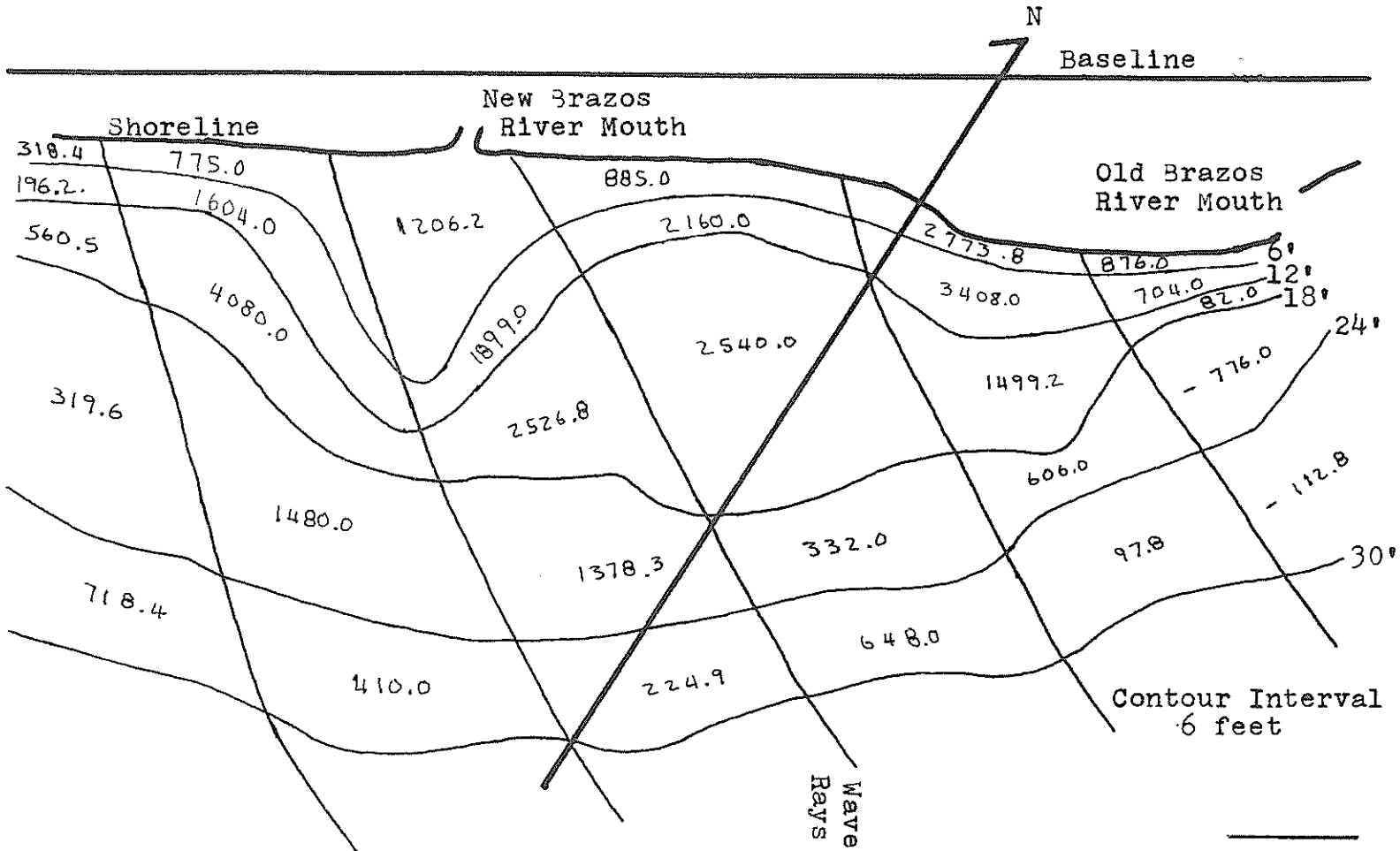

Fig. 40. Wave ray diagram for August, 1937, for waves approaching from the East-Southeast. Values given are 10^6 pounds.

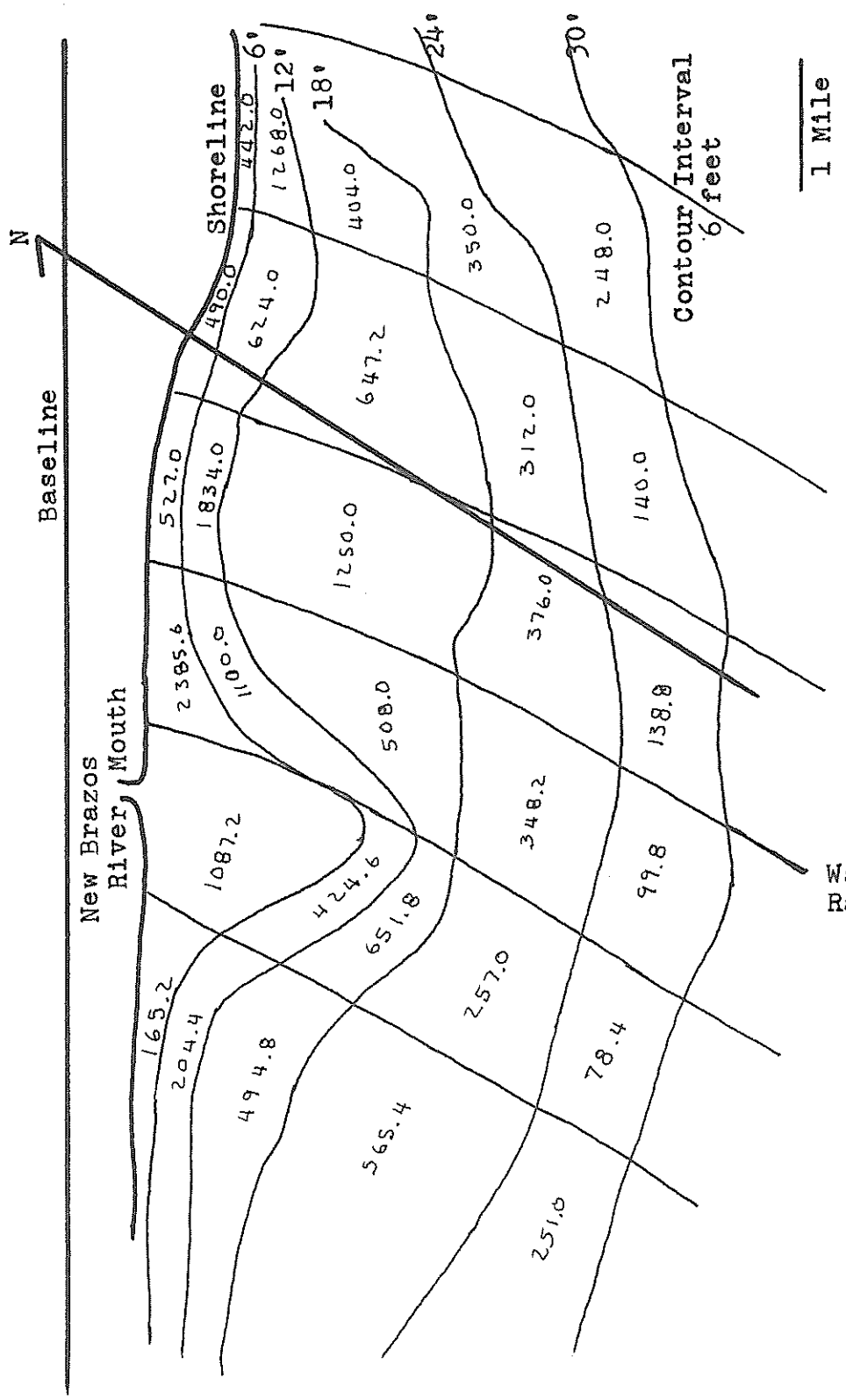

Fig. 41. Wave ray diagram for August, 1937, for waves approaching from the South. Values given are 10^6 pounds.

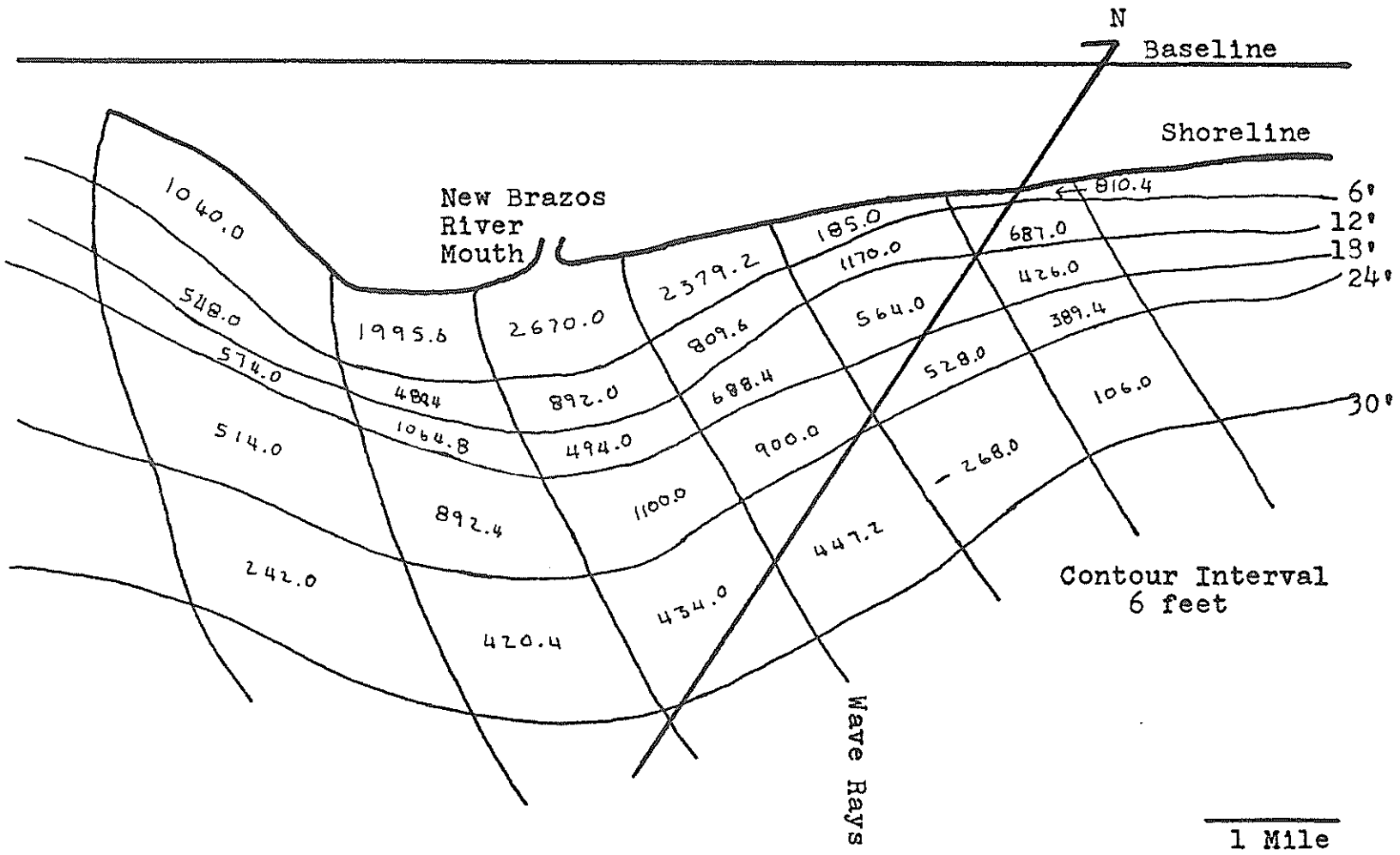

Fig. 42. Wave ray diagram for May, 1973, for waves approaching from the East-Southeast. Values given are 10^6 pounds.

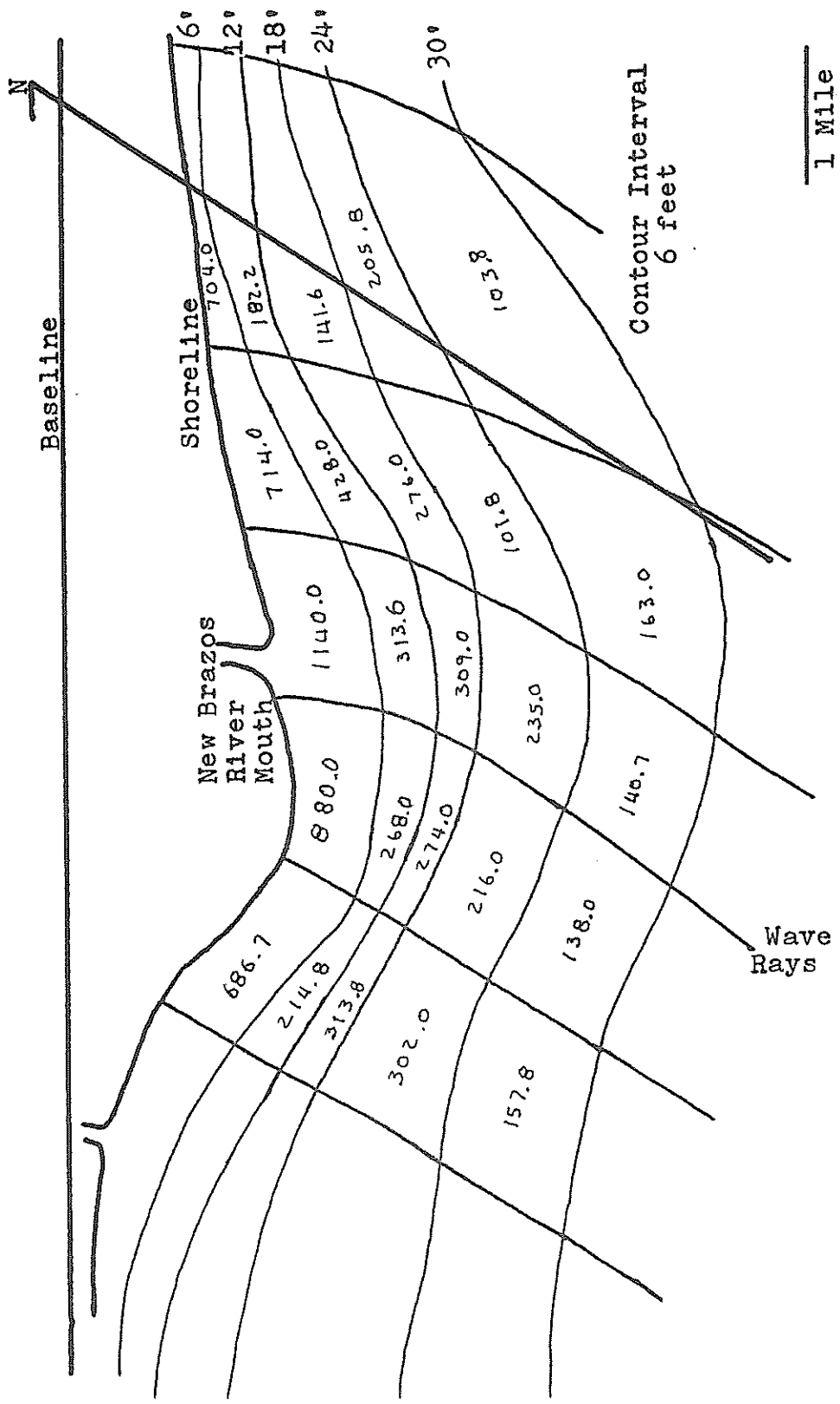

Fig. 43. Wave ray diagram for May, 1973, for waves approaching from the South. Values given are 10^6 pounds.

shoreline and of local land features would make this comparison difficult otherwise.

The numbers inside each area or "compartment" formed by the wave rays and the depth contours on these wave ray charts will be discussed later.

Having constructed the wave orthogonals, several parameters must be measured for each compartment: 1) θ, the angle between a normal to the contour and the orthogonal, 2) b, the distance between rays, measured perpendicular to the wave orthogonals, and 3) X, the distance between contours, measured along the wave orthogonals. The measurement of the values is depicted in Figure 44. After the measurement of all these values, an average value of each parameter for each compartment is taken; X_{AB} and X_{BC} in Figure 44 are averaged to give X_B. Likewise, the θ measured on the two sides of compartment B at the 30 foot contour is averaged to give a θ_{30B}, while the two measured at the 24 foot contour are averaged to give θ_{24B}. Note in Figure 44 that while the wave orthogonals striking the depth contours and forming compartments B and C show a wave regime causing longshore movement to the left of the page, the wave orthogonal at the right of the page shows a wave regime causing longshore movement to the right.

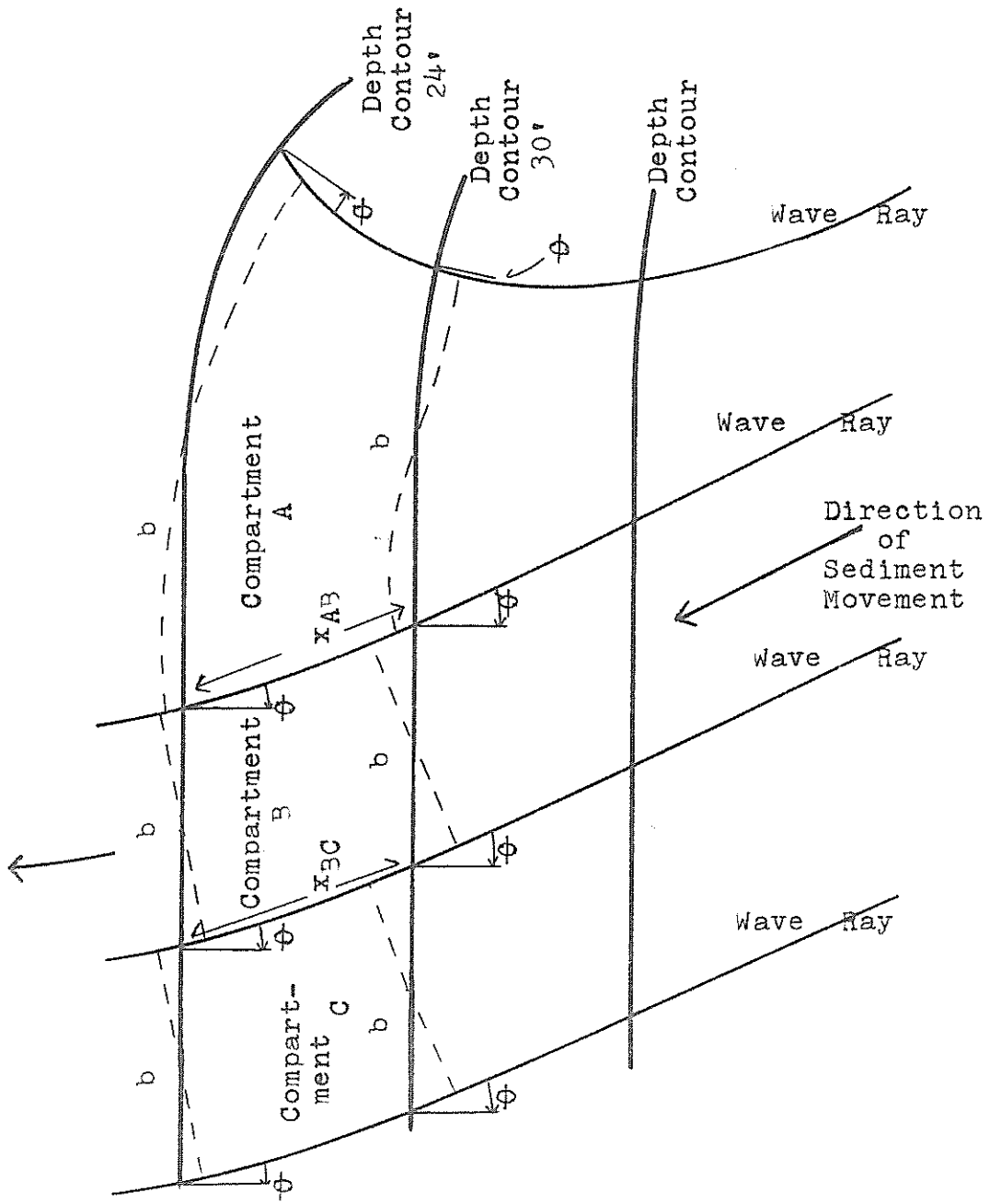

Fig. 44. Diagram showing the measurement of θ, b, and x for several wave ray-depth contour "compartments".

These measured parameters along with the parameters of the characteristic waves, are sufficient for the calculation of the wave energy dissipated in frictional contact with the sea bottom in each compartment. In Figure 44, the total wave energy entering compartment B is $b_o E_o k_{s30} k_{fp30} k_{r30}$ (see Eqs. 10 and 12). Refraction seaward of the 30 foot contour has been ignored here and this expression simplifies to $b_o E_o k_{s30} k_{fp30}$. The term k_s is calculated using Equations 9 and 11; k_{fp} is assumed to equal one, and k_{fp} at the 24 foot depth was consistently found to be .98 or higher. Thus the total wave energy entering the compartment B along a wave crest of length b_o (b_{30}) is $b_o E_o k_{s30}$. The amount of this energy which would be propagated shoreward of compartment B if there were no frictional dissipation of energy is $(k_{s24} k_{r24})$ $(b_o E_o k_{s30})$. Again, k_{s24} can be calculated from Equations 9 and 11, while k_{r24} is taken here to be:

$$\frac{b_{24_B}}{b_{30_B}} .$$

Taking frictional dissipation of energy into account changes the energy propagated shoreward to:

$$k_{fp24} (k_{s24} k_{r24}) (b_o E_o k_{s30}).$$

Here, k_{fp} can be found using Figure 10 and X_B. Figure 10 is based on bottoms of constant depth, so one must assume for use in the figure that the water depth in compartment B is 24 + 30/2 = 27'. The total amount of energy dissipated in bottom friction inside compartment is then found to be:

$$(k_{s24}\ k_{r24})\ (b_o\ E_o\ k_{s30})\ (1-k_{fp27}).$$

The energy dissipated in bottom friction in compartments shoreward of B is then calculated in the same manner.

It will be assumed that all of the wave energy dissipated in bottom friction causes sediment movement. The initial sediment movement will be in the direction of the wave orthogonals. Under the assumption stated earlier, however, the sediments in compartment B of Figure 44 cannot move shoreward of the 24' contour. The average one pound mass of sediment can gain only three feet of elevation in moving from its position inside compartment B to the 24' contour, and thereby gains three foot-pounds of energy. Because a one-pound mass of sediment weighs only .622 pounds in water, the actual gain in energy is 1.866 foot-pounds. After the initial expenditure of 1.866 foot-pounds of wave energy moves the average one-pound unit of sediment to the 24' contour in Figure 44, every additional 1.866 foot-pounds is capable of moving the wave a dis-

tance parallel to the 24' contour given by $X_b \cos \theta_B$ (see Fig. 11). Therefore, to find the total number of one-pound mass units of sediment which can be moved out of compartment B, take the ratio:

$$\frac{\text{Energy expended in bottom friction in compartment B}}{\left(\frac{b_B}{X_B \cos \theta_B} \quad 1.866\right)}$$

where b_B = the average width of compartment B

$\frac{b_B}{X_B \cos \theta_B}$ = the number of 1.866 foot-pound units necessary to get the sediment out of the compartment (the number of movements of length $X_B \cos \theta_B$ necessary to equal b_B).

After this procedure was followed for each compartment in each of Figures 32 through 43, the result was adjusted to account for the total number of waves which propagate into the area per year; these numbers are found by dividing one year by the periods of the two characteristic waves.

This answer is then divided by 90 pounds per cubic foot to give the final result, i.e., the number of cubic feet of sediment which can be transported out of each compartment by the friction dissipated wave energy. These are the values written in each compartment on Figures 32 through 43. Negative values are those in which the move-

ment of the sediment is opposite to the normal longshore flow, similar to that in compartment A of Figure 44.

It is necessary to make some assumption as to the amount of wave energy which is lost in breaking. Because there are no guidelines to follow, it was assumed that approximately 1/2 of the wave energy at the 6' depth contour was lost in breaking (Galvin and Eagleson, 1965), and for the sake of consistency it was assumed that none of this energy would cause sediment transport, i.e., it is all lost in heat in the breaking process.

Longshore Movement

The values recorded on Figures 32 through 43 could be termed the gross potential for longshore sediment displacement from each compartment; however, the sediment transported from one compartment moves into the next, where it either is deposited or transported onward to the next compartment. Thus, one cubic foot of sediment eroded from compartment B (Fig. 44) must also be eroded from compartment C. The net erosion from compartment C is the difference between the gross displacement potentials for compartments B and C. Figure 45 shows the values obtained using this procedure for the chart dated June, 1932, for the waves from the East-Southeast. The

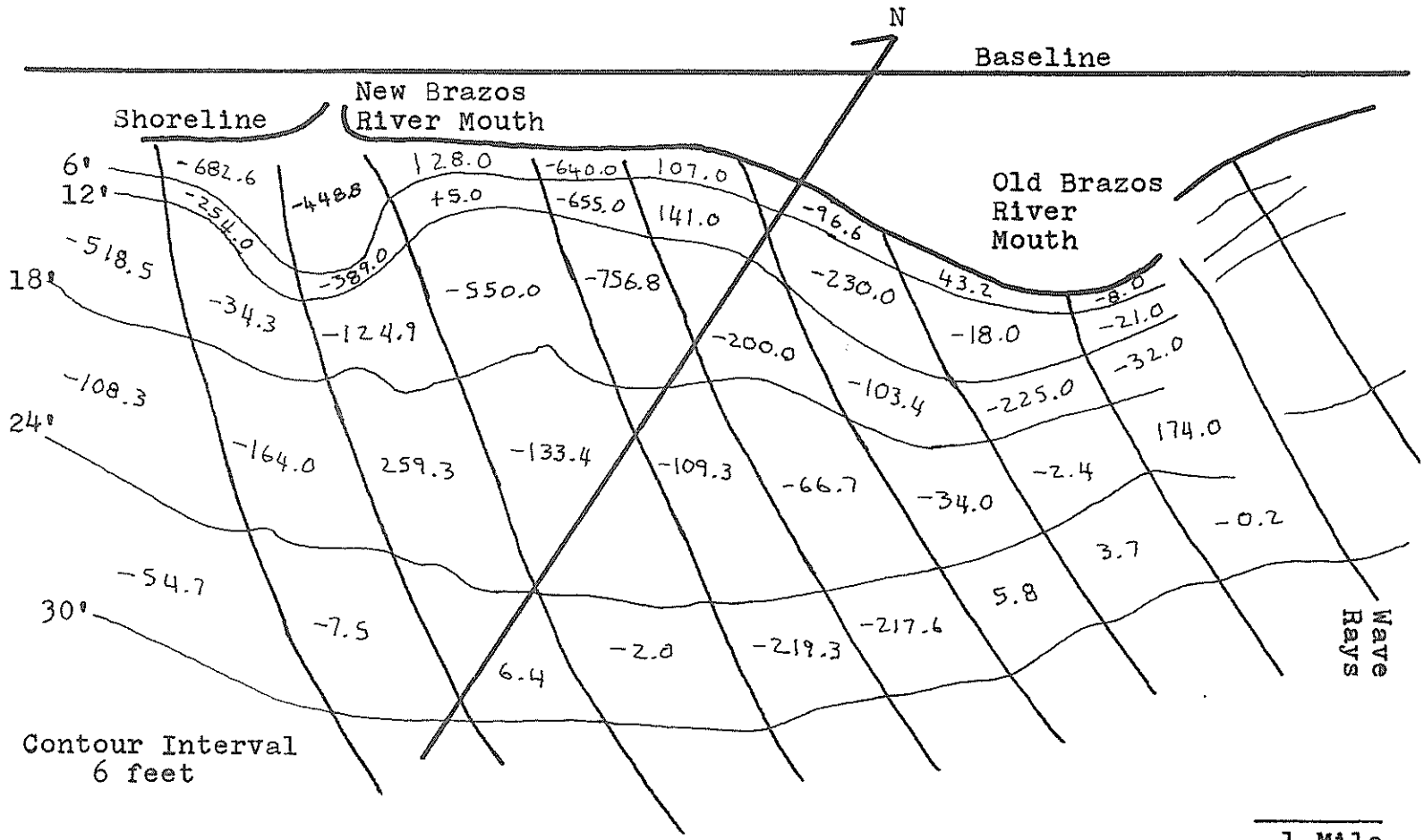

Fig. 45. Sediment displacement potential, corrected for longshore transport, for waves approaching from the East-Southeast, June, 1932. Potential values are given in pounds X 10^6.

negative value in the 18°-12° compartment at the far west means that the gross value in this compartment is larger than the gross value in the compartment to the east, and thus more sediment can be eroded than is transported in. This negative value will correspond to a negative isopach value.

When the gross longshore displacement potentials of any of the compartments in Figures 32 - 43 is negative, there is no longshore flow through this compartment. In Figure 46a, let the values given be the gross longshore sediment displacement potentials for the compartments D, E and F. The direction in which the sediment of each compartment moves is shown by the arrows. Figure 46b, shows the net longshore sediment displacement potential; compartment E has a positive value, showing that sediment eroded from D is deposited in E; that is, the waves could erode only 5000 cubic feet of sediment from compartment E, but 7000 cubic feet were transported into E, leading to the deposition of 2000 cubic feet. The sign of the value is positive to coincide with the positive isopach value resulting from deposition. The 5000 cubic feet which are eroded from compartment E, however, are not transported into compartment F; in F, the flow is in the opposite direction. Thus the net loss to compartment F

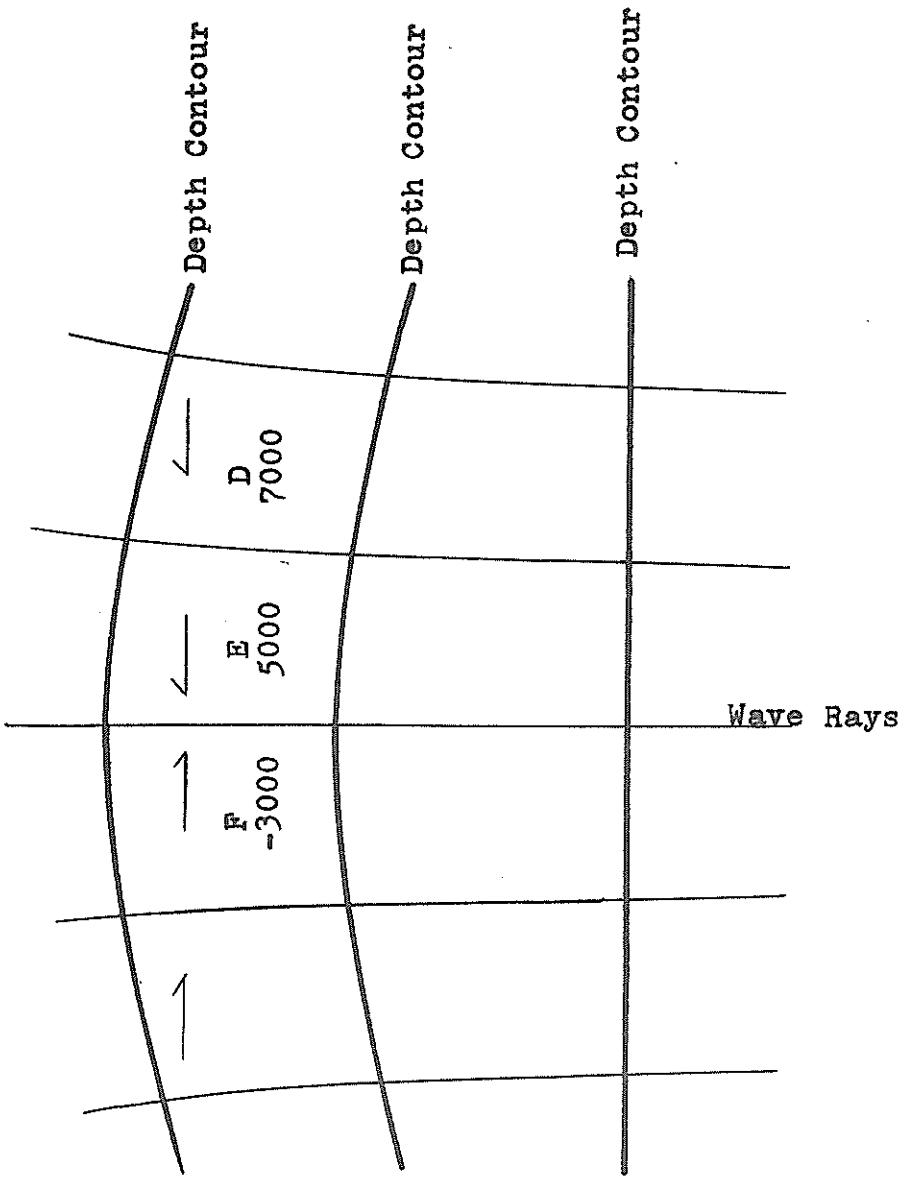

Fig. 46 a. Diagram showing gross longshore sediment movement in opposite directions.

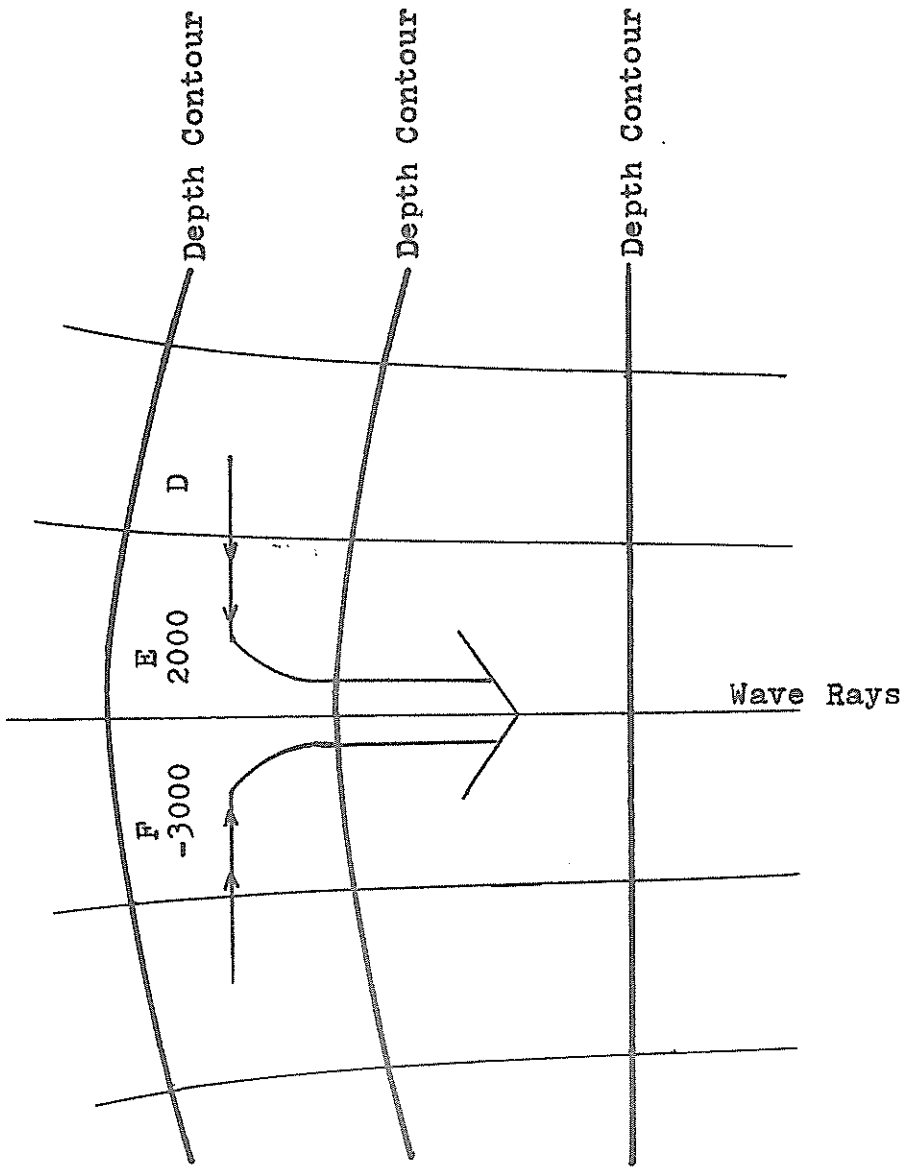

Fig. 46 b. Diagram showing net longshore sediment movement and the development of a localized rip current.

is the same as the gross loss. The sign of the value is negative to coincide with the negative isopach value resulting from erosion. In this way, the model has shown the development of a localized rip current.

Thus far the longshore sediment displacement potentials calculated for the two characteristic waves have been kept separate. The next step is to superimpose the two figures (of Figs. 32 through 43) that are drawn for each year. The values of net longshore sediment displacement potentials are added algebraically; the result of such a procedure is shown in Figure 47 for the chart dated July, 1930. On this figure, one added step has been taken; the longshore sediment displacement potential values have been converted from cubic feet to feet of thickness covering each small compartment by estimating the area of each compartment. Once this is done for each of the charts, any two of these resultant potential maps can then be overlain and algebraically added to obtain the longshore sediment displacement potential for a given time interval. Figure 48 shows the result of this procedure for the time interval July, 1930, to July, 1931. Figures 49 through 53 are contour maps of the sediment displacement potentials calculated for the time intervals July, 1930 to July, 1931; July, 1931 to June, 1932; July,

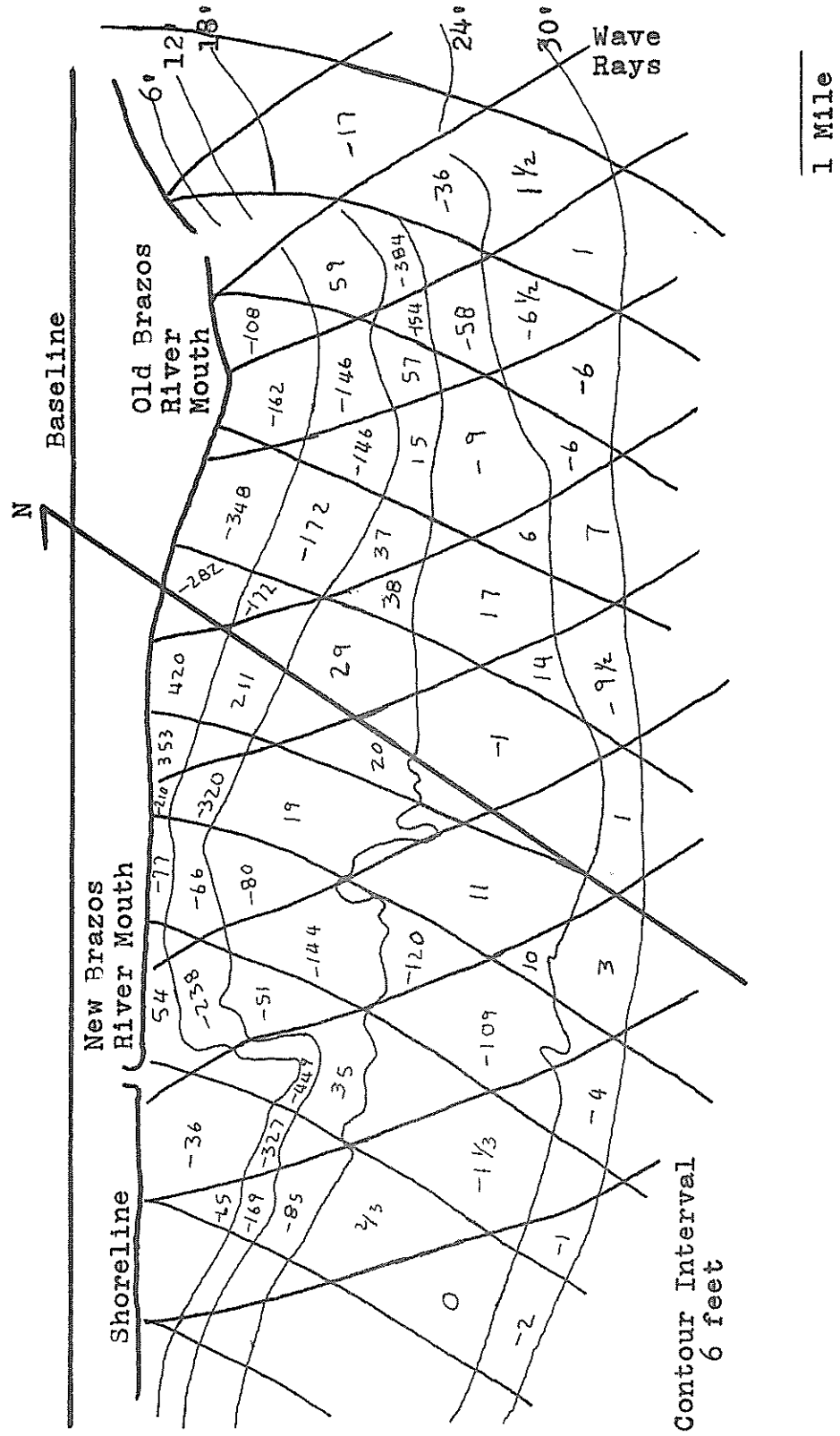

Fig. 47. Combined sediment displacement potential for July, 1930. Potential values in feet X 10^6.

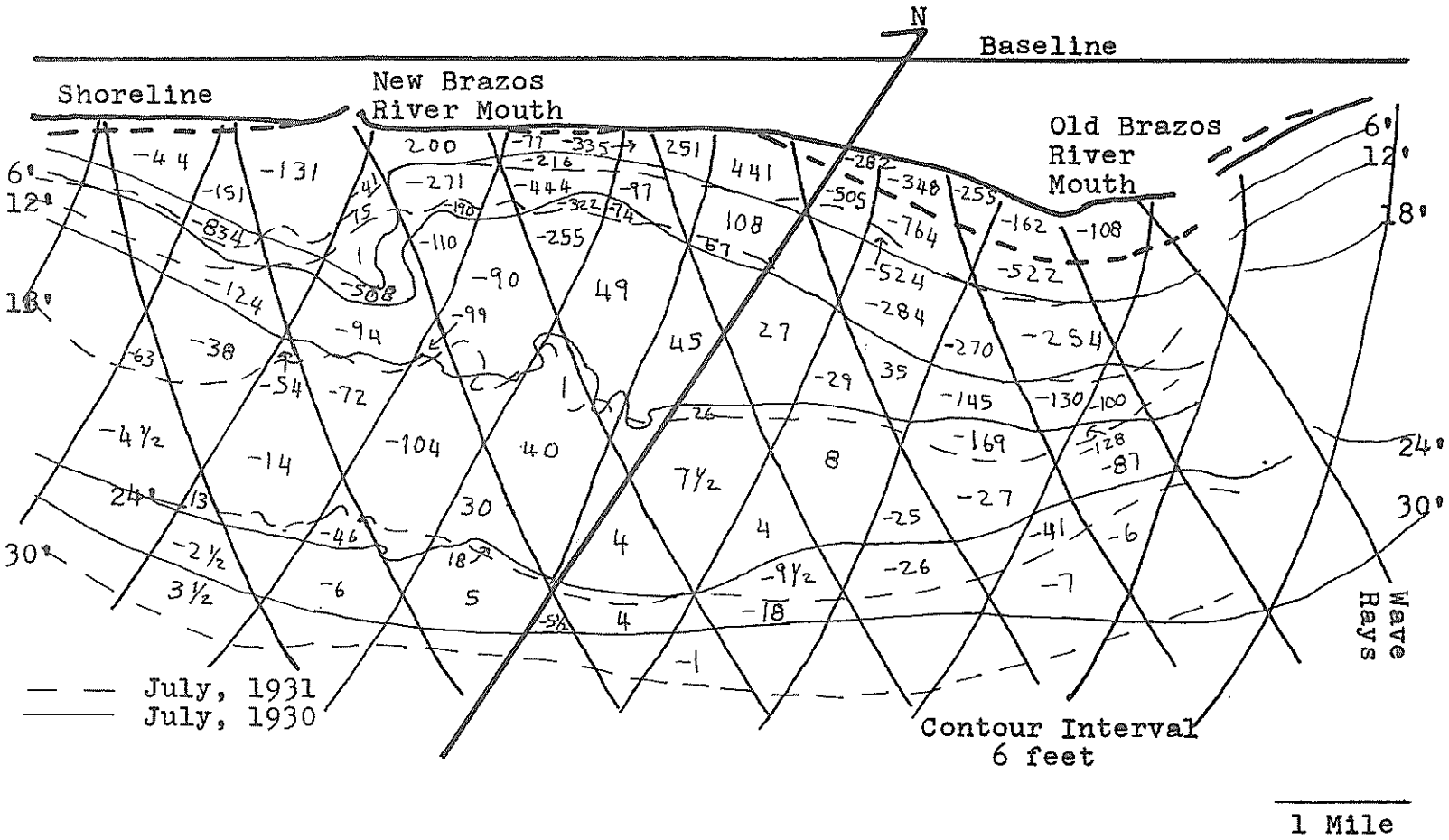

Fig. 48. Combined sediment displacement potential for the time interval July, 1930 to July, 1931. Potential values in feet X 10^6.

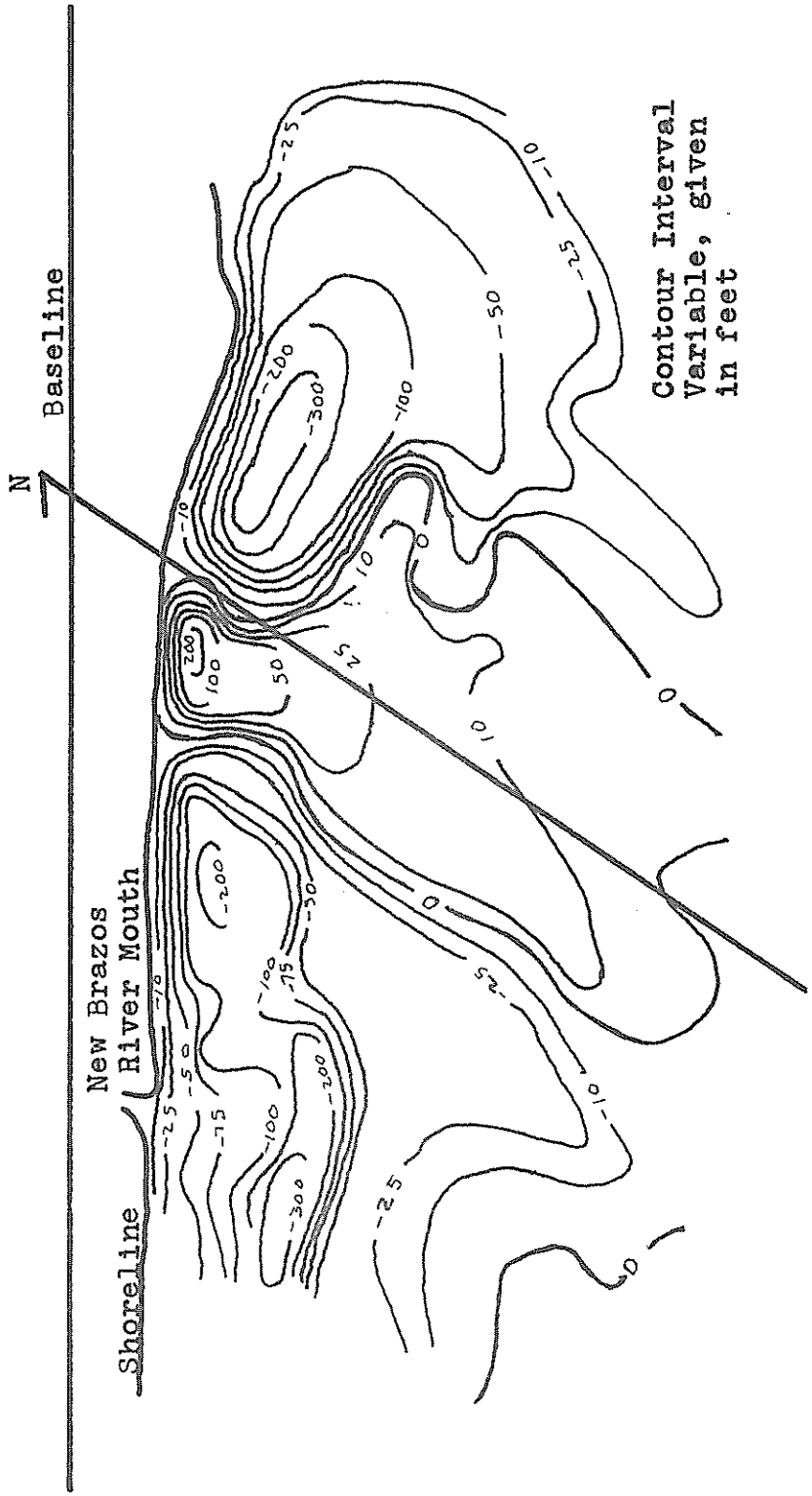

Fig. 49. Sediment displacement potential calculated for the time interval July, 1930 to July, 1931. Potential values given in feet X 10^6.

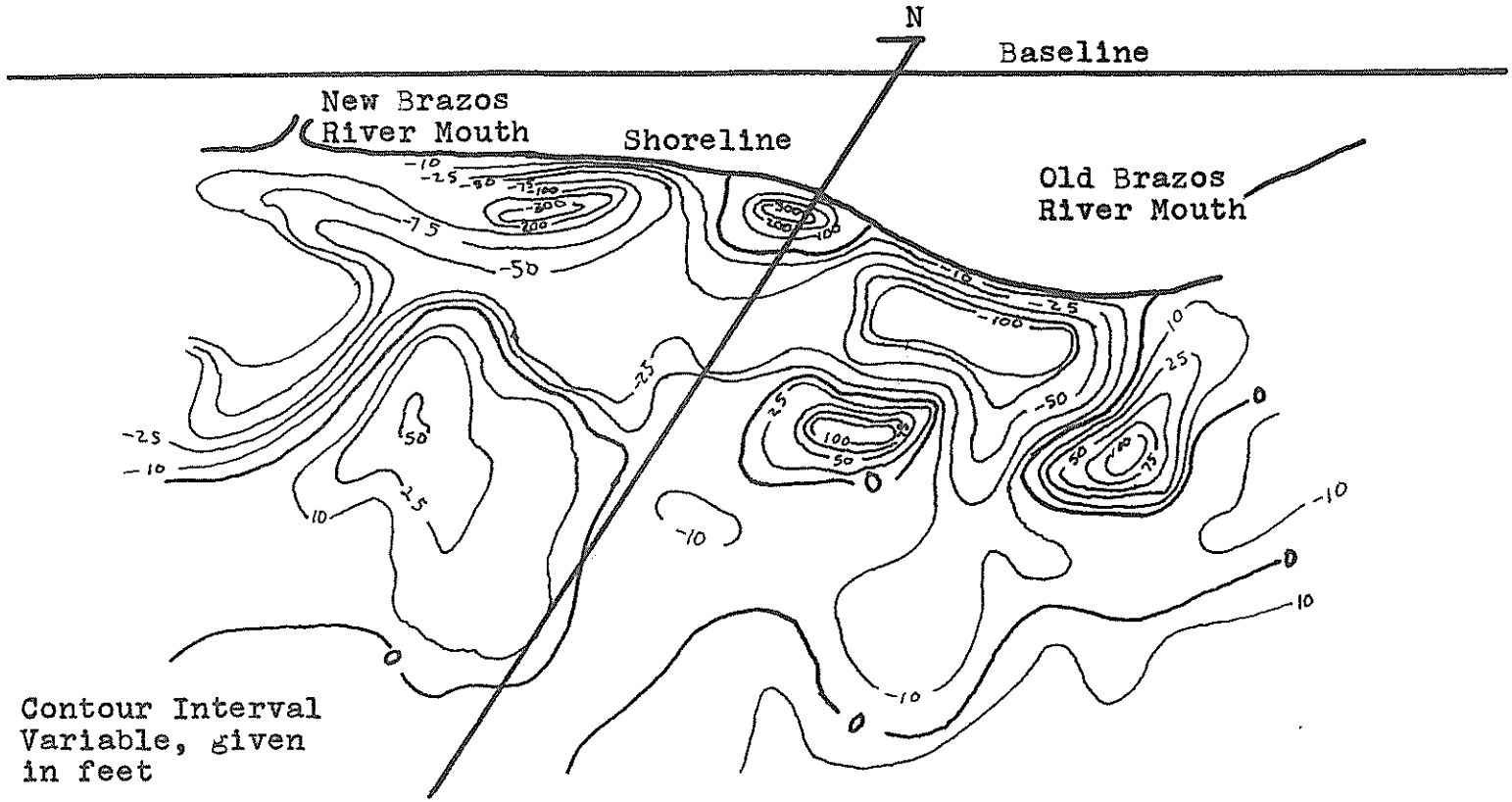

Fig. 50. Sediment displacement potential calculated for the time interval July, 1931 to June, 1932. Potential values given in feet X 10^6.

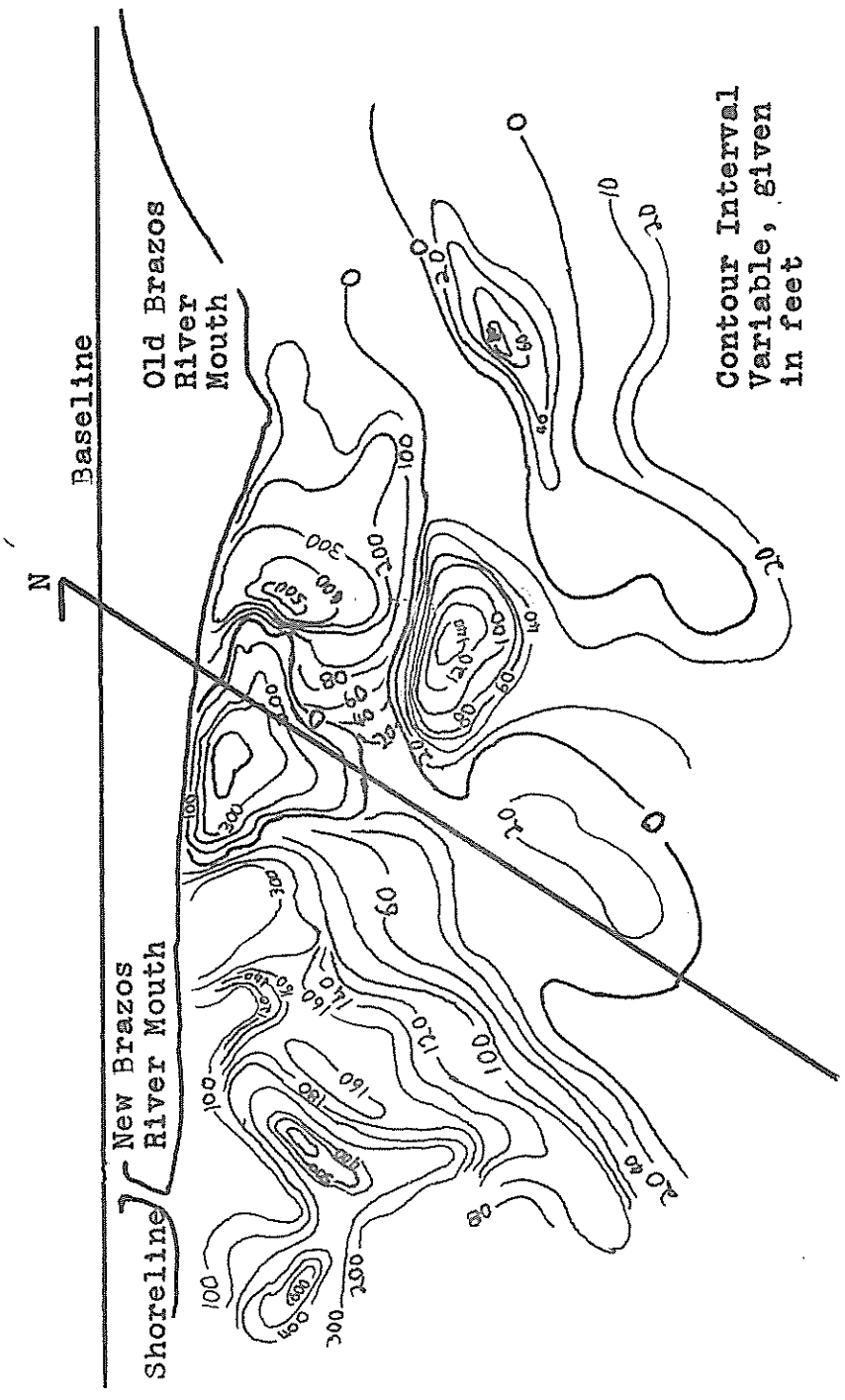

Fig. 51. Sediment displacement potential calculated for the time interval July, 1930 to June, 1932. Potential values given in feet X 10^6.

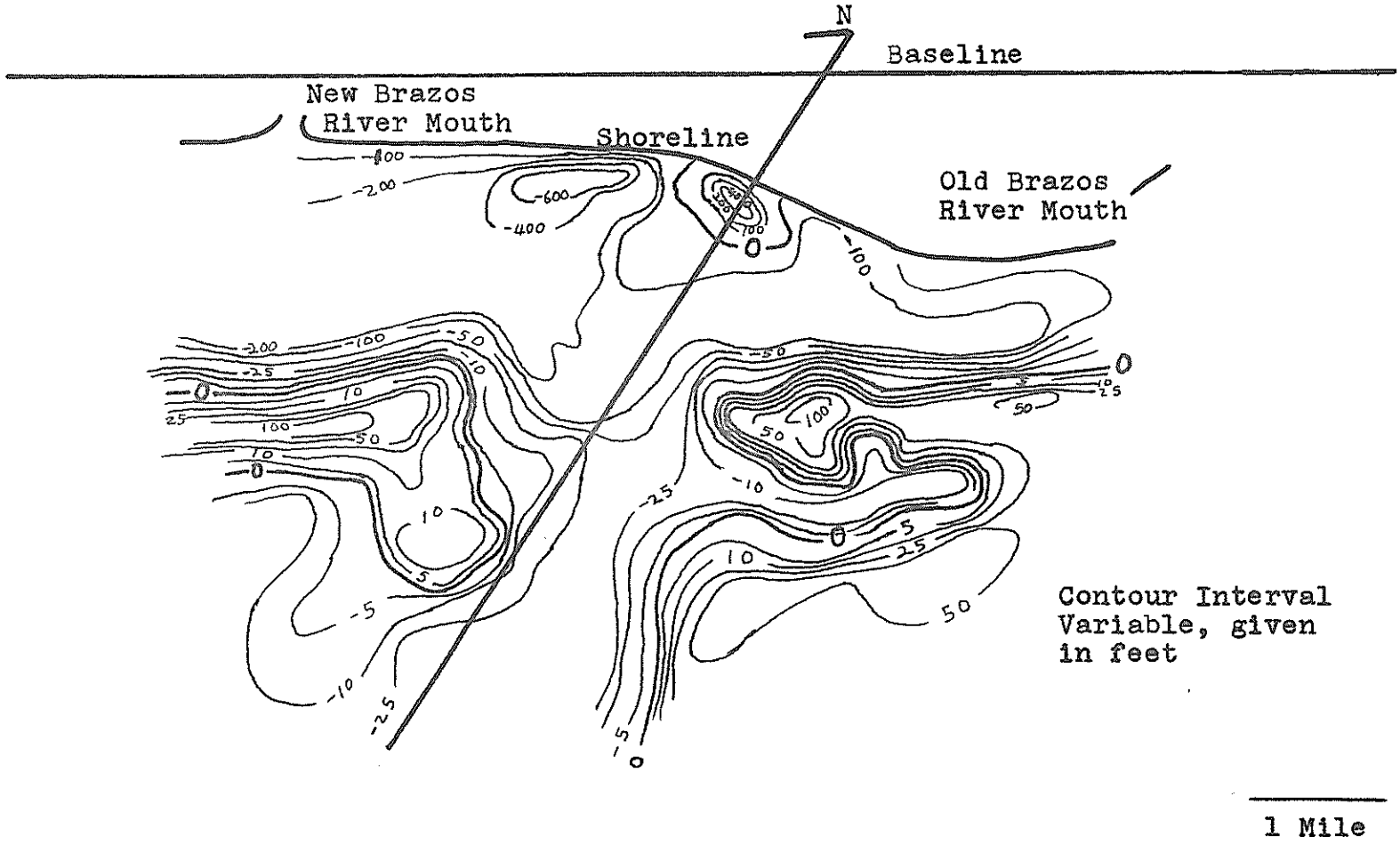

Fig. 52. Sediment displacement potential calculated for the time interval June, 1932 to October, 1934. Potential values given in feet X 10^6.

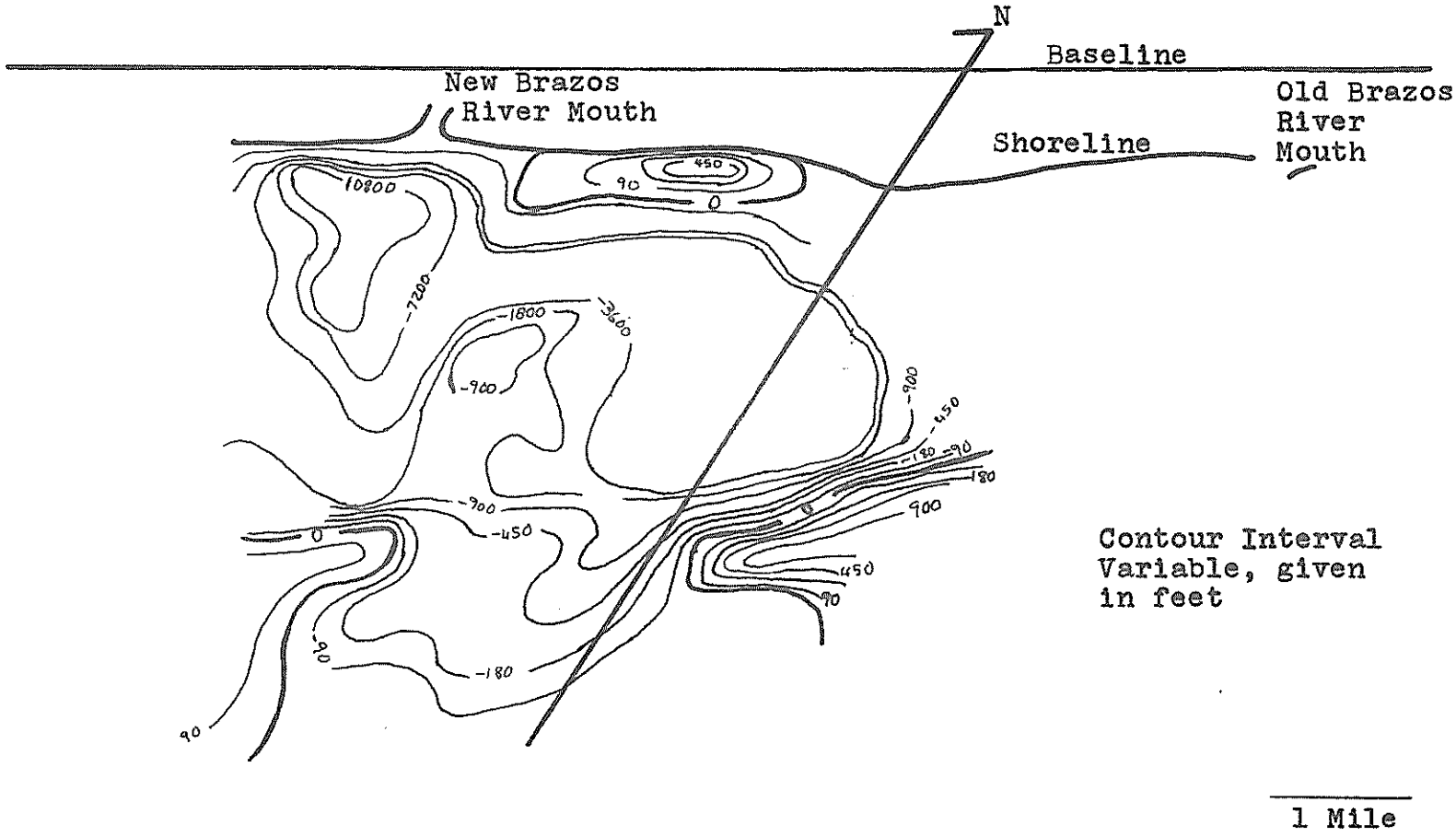

Fig. 53. Sediment displacement potential calculated for the time interval August, 1937 to May, 1973. Potential values given in feet X 10^6.

1930 to June 1932; June, 1932 to October, 1934; and August, 1937 to May, 1973. Figure 54 is a similar map contoured on the values calculated for 1973 alone.

The Erosional Correction Factors

One of the original assumptions made in this approach was that 100% of the friction-dissipated wave energy caused sediment movement, with no energy loss. This was obviously not a valid assumption, and a correction factor must be found which correlates the actual sediment erosion and deposition rates to those predicted. To facilitate this process, isopach maps have been drawn from the charts for time periods which coincide with those in Figures 49 through 53. These are given in Figures 55 through 59.

In order to choose a correction factor Figures 50 and 56, the actual and predicted depth changes for July, 1931, to June, 1932, were compared. This time interval was chosen at random as the control interval. The deposition of the Brazos River has not yet been added to the sediment displacement potential map, so that the areas which should reasonably be expected to coincide are those negative values on the two maps. Note that the ratio of the predicted erosion values to the actual values is much

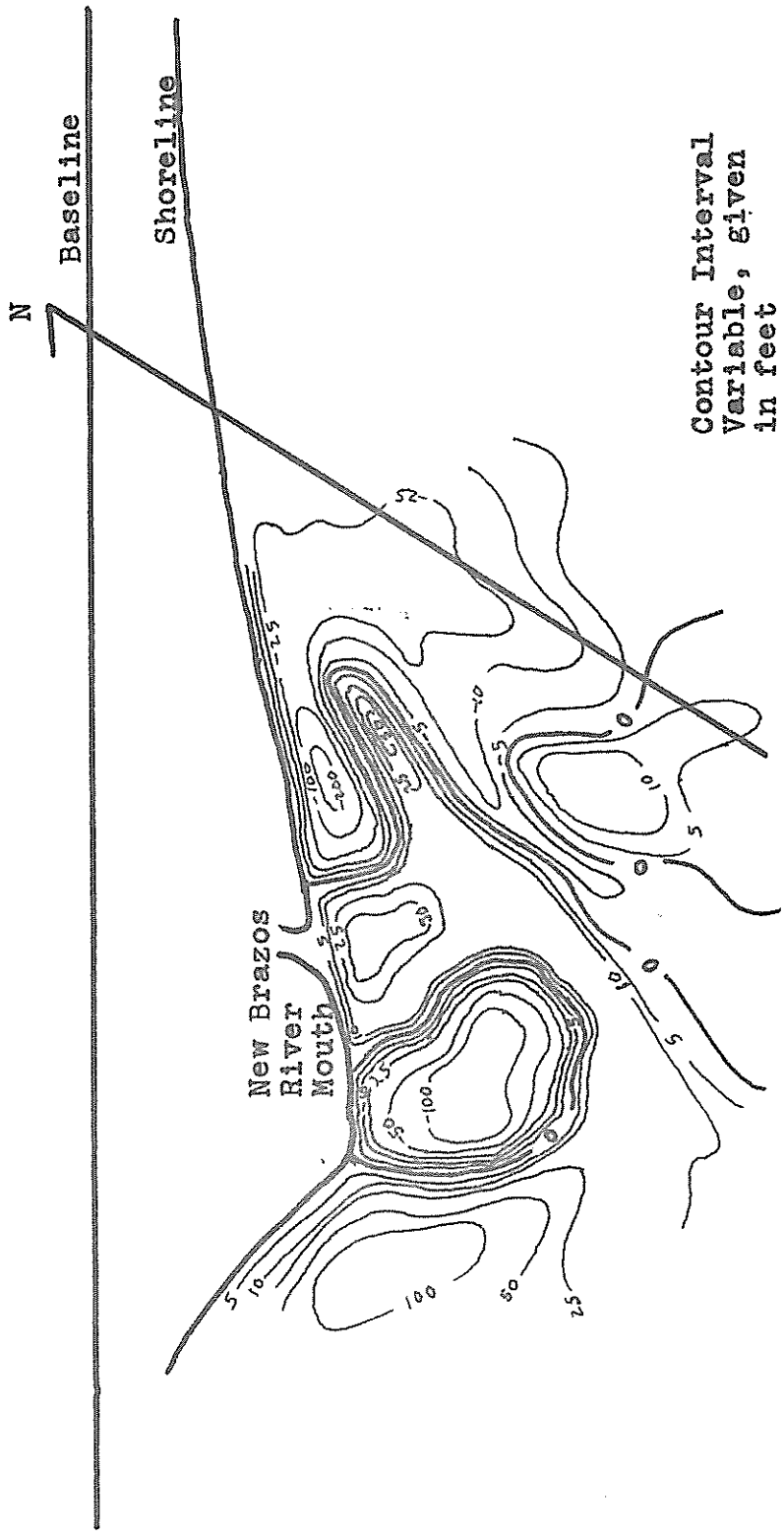

Fig. 54. Sediment displacement potential calgulated for 1973.
Potential values given in feet X 10⁶.

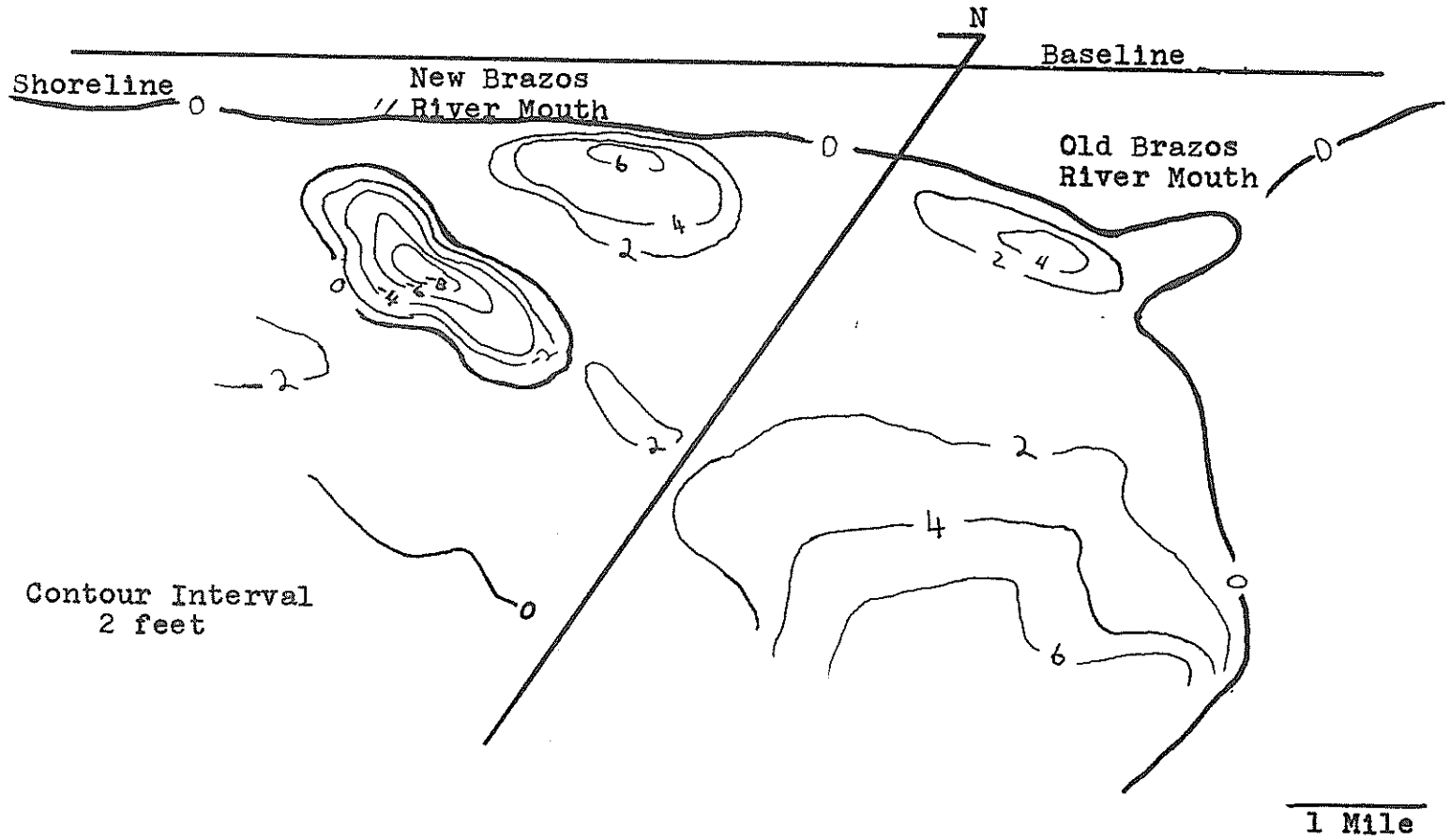

Fig. 55. Isopach map for the time interval July, 1930 to July, 1931.

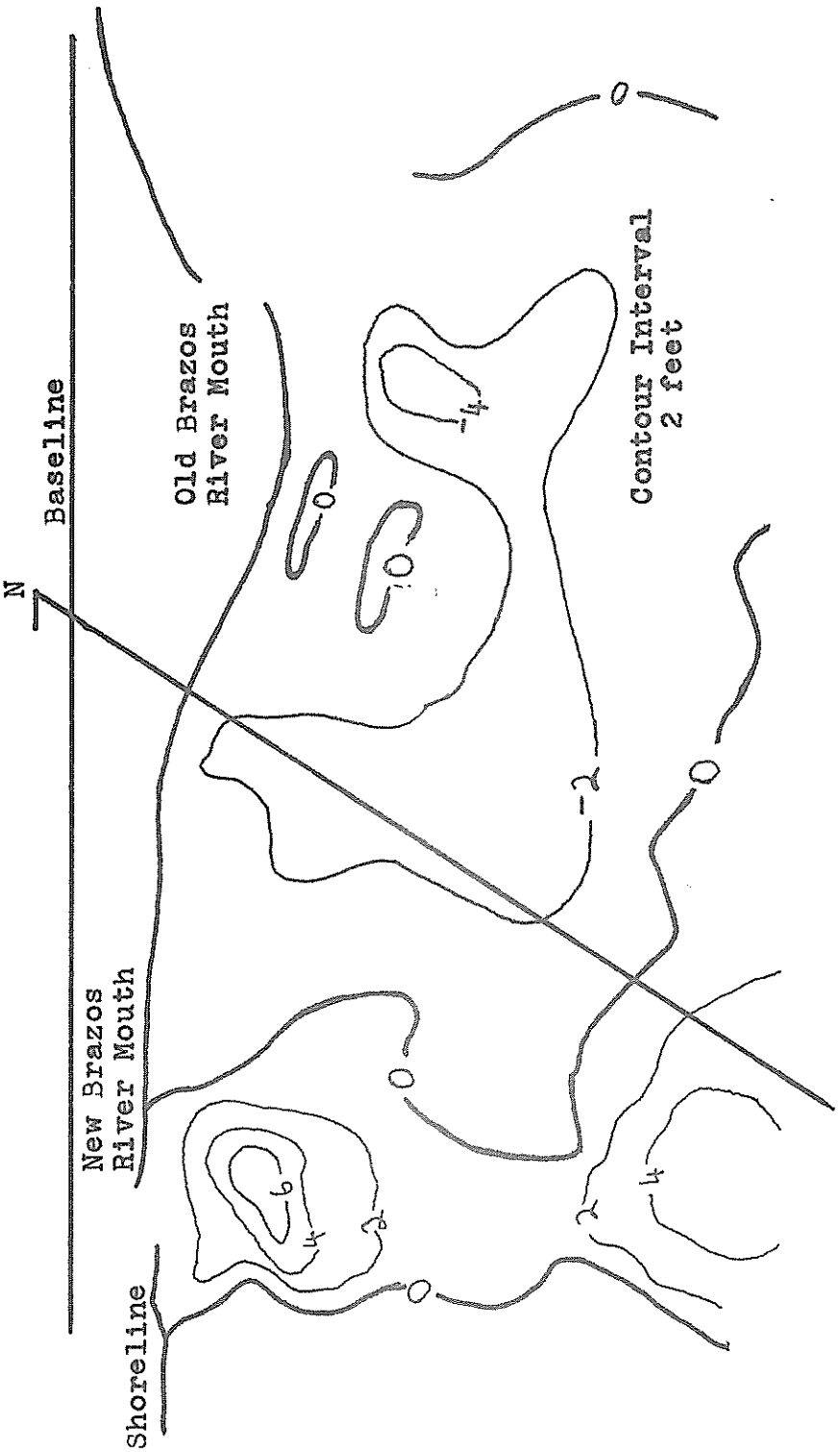

Fig. 56. Isopach map for the time interval July, 1931 to June, 1932.

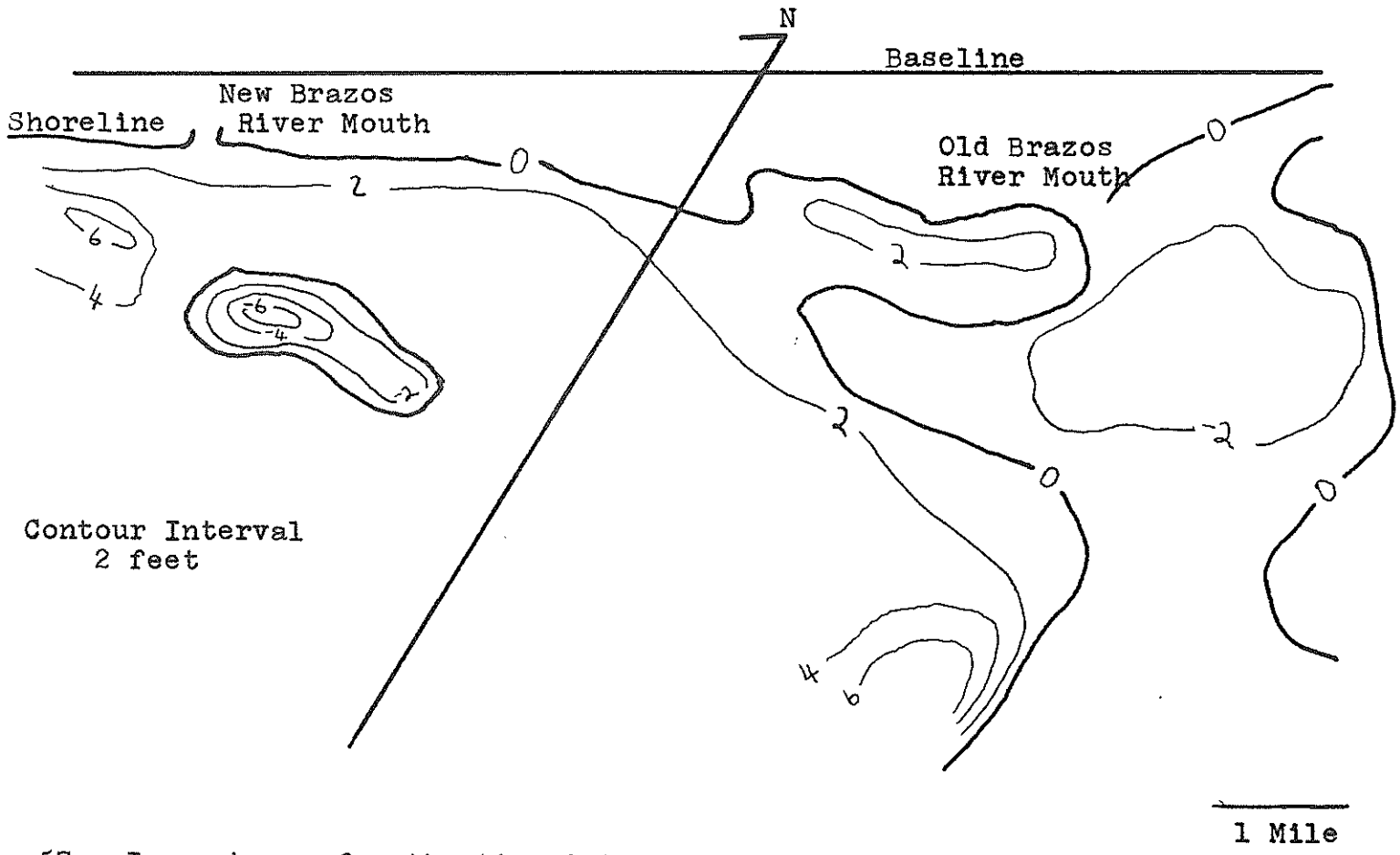

Fig. 57. Isopach map for the time interval July, 1930 to June, 1932.

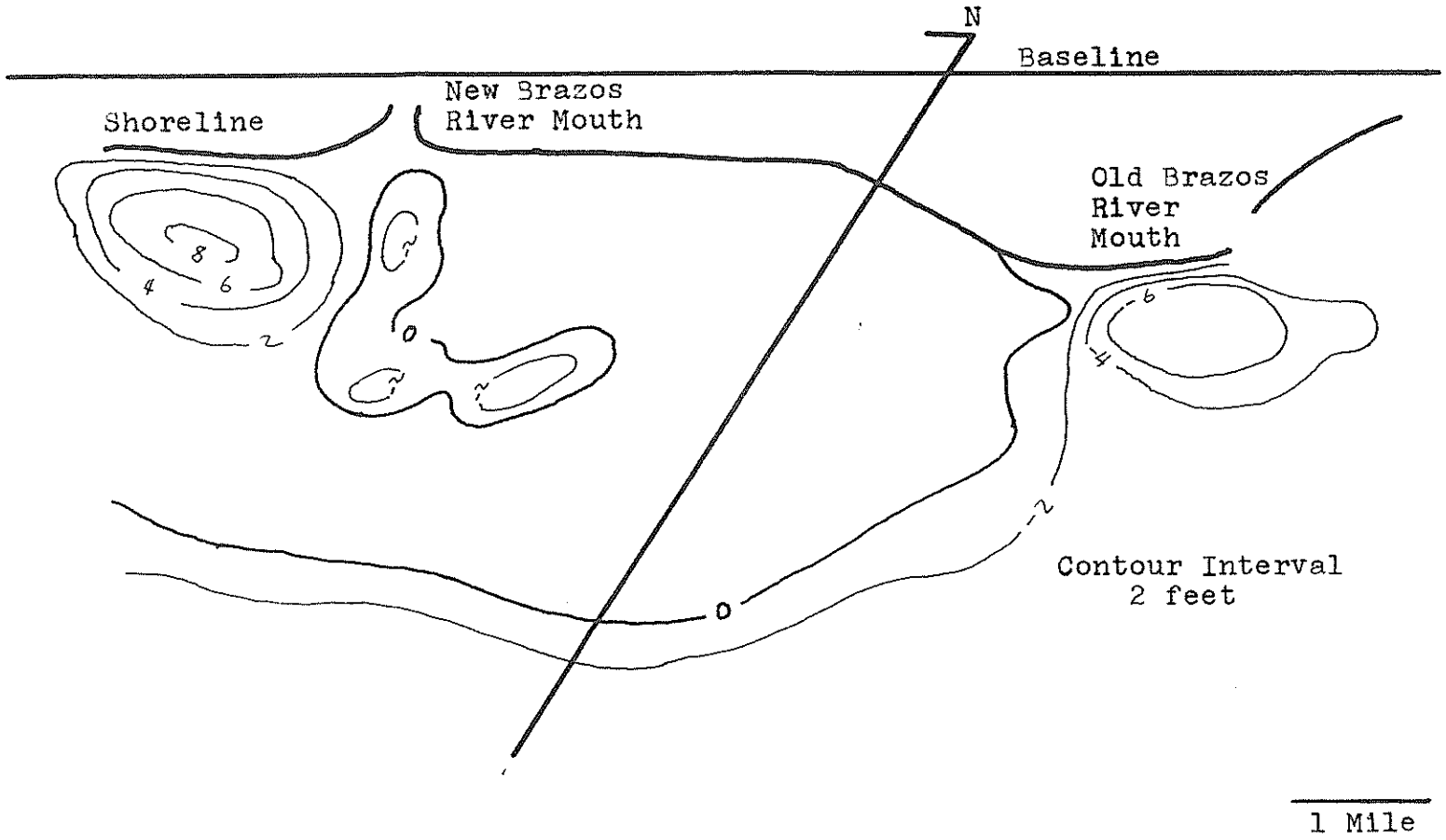

Fig. 58. Isopach map for the time interval June, 1932 to October, 1934.

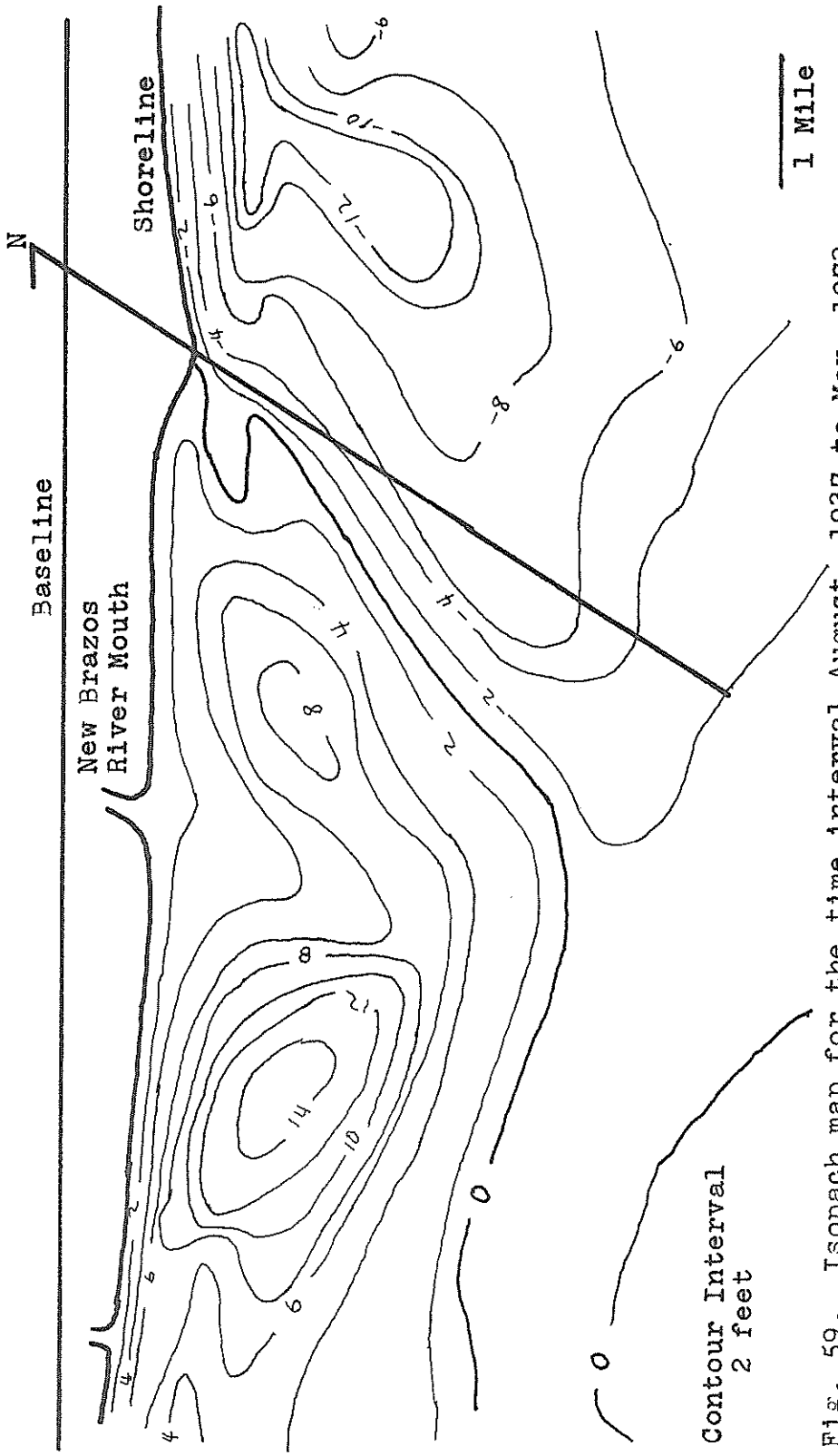

Fig. 59. Isopach map for the time interval August, 1937 to May, 1973.

higher nearshore than offshore. This is an would be expected; much more of the wave energy dissipated at the 6' depth should be lost in internal and surface turbulence and heat than is lost in this manner at deeper contours. For this reason, different correction factors were applied to Figure 57 for each of the depth intervals 0-6 feet, 6-12 feet, 12-18 feet, 18-24 feet and 24-30 feet; the contours used were those of July, 1931. The correction factors were found to be $2/150 \times 10^6$, $2/150 \times 10^6$, $2/25 \times 10^6$, $2/5 \times 10^6$) and $2/10^7$, where the shallow water correction factor is listed first. These correction factors were then applied to each of the Figures 55, 57, 58, 59, using the bottom contours of the first year of each time interval to determine where the correction factors should be applied. The results, corrected sediment displacement potentials, are shown in Figures 60, 61, 62, 63 and 64. Figure 65 is the corrected sediment displacement potential based on the 1973 map alone.

The Depositional Correction Factor

The patterns of deposition of the suspended load for each of the time intervals were calculated using Equation 27, with the distribution as was shown in Figure

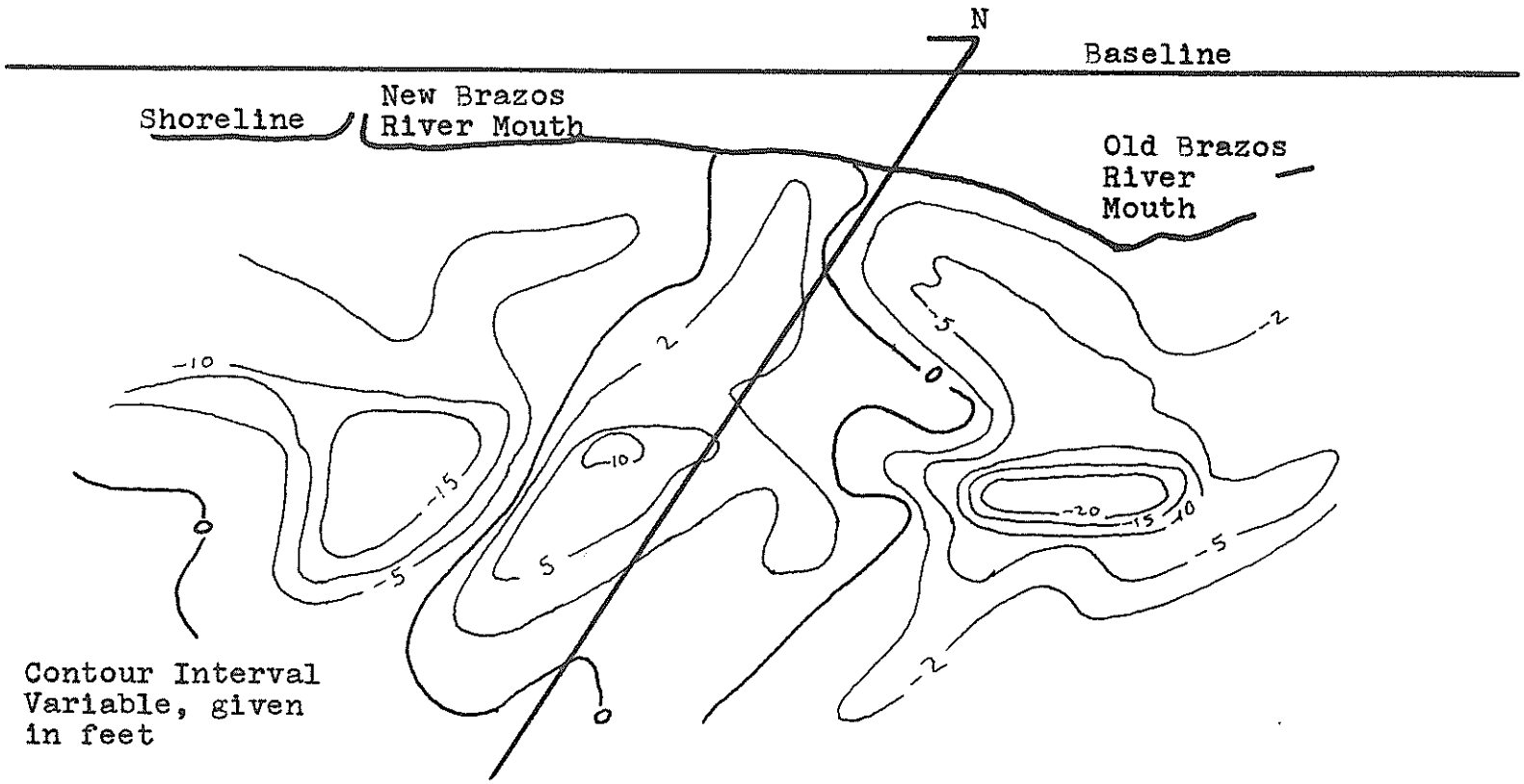

Fig. 60. Corrected sediment displacement potential calculated for the time interval July, 1930 to July, 1931.

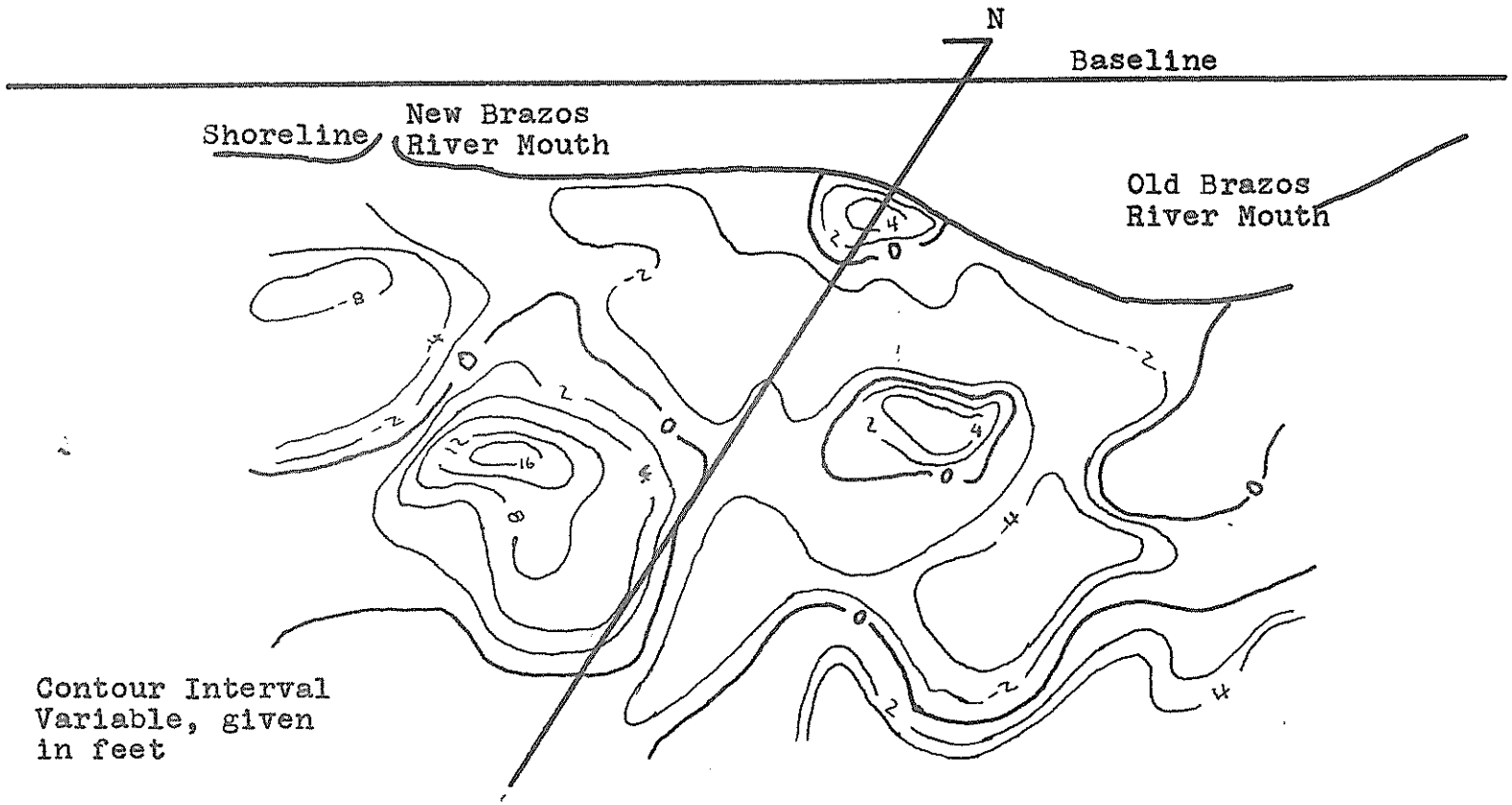

Fig. 61. Corrected sediment displacement potential for the time interval July, 1931 to June, 1932.

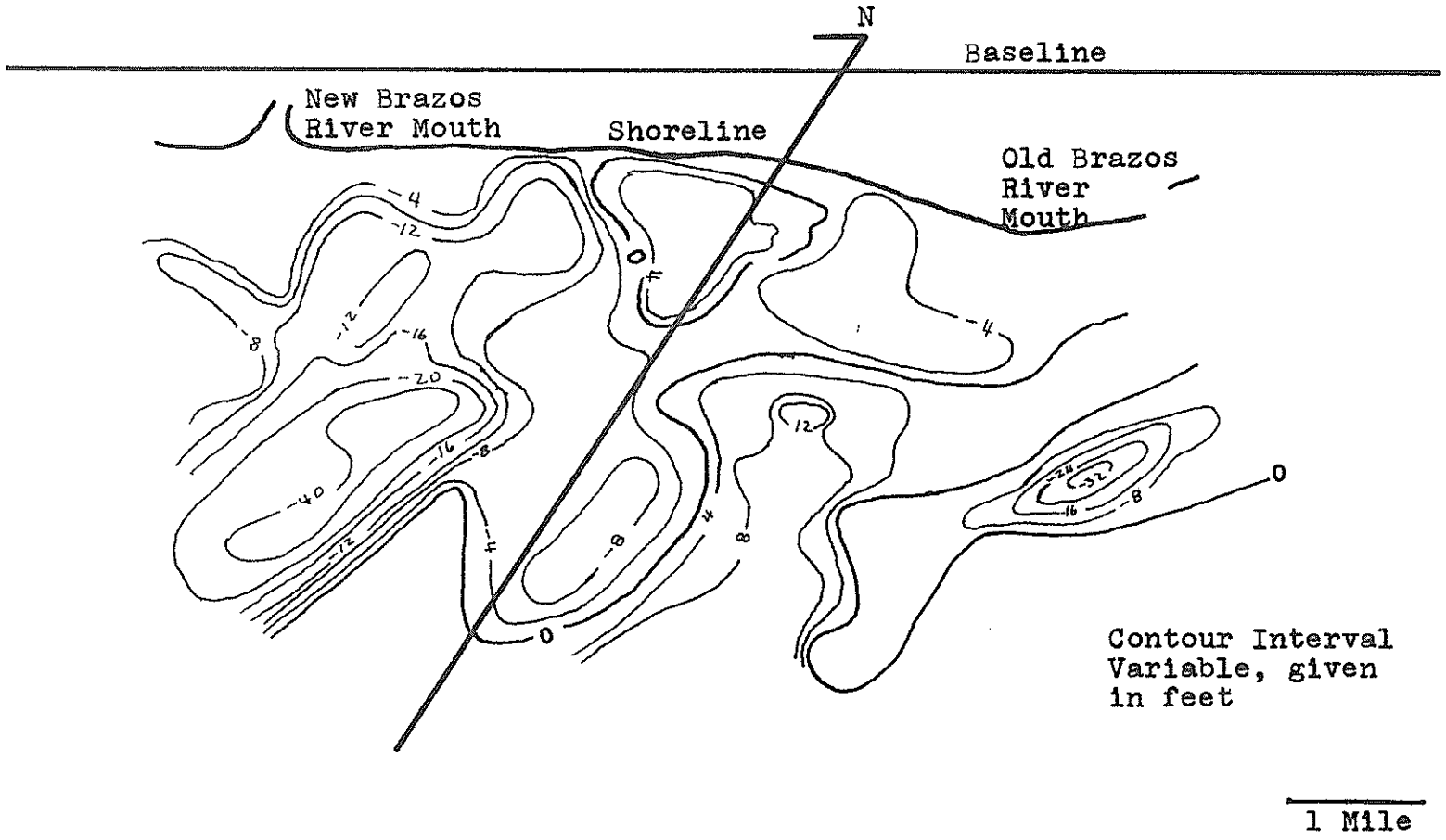

Fig. 62. Corrected sediment displacement potential for the time interval July, 1930 to June, 1932.

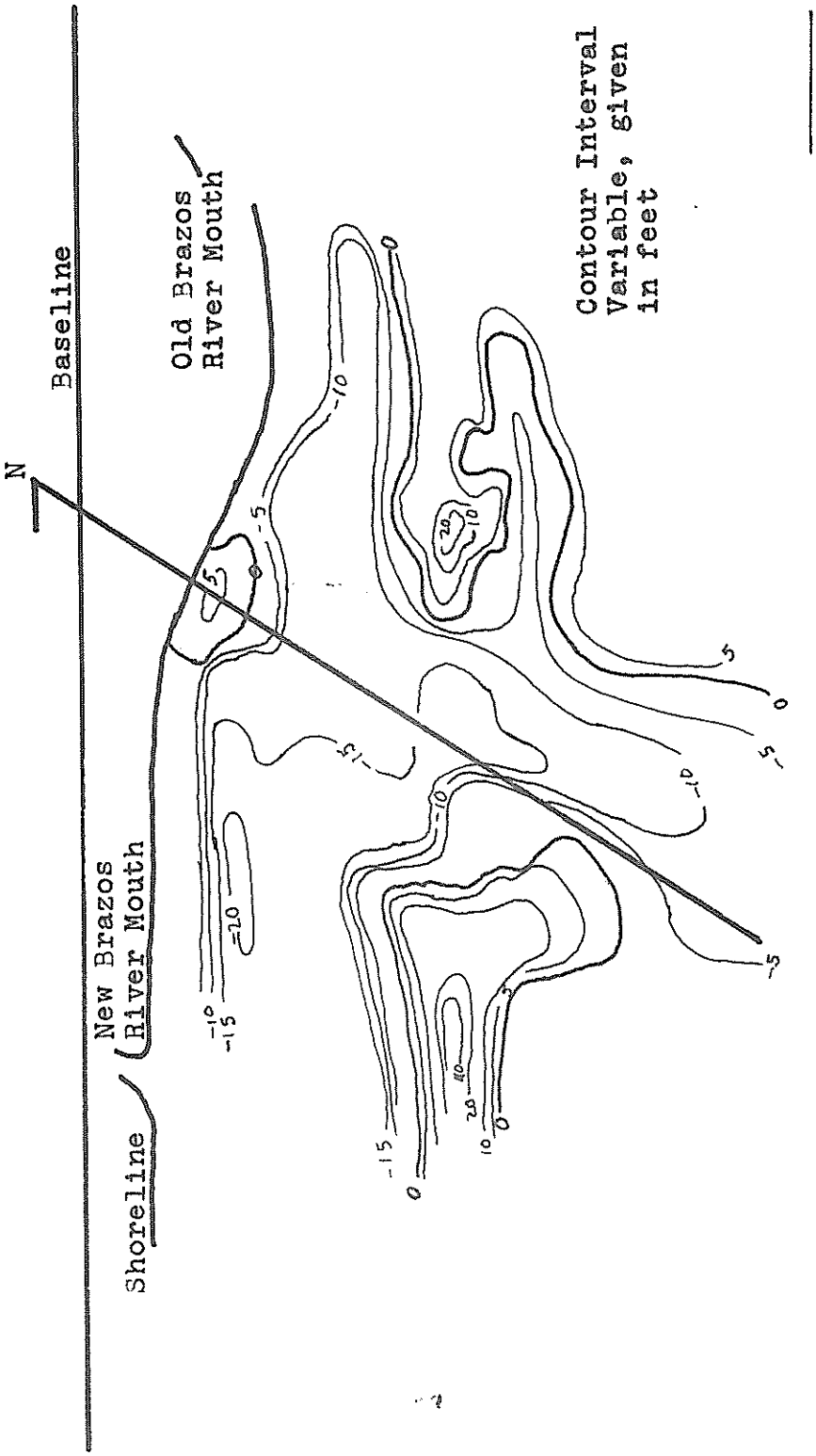

Fig. 63. Corrected sediment displacement potential for the time interval June, 1932 to October, 1934.

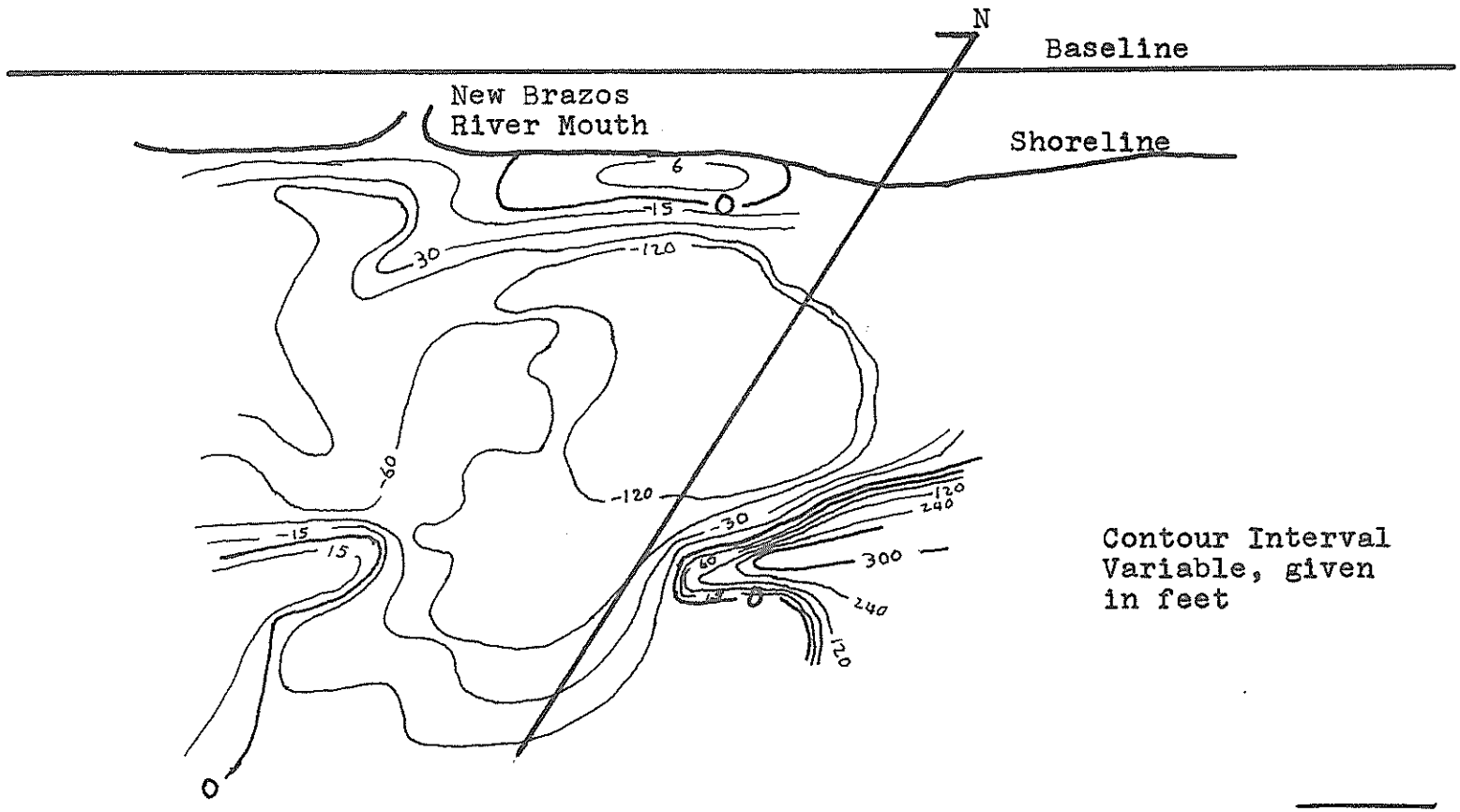

Fig. 64. Corrected sediment displacement potential for the time interval August, 1937 to May, 1973.

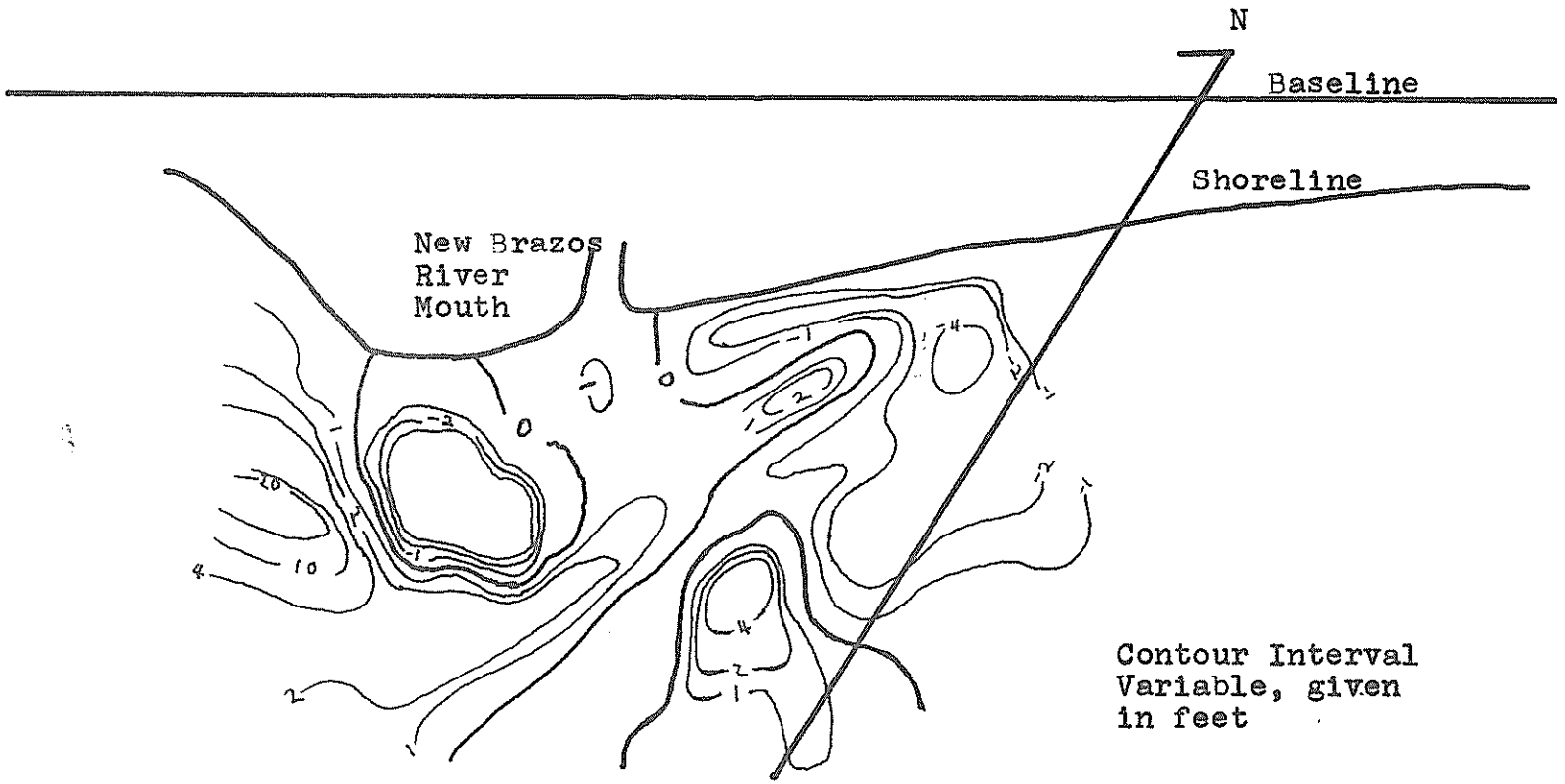

Fig. 65. Corrected sediment displacement potential for 1973.

21d. The bedload deposition pattern was also calculated using Equation 27; however, it was assumed that bedload deposition pattern would be circular rather than elliptical, as the entire bedload would tend to be deposited at the river mouth where the streamflow becomes completely separated from the bed by denser Gulf waters. The deposition patterns for the time intervals July, 1930 to July, 1931; July, 1931 to June, 1932; July, 1930 to June, 1932; June, 1932 to October, 1934; and August, 1931 to May, 1973 are shown in Figures 66, 67, 68, 69 and 70.

Comparison of Figures 66 through 70 with the isopach maps (Figs. 55 through 59) shows that the predicted deposition rates are much higher than the observed rates. This discrepancy has two probable causes: 1) the assumption that deposition is linearly related to decreasing velocities, and 2) the assumption that 10% of the total sediment is lost in the delta. Inspection of Figure 8 or Figure 14 shows that stream velocity is not linearly related to the suspended sediment concentration; thus it is not correct to assume at the point in the Gulf where, according to Bates (1957), the "stream" has a velocity of $V_o/2$, that the suspended sediment concentration will be equal to $C_{so}/2$. There is no known way of estimating a true relationship. Therefore, the method chosen was to

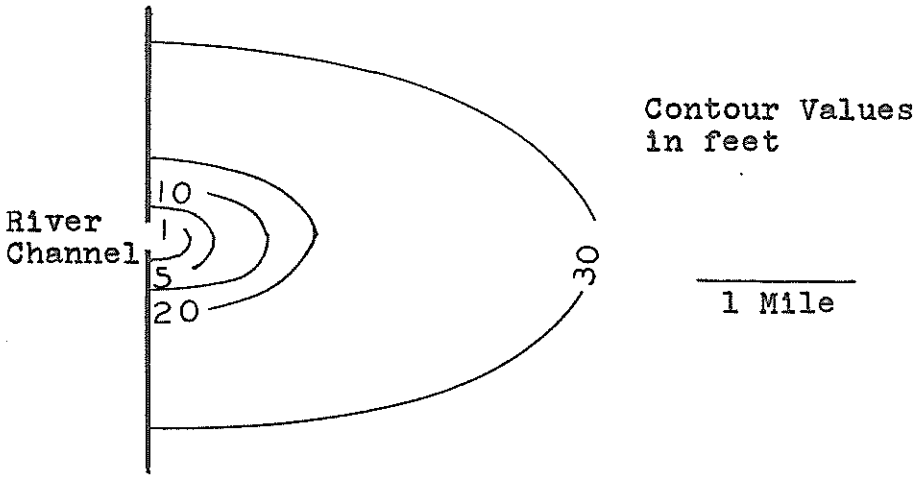

Fig. 66. Isopach map of the deposition of the Brazos River sediment load for the time interval July, 1930 to July, 1931.

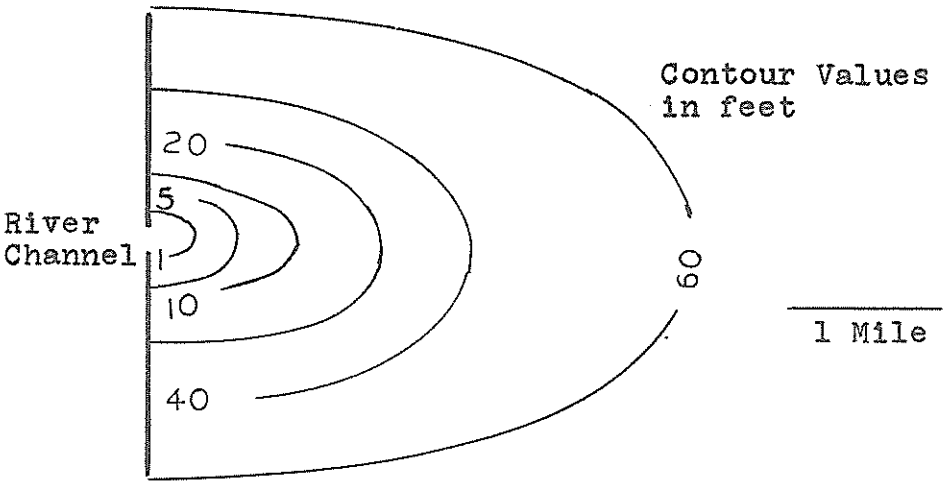

Fig. 67. Isopach map of the deposition of the Brazos River sediment load for the time interval July, 1931 to June, 1932.

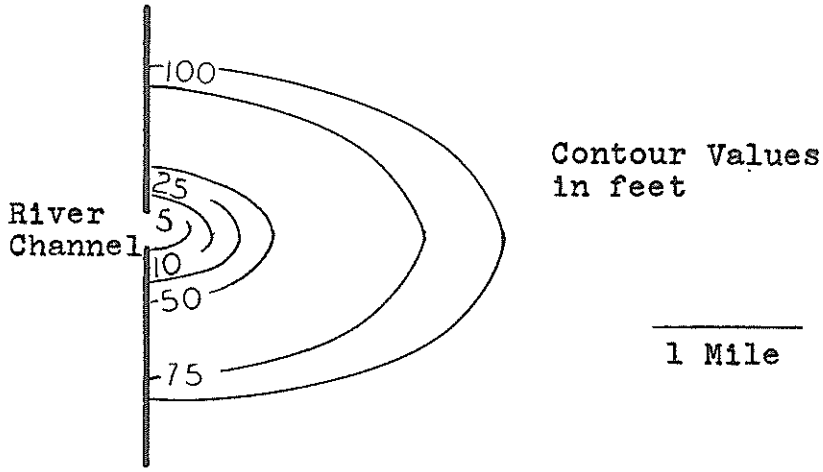

Fig. 68. Isopach map of the deposition of the Brazos River sediment load for the time interval July, 1930 to June, 1932.

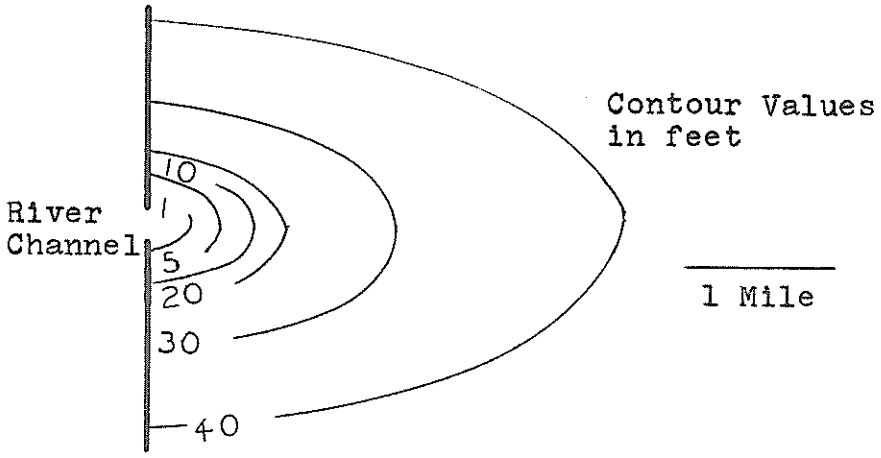

Fig. 69. Isopach map of the deposition of the Brazos River sediment load for the time interval June, 1932 to October, 1934.

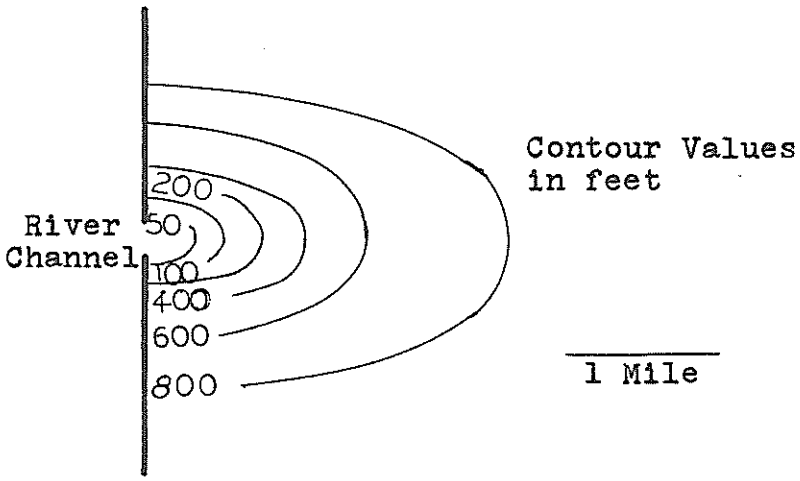

Fig. 70. Isopach map of the deposition of the Brazos River sediment load for the time interval August, 1937 to May, 1973.

assume direct proportionality and then to use a correction factor for correlation of the predicted and observed values. The second cause is related to the first: if the sediment does not fall out of suspension at as fast a rate as has been predicted, obviously more is lost to the delta region, either through the Bates stream type flow or through a diffusion process. The correction factor method does not point out the cause of the discrepancies.

To apply a correction factor, the time interval July, 1931 to June, 1932, was again chosen as a control year. A comparison of Figures 67, 56 and 61 shows that a best fit is obtained if it is assumed that 23% of the predicted deposition actually takes place; this means that approximately 20.7% of the total sediment load is deposited, the rest being lost to the delta. This would seem to indicate that much more sediment than was initially assumed flows out past the delta with the river flow.

It was noted that in most cases the isopach maps showed the highest rate of deposition offshore from the mouth rather than directly at the mouth; therefore, to achieve a best fit of the predicted and observed depositional patterns for the control year, it was assumed that the baseline in Figure 67 was approximately 1/2

mile directly offshore from the river mouth. This same correction factor was then applied to figures 66, 68, 69 and 70. After contouring to the points of intersection of the contours on two or more figures, the corrected Figures 66 through 70 with Figures 60 through 64, the final results shown in Figures 71 through 75 were obtained. These are the calculated isopach maps for the time intervals July, 1930 to July, 1931; July, 1931 to June, 1932; July, 1930 to June, 1932; June, 1932 to October, 1934; and August, 1937 to May, 1973, respectively.

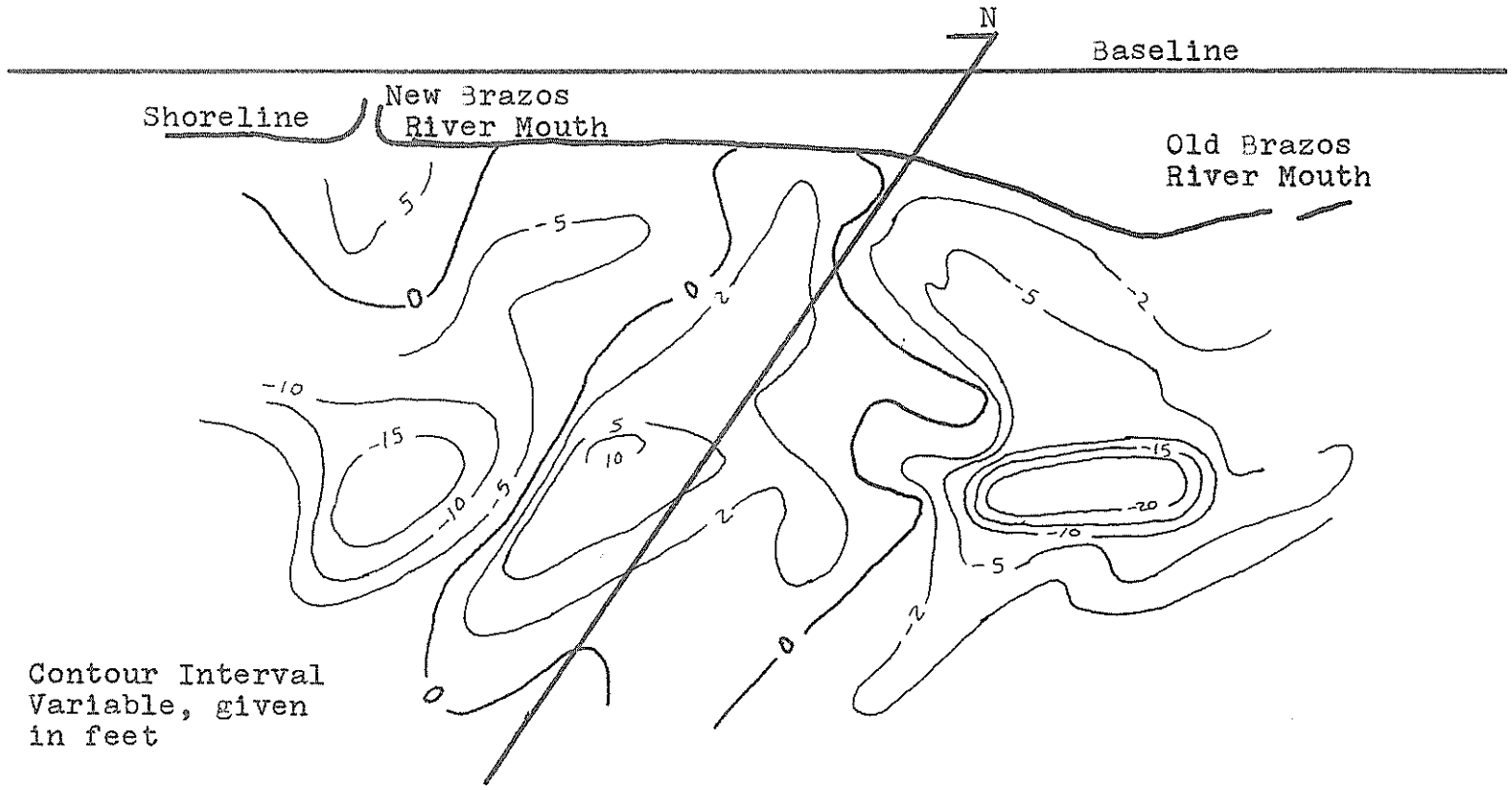

Fig. 71. Calculated isopach map for the time interval July, 1930 to July, 1931.

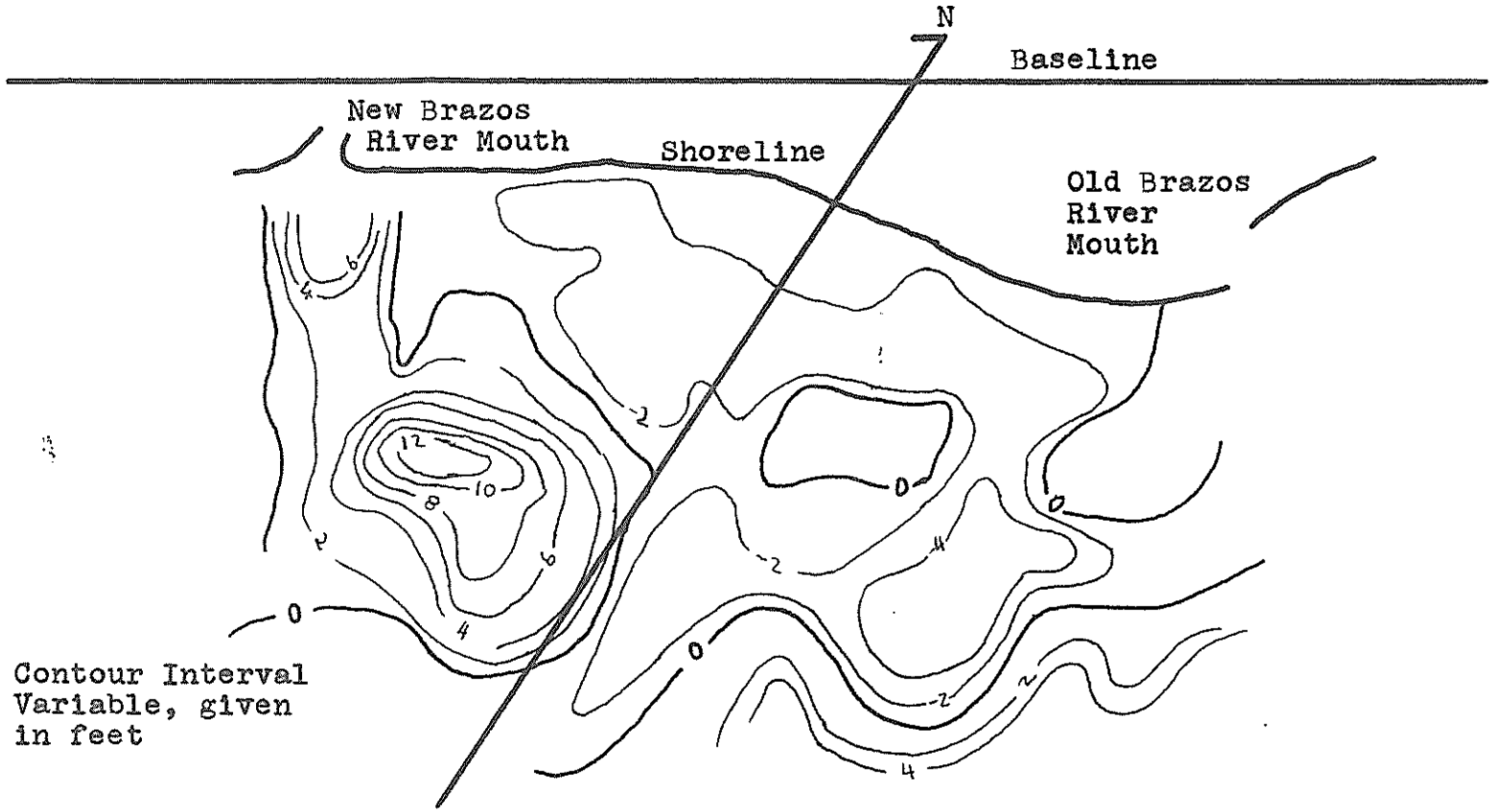

Fig. 72. Calculated isopach map for the time interval July, 1931 to June, 1932.

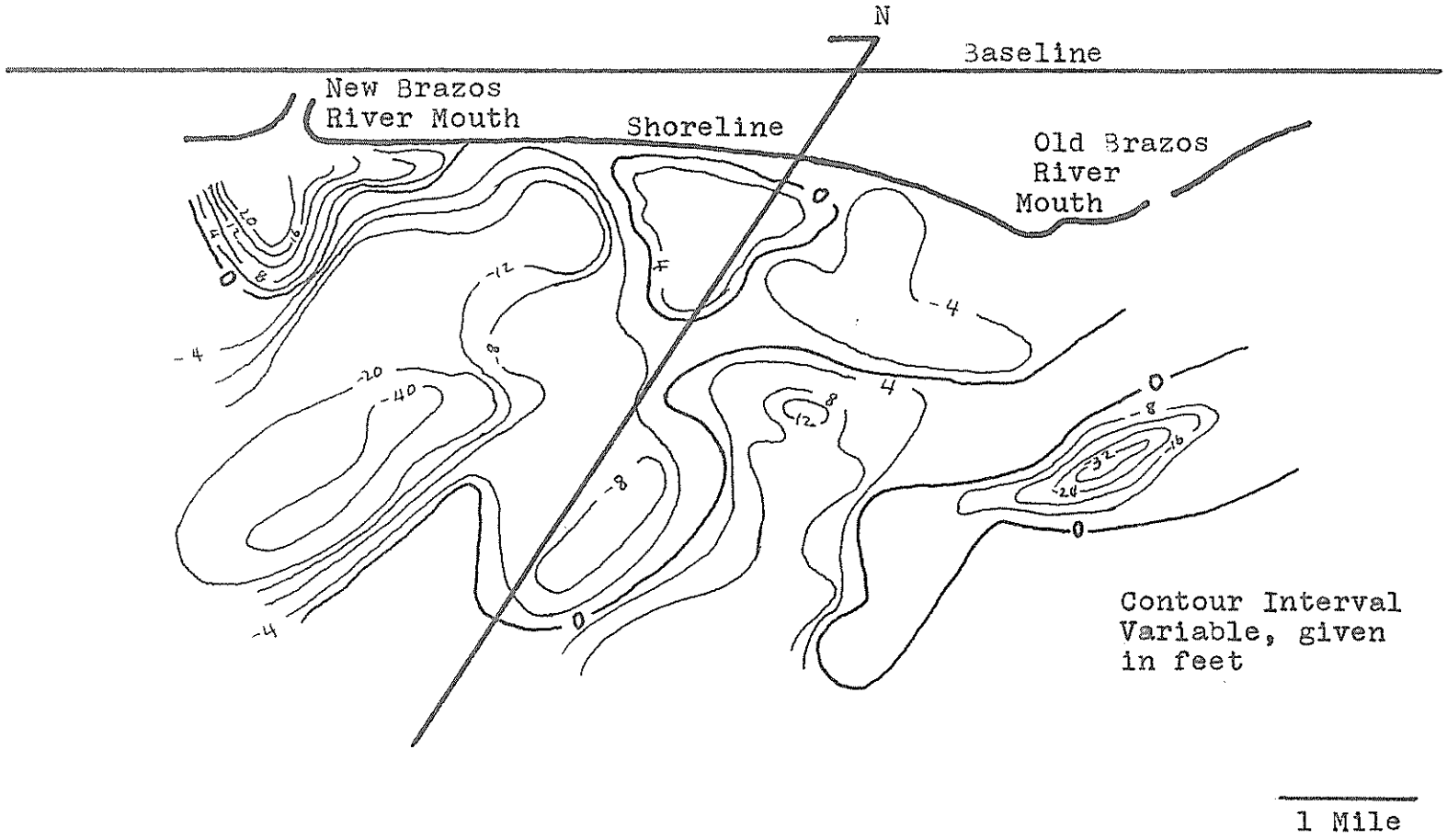

Fig. 73. Calculated isopach map for the time interval July, 1930 to June, 1932.

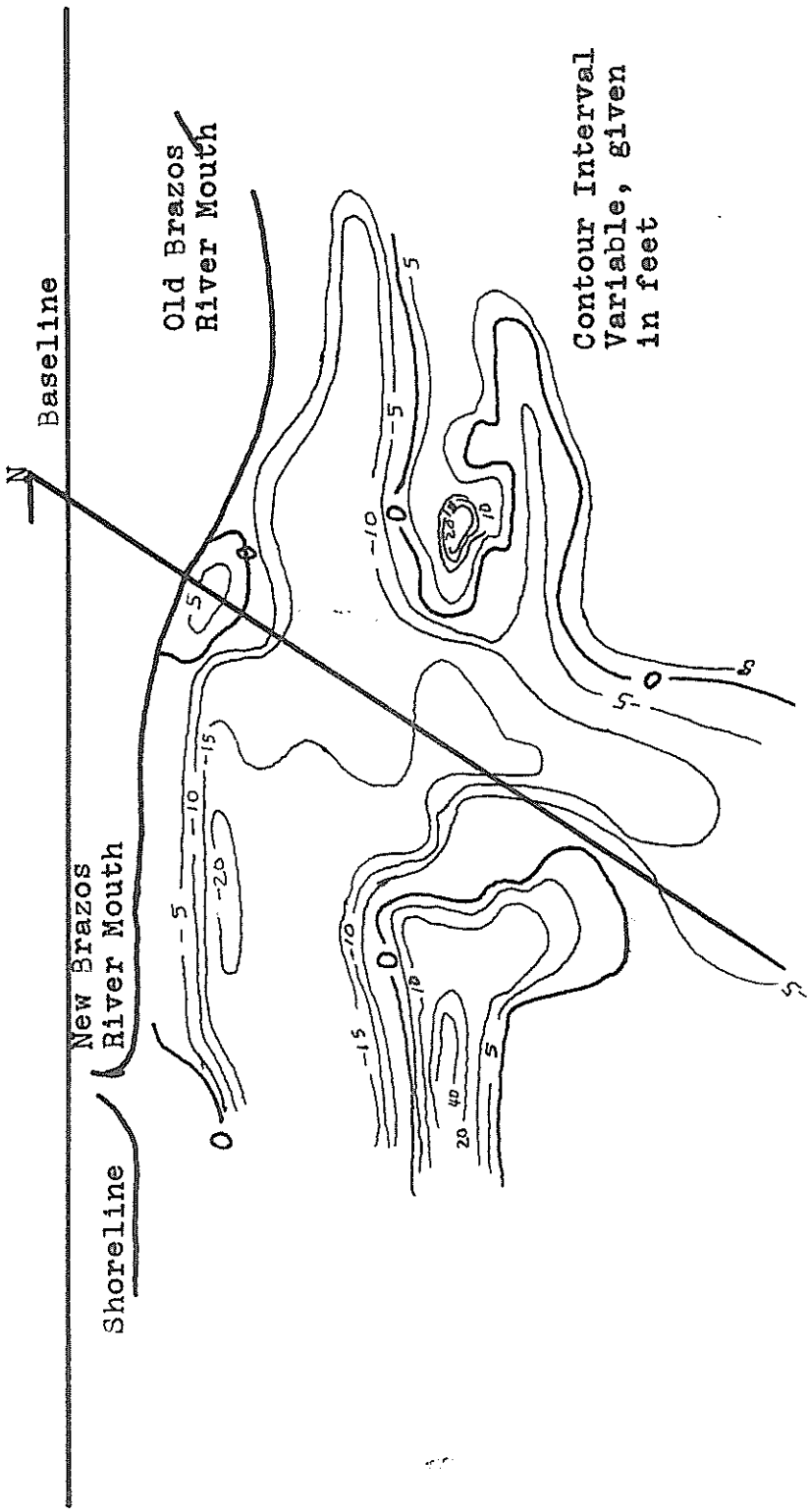

Fig. 74. Calculated isopach map for the time interval June, 1932 to October, 1934.

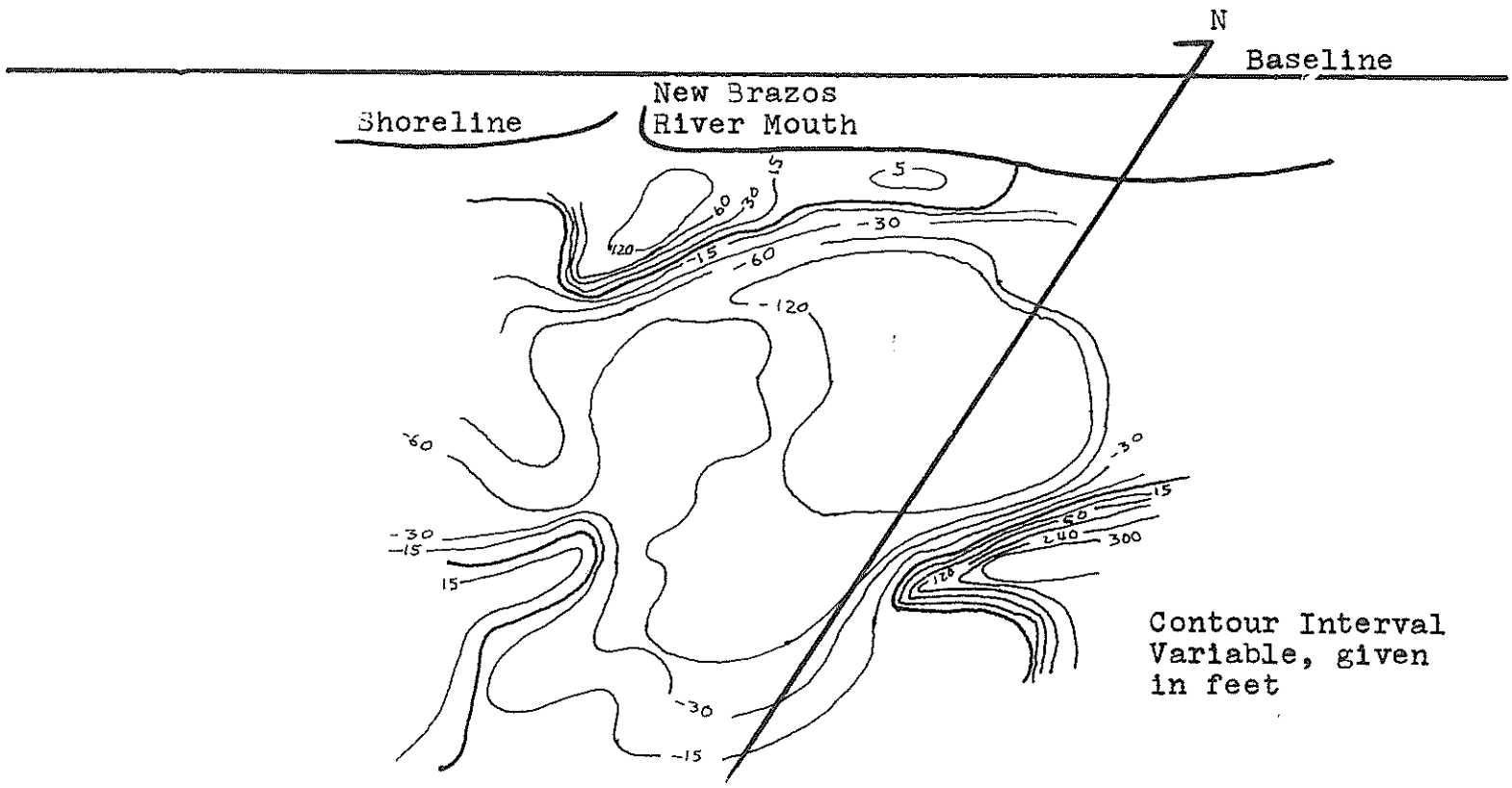

Fig. 75. Calculated isopach map for the time interval August, 1937 to May, 1973.

RESULTS

The calculated and observed isopach maps (Figs. 56 and 69) for the control year, July, 1930 to July, 1931, are very similar. They differ only in the thickness of the center of deposition furthest offshore; the thickness (12') of the predicted isopach map is due to deposition by the longshore current, as is shown by the high positive values in this area on Figure 50. The broadening of this positive area on the isopach map is related to longshore current activity because the area is too far offshore to be directly related to river deposition. The close fit of these maps is to be expected in that the calculated map was corrected to give as close a fit as possible. However, the closeness of the trends, regardless of the scaling effect of the correction factor, indicates that the method used in this thesis is effective in delineating the areas in which deposition and erosion should occur.

A comparison of Figures 68 and 55, the maps for the year July, 1930 to July, 1931, once again shows a general similarity in trend between the calculated and observed isopachs. Both maps show an area of erosion offshore from the area of primary deposition, with a wide area of deposition to the northeast of the river mouth. The cal-

culated isopach map shows the erosion which would be expected at the site of the old delta; this erosion is not observed on the isopach map, however.

The maps calculated for the time period July, 1930 to June, 1932, were made independently of those for July, 1930 to July, 1931, and July, 1931 to June, 1930, i.e., they were not constructed by cross-contouring those two maps. The calculated and observed isopach maps for this time interval, Figures 57 and 73, show a similarity of trend, but the fit is very poor. The calculated isopach map shows erosion at the site of the old Brazos River Delta, as does the observed isopach map. The observed isopach map shows a very broad positive area and a small negative area seaward and northeastward of the river mouth but on the calculated isopach map, the negative area is much broader and shows much more predicted erosion offshore from the river mouth. Nonetheless, the trends shown in both maps are similar.

The calculated and observed isopach maps for the last two intervals, June, 1932 to October, 1934 (Figs. 74 and 58) and August, 1937 to May, 1973, are in no way similar in trend or in scale of erosion and deposition. There are several possible reasons for this: 1) the displacement correction factor applied may cease to be

applicable after a radical change in the shape of the contours when, for example, the slopes of the various depth intervals may be considerably different than they were in 1930-1932; 2) it is possible that the corrected annual bedload figures (Appendix I) are not high enough for years prior to 1945, and that the deposition correction factor, based on low numbers, led to an inordinately low estimate of deposition for the years following 1945; 3) the hurricanes which struck the Sargent-Freeport coastline during both of these intervals may have caused a complete reversal of normal deposition-erosion patterns, at least temporarily. Severe storms are thought to be the cause for the disparity between the calculated and observed isopachs for 1932 to 1934 because reasons (1) and (2) would have had little effect during that time interval. Seelig (1973) states that in September of 1933, a two-day hurricane may have moved as much sediment along shore as would normally have been transported in an entire non-hurricane year. Only the most general of parameters have been measured for hurricanes, none of which can easily be correlated to sediment erosion.

Very little can be said concerning loss of energy during wave-breaking, because of the scale at which this work was done. However, the very large correction

factor ($2/150 \times 10^6$) in the 0-6' depth interval shows that there is very little agreement between the assumptions and the observed behavior; obviously in this depth range the fit of the model is very poor, probably because; 1) the energy dissipated in breaking is lost as heat and causes very little actual sediment erosion (although it may cause the suspension of large amounts of sediments which is then moved by the open-channel flow style of the conventional longshore current), and 2) wave reflection, diffraction and absorption increases nearshore and may dissipate large amounts of energy.

The charts and maps showing the offshore topography of the Sargent-Freeport area are reworked only occasionally, and there is no map showing the configuration of this entire segment of the coastline for any one date; it was therefore impossible to extend the prediction procedure all the way from the Brazos River delta to Sargent. Based on comparisons of the calculated and observed isopach maps, however, a few general observations are possible. Even though the total amount of sediment which is transported through the Brazos River delta area by the longshore current is very large, the difference in the capacity of the current from one place to another was initially very small, therefore the corrected sedi-

ment displacement potentials for the first three time periods show the erosion or deposition of only a few tens of feet. These amounts are comparable to the corrected river deposition thicknesses. The same phenomenon probably obtained at the site of the old Brazos River delta, so that the river and the longshore currents may have been in near equilibrium. If, however, the river deposition rate were decreased by dam construction which dampened the hydrologic cycle, the longshore drift would determine shoreline stability. The longshore current would then become sediment starved as it flowed southwest and through the delta area for two reasons: 1) the continued deposition by the longshore current; that is, the deposition trends shown in the corrected sediment displacement potential maps (Figs. 60 and 61) should be unchanged; and 2) the decrease in erosion rates in some of the areas furthest offshore, because of a lack of easily erodable sediment. In areas where the longshore current must erode mud bottom rather than loose silt, more energy will be dissipated in erosion, and smaller amounts of sediment can be moved. It seems likely that the increase in erosion rates downdrift from the Brazos River delta are causally related to the delta. The erosion is probably much more related to dam construction

on the Brazos than to the diversion of the river and the resultant shift in the position of the river delta.

Finally, it has been determined (Fig. 65) that the delta is a barrier to longshore current flow to depths as great as 30'. This observation and the fact that erosion rates seem to be lower on the crest of the delta than on the sides, may explain why the delta has continued to grow subaerially since 1937, but has remained essentially static at the thirty foot depth. It may also explain how the new Brazos delta has grown at a much higher rate than did the old, even though the sediment load has been cut drastically.

CONCLUSIONS

The method developed here for the prediction of deposition and erosion caused by river sedimentation and longshore currents is successful for short-term predictions in the Brazos River delta area in that the predicted trends approximate the observed trends of erosion and deposition. The control was insufficient to account for long term systematic changes, such as the inferred changes in the values of the deposition and erosional correction factors. The method does not account for catastrophic changes such as those caused by hurricane waves and winds. If future studies reveal a relationship between hurricane-caused erosion and deposition and some combination of hurricane parameters, then a method similar to the one used in this study might be used on a much larger scale to predict coastline stability, if there is sufficient control to establish the trend of the correction factor changes. In the meantime, this method seems best suited for areas where there are no catastrophic inputs of sediment and energy resulting from hurricanes.

The success of the predictions for the first three time intervals shows that a combination of some process similar to the one developed here with the more typical

engineering studies of beach erosion rates might lead to a greater understanding of shoreline dynamics than is currently achieved from beach erosion studies alone.

REFERENCES

Adey, E. A., and H. M. Cook, 1964, Suspended-sediment load of Texas streams, compilation report, October, 1959-September, 1961: Texas Water Commission Bull. 6410, Austin, Texas, 49 p.

Bakker, W.T.J.N.P., and T. Edelmann, 1964, The coastline of river deltas: Conf. Coast. Eng., 9th, Lisbon, 1964, Proc., p. 199-218, Am. Soc. Civ. Eng., New York, 921 p.

Bates, C. C., 1953, Rational theory of delta formation: Am. Assoc. Petroleum Geologists Bull., v. 37, no. 9, p. 2119-2162.

Bretschneider, C. L., and R. D. Gaul, 1956, Wave statistics for the Gulf of Mexico off Caplan, Texas: U.S. Army Corps of Engineers, Beach Erosion Board Tech. Rep. 86.

Carr, J. T., Jr., 1967, Hurricanes affecting the Texas Gulf Coast: Texas Water Development Board Rep. 49, Austin, Texas, 58 p.

Colby, B. R., 1957, Relationship of unmeasured sediment discharge to mean velocity: Trans. Am. Geophys. Union, v. 35, no. 5, p. 708-717.

_____, and D. W. Hubbell, 1961, Simplified methods for computing total sediment discharge with the modified Einstein procedure: U.S. Geol. Survey Water Supply Paper 1593, Washington, D. C., U.S. Govt. Printing Office, 17 p.

Cook, H. M., 1967, Suspended-sediment load of Texas streams, compilation report, October, 1959-September, 1961: Texas Water Development Board Rep. 45, Austin, Texas, 61 p.

_____, 1970, Suspended-sediment load of Texas streams, compilation report, October, 1963-September, 1965: Texas Water Development Board Rep. 106, Austin, Texas, 61 p.

Fowler, L. C., 1957, Determination of the rate of growth and location of delta formations: U.S. Army Corps Eng. Memo. 6, 13 p.

Fox, M. P., 1931, Improving the Brazos River: Civ. Eng., v. 1, no. 4, p. 287-292.

Galvin, C. J., 1967, Longshore current velocity: a review of theory and data: Rev. Geophys, v. 5, no. 3, p. 287-303.

_____, and P. S. Eagleson, 1965, Experimental study of longshore currents on a plane beach: U.S. Army Coast Eng. Res. Center, Tech. Memo. no. 10, 80 p.

Gilbert, G. K., 1885, The topographic features of lake shores: U.S. Geol. Survey, 5th, Ann. Rep., p. 69-123.

Graf, W. H., 1971, Hydraulics of sediment transport: McGraw-Hill Book Co., New York, 513 p.

Grijm, W., 1960, Theoretical forms of shorelines: Conf. Coast. Eng., 7th, Berkeley, California, 1960, Proc., p. 197-202, Council on Wave Res., The Engineering Foundation, 484 p.

_____, 1964, Theoretical forms of shorelines: Conf. Coast Eng., 9th, Lisbon, 1964, Proc., p. 219-235.

Ippen, A. T., ed., 1966, Estuary and coastline hydrodynamics: McGraw-Hill Book Co., New York, 744 p.

Johnson, D. W., 1919, Shore processes and shoreline development: John Wiley and Sons, Inc., New York, 584 p.

King, C.A.M., 1959, Beaches and coasts: London, Edward Arnold Ltd., 403 p.

Lamb, Horace, 1924, Hydrodynamics: Cambridge University Press, 687 p.

Leblanc, R. J., and W. D. Hodgson, 1959, Origin and development of the Texas shoreline, Gulf Coast Assoc. Geol. Soc. Trans., v. 9, p. 197-220.

Matthews, M. D., 1972, Flocculation in the turbidity maximum of Acharon Channel, Yukon River Delta, Alaska: Geol. Soc. America Abst. with Programs, v. 4, no. 7, Boulder, Colorado, p. 585.

Nienaber, J. H., 1963, Shallow marine sediments offshore from the Brazos River, Texas: Pub. Inst. Mar. Sci., v. 9, p. 311-372.

Odem, W. I., 1953, Delta of the diverted Brazos River of Texas: unpub. Master's thesis, University of Kansas, 112 p.

Seelig, W. N., 1973, Dynamics and stability of a Texas beach: unpub. Master's thesis, Texas A & M University.

Seelig, W. N., and R. M. Sorensen, 1973, Historic shoreline changes in Texas: Sea Grant Publication, no. TAMU-SG-73-200, Coastal and Ocean Engineering Division Rep. 165-C.O.E., 19 p.

Shepard, F. P., 1948, Submarine geology: New York, Harper and Row, 557 p.

Stout, I. M., L. C. Bentz, and H. W. Ingram, 1961, Silt load of Texas streams, compilation report, June, 1889-September, 1959: Texas Board Water Engineers Bull., 6108, 236 p.

Task Committee for Preparation of Sedimentation Manual, Committee on Sedimentation of the Hydraulics Division, 1969, Sediment measurement techniques: A. fluvial sediments: Jour. Hydraulics Div., Proc. Am. Soc. Civ. Eng., v. 95, no. HY5, p. 1477-1514.

_____, 1971, Sediment transportation mechanics: H. sediment discharge formulas: Jour. Hydraulics Div., Proc. Am. Soc. Civ. Eng., v. 97, no. HY4, p. 523-567.

United States Coast and Geodetic Survey, 1931, U.S. Gulf Coast, San Luis Pass to Matagorda Bay, Chart no. 1283, January, 1931, 1:80000.

_____, 1931, U.S. Gulf Coast, San Luis Pass to Matagorda Bay, Chart no. 1283, December, 1931, 1:80000.

_____, 1933, U.S. Gulf Coast, San Luis Pass to Matagorda Bay, Chart no. 1283, April, 1933, 1:80000.

_____, 1935, U.S. Gulf Coast, San Luis Pass to Matagorda Bay, Chart no. 1283, September, 1935, 1:80000.

United States Coast Chart, 1858: Chart 106, April, 1858, 1:20000.

United States Geological Survey, 1966, Water resource data for Texas: U.S. Dep. Int., Austin, Texas 714 p.

_____, 1967, Water resource data for Texas: U.S. Dep. Int., Austin, Texas, 279 p.

_____, 1968, Water resource data for Texas: U.S. Dep. Int., Austin, Texas, 746 p.

_____, 1969, Water resource data for Texas: U.S. Dep. Int., Austin, Texas, 642 p.

_____, 1973, Water resource data for Texas: U.S. Dep. Int., Austin, Texas, 714 p.

Vanoni, V. A., 1946, Transportation of suspended sediment by water, Am. Soc. Civ. Eng. Trans., v. III, p. 67-102.

Welborn, C. T., date unknown, Method for computing daily unmeasured sediment discharge: unpub. paper, U.S. Geol. Survey, Austin, Texas, 4 p.

Wisner, G. Y., 1891, Brazos River harbor improvement: Am. Soc. Civ. Eng. Trans., v. 25, p. 519-537.

Zenkovich, V. P., 1967, Processes of coastal development: John Wiley and Sons, Inc., New York, 738 p.

APPENDIX I

STREAMFLOW AND SEDIMENT LOAD DATA FOR THE BRAZOS RIVER, 1924 - 1972

Water Year	Total Discharge (in 10^6 acre feet)	Total Suspended Sediment Discharge (in 10^6 tons)	Average Suspended Sediment Concentration, (in p.p.m.)	Total Bedload Discharge (in 10^6 cubic feet)
1924	8.348			
1925	1.237	12.677	7530	2
1926	8.763	44.939	3770	17
1927	5.563	34.377	4540	9
1928	3.318	28.164	6240	5
1929	6.000	32.284	3950	15
1930	5.219	38.686	5450	15
1931	5.639	27.766	3620	8
1932	8.040	63.649	5820	14
1933	2.560	15.175	4350	5
1934	3.370	23.319	5080	5
1935	7.334	63.473	6360	23
1936	6.032	40.331	4910	9
1937	5.406	23.532	3470	9
1938	7.204	55.713	5680	11
1939	1.966	14.743	5510	3
1940	3.161	23.679	5500	5
1941	16.120	97.307	4430	36
1942	8.523	71.490	6160	15
1943	3.255	11.426	2580	5
1944	7.627	46.736	4500	15
1945	9.305	57.254	4290	17
1946	7.400	35.434	3520	10
1947	6.346	21.011	2430	3
1948	1.951	3.950	1490	3

Water Year	Total Discharge (in 10^6 acre feet)	Total Suspended Sediment Discharge (in 10^6 tons)	Average Suspended Sediment Concentration (in p.p.m.)	Total Bedload Discharge (in 10^6 cubic feet)
1949	3.363	14.457	3160	4
1950	4.186	9.544	1670	6
1951	1.027	1.079	770	1
1952	1.321	4.126	2290	2
1953	2.972	9.543	2360	4
1954	1.974	3.535	1320	2
1955	1.569	2.786	1300	2
1956	1.566	2.890	1360	2
1957	11.070	48.447	3220	30
1958	8.590	24.453	2180	10
1959	3.222	5.198	1190	4
1960	6.440	13.829	1580	7
1961	11.674	38.681	2430	17
1962	3.264	3.981	900	4
1963	1.998	2.315	850	2
1964	1.245	1.850	1090	1
1965	7.430	18.877	1870	13
1966	5.181	18.123	2569	10
1967	1.351	1.072	583	2
1968	9.599	30.867	2362	13
1969	5.949	15.635	1931	6
1970	4.675	9.202	1446	5
1971				2
1972				4

These data are given for each "water-year", which begins October 1 and extends through the following September 30, and is identified by the year in which it ends.

The columns giving stream discharge, suspended sediment discharge, and suspended sediment concentration are from publications of the Texas Water Development Board and its predecessors.

These data are those given for the Brazos River at Richmond in the publications of the Water Development Board. The gaging station is located on a bridge on U.S. Highway 59, on the northeast edge of Richmond, Texas.

APPENDIX II

DAMS AND RESERVOIRS WHICH COULD SIGNIFICANTLY AFFECT THE SEDIMENT LOAD OF THE BRAZOS RIVER

Name	Completion Date	Capacity (acre feet)
Waco Dam	1929	22030
Possum Kingdom Dam	1941	724700
Camp Creek Dam	1948	8550
Leon Dam	1951	2017500
Belton Dam	1953	27290
Smithers Lake Dam	1954	1097600
Palo Pinto Dam	1957	18000
Stillhouse Hollow Dam	1963	34250
Somerville Dam	post 1963	630400